CasaXPS XPS Manual

Contents

Introduction

CasaXPS is a data system primarily designed for the analysis of X-ray Photoelectron Spectroscopy (XPS) data. Data from other techniques are supported within CasaXPS however the core functionality in CasaXPS is aimed at XPS. The topics covered in this manual are designed to aid an understanding of both the XPS technique and data treatment leading to scientifically meaningful results.

CasaXPS is designed around the VAMAS (ISO 14976) file format, which was in turn designed to allow the easy and complete sharing of experimental data between research scientists. Complete sharing of data is significant because without experimental context, spectral or imaging data are simply lists of numbers. Experimental design and acquisition parameters used to collect data are as important to a scientist as the measured signal. Establishing scientific meaning to these lists of counts is the challenge for those making use of XPS therefore the use of a well-defined file format visualised through the windows of CasaXPS is as important as the basic functionality expected of an XPS data system such as curve fitting or chemical state quantification.

This manual therefore presents an introduction to the XPS technique as well as user interface features aimed at providing experimental context for data. The core XPS data analysis features are then presented through as selection of examples. The primary purpose of the following text is to expand on the software tools and tricks presented in video format on the internet. Videos found on YouTube and the CasaXPS video channel web-site https://www.casa-software.com/ follow paths through an analysis that, due to time constraints, omit details about CasaXPS that are herein described in detail. Similarly, published insight notes and practical guides do not permit the full detail of how the results presented therein are achieved. It is therefore the objective for this book to fill in the missing details from videos and papers to make possible the analysis of XPS data by the wider XPS community.

Energy Spectra

When a material is exposed to X-rays, electrons are emitted from the sample with a range of energies. To create an energy spectrum from electrons leaving the sample these electrons must be transferred from the point of emission to a point of detection via a lens system and energy filter designed to allow detection of electrons with specific energies at any one time-interval. An energy spectrum per se is the result of counting electrons for a given time interval (dwell-time) at a given energy, then stepping energy-retarding lenses to a new energy. Repeating measurements over a range of energies results in spectra, an example of which is shown in Figure 1.

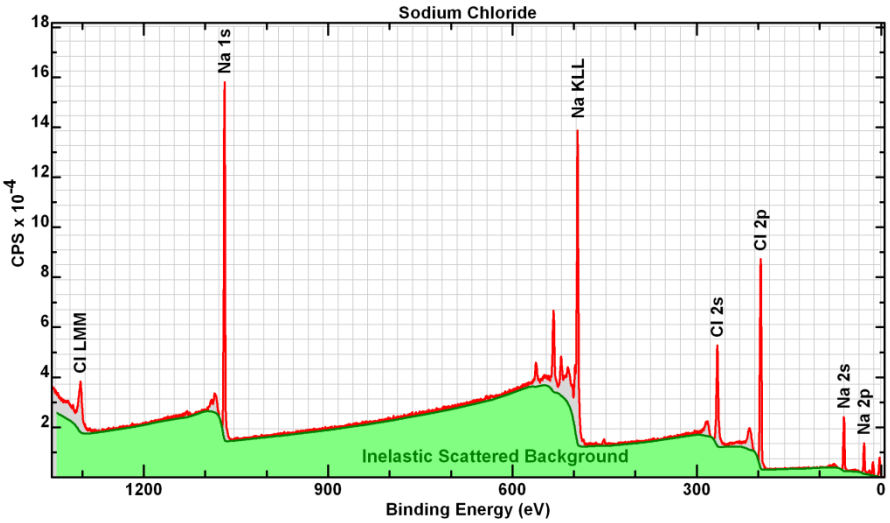

Figure 1. Energy spectrum spanning an energy interval appropriate for surveying photoelectron and Auger peaks emitted from sodium chloride when irradiated by an aluminium X-ray source.

XPS allows quantification of a sample in terms of chemical state. While the intensity of photoelectron peaks depends on the amount of substance within the sample, the spectra are often mixtures of information necessary for quantification of a sample. Photoemission resonance peaks originate from an atom. These resonance peaks are combined with electrons from other atoms and electronic states of these atoms that have lost energy due to interactions with the sample prior to escaping the sample surface. Further, each different element generates multiple photoelectron resonance peaks shifted in energy by differing chemical bonding between atoms. As a consequence, interpretation of energy spectra is seldom simple and requires a degree of knowledge regarding the best use of instrumentation for a specific sample and methods of analysis that are best used to extract information from resulting data.

Collecting Energy Spectra

A typical XPS instrument (Figure 2) makes use of a hemispherical analyser (HSA) to limit the energy of electrons detected to a narrow energy interval. A set of detectors, logical or otherwise, are distributed in the energy dispersive direction with respect to the geometry of the HSA. These individual detectors provide further partitioning of electrons into distinct energy bins, which potentially offer additional energy filtering subject to appropriate dimensions for an entrance aperture to the HSA and pass energy (see below) for the HSA.

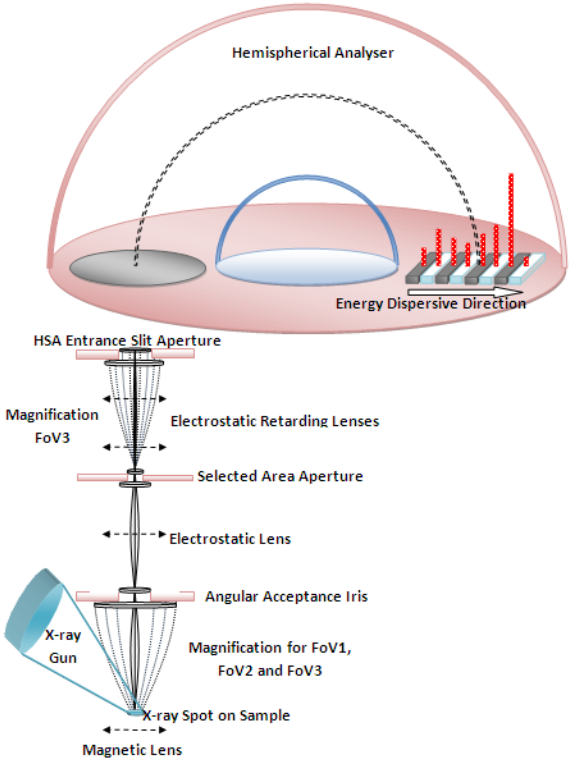

Figure 2. Aspects of a typical spectrometer that includes an X-ray source, a transfer lens column to guide electrons from the sample to the entrance aperture of the hemispherical analyser that filters in energy the electrons available to the detectors.

When the sample is irradiated with X-rays of a specific energy, photoemission occurs with electron kinetic energy ranging over an energy interval limited by the photon energy of the X-rays. A proportion of these electrons emitted from the sample are allowed to arrive at the detector by

means of a constant potential difference applied between the inner and outer hemispheres of the HSA (Figure 3). The constant potential difference applied between the inner and outer hemispheres of the HSA creates a pass energy (PE), meaning only electrons with kinetic energy equal to the pass energy travelling along the mean radius for the two hemispheres will arrive at the same radial position on the detector as the position within the entrance slit at which the electrons entered the HSA. An instrument functioning with constant pass energy is said to be operating in Fixed Analyser Transmission (FAT) mode or Constant Analyser Energy (CAE) mode. Since photoemission occurs over a wide range of energies, to make use of FAT mode for the HSA the transfer lens system must apply a retarding voltage to electrons leaving the sample causing electrons with energies different from that of the pass energy to arrive at the entrance to the HSA with energy matching the pass energy of the HSA. An energy spectrum is therefore collected by scanning the retarding voltages applied via the transfer lens system to electrons emitted from the sample and counting the number of electrons arriving at detectors for these different retarding voltages.

When an energy spectrum is collected there are a number of choices that must be made in terms of how the scan of these retarding voltages should be performed. The first choice is selecting the appropriate pass energy, which determines the best choices for energy step-sizes during a scan and the length of time required to collect signal with acceptable signal-to-noise for the purposes of the measurement.

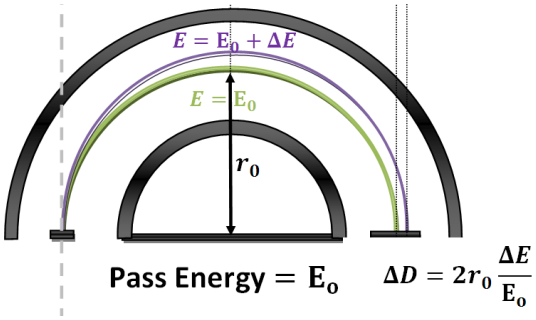

Figure 3. Schematic of a hemispherical analyser consisting of two concentric hemispherical electrodes that in FAT mode are held at a constant potential difference between these two electrodes during the acquisition of spectra. Only electrons with energies close to the pass energy are available for detection.

Pass energy has an influence on the ability to distinguish between two photoemission peaks with similar kinetic energy. Pass energy also influences count rate reported by the detectors. The role played by pass energy is that of specifying the level of dispersion of electrons achieved by the HSA. The greater the potential difference between the hemispheres in the HSA the lesser is the dispersion of electrons with energies different from the pass energy selected. Using a higher pass energy result in more electrons at one time arriving at the detectors compared to lower pass energies and therefore signal-to-noise is improved by increasing the pass energy for a measurement. The cost of increasing the pass energy is the blurring of peaks close-in-energy which impairs ability to resolve or separate signal from different origins, e.g. different chemical states of an atom. The energy resolution for an operating mode is typically characterised in terms of the full width at half maximum (FWHM) for a photoemission peak, often Ag $3d_{5/2}$ measured from a clean silver foil.

For an instrument with fixed size entrance and exit apertures to the HSA, pass energy is often considered as synonymous with energy resolving power for an instrument mode. There are however many instruments with the ability to change the width and length of the entrance aperture to the HSA and when coupled with multiple detectors arranged at the exit aperture to the HSA, the energy resolution for data collected using different aperture and detector arrangements differs for data collected using the same pass energy. The reason energy resolution depends on these apertures at the entrance and exit to the HSA is, for electrons of a specific energy, an image of the entrance aperture is formed at the exit aperture plane (Figure 4). If the image of the entrance aperture for electrons of a given energy falls across multiple detector channels, then energy filtering by detector channel is compromised limiting the separation of electrons with similar energies by means of these multiple channel detectors. Hence energy resolution is also determined by widths of apertures and also by the mean radius of the two hemispheres in the HSA, the latter for a specific instrument is of fixed radius and therefore only pass-energy and aperture widths determine energy resolution for an instrument properly tuned and calibrated.

$$\Delta E = \frac{\Delta D \times \mathrm{PE}}{2r_0}$$

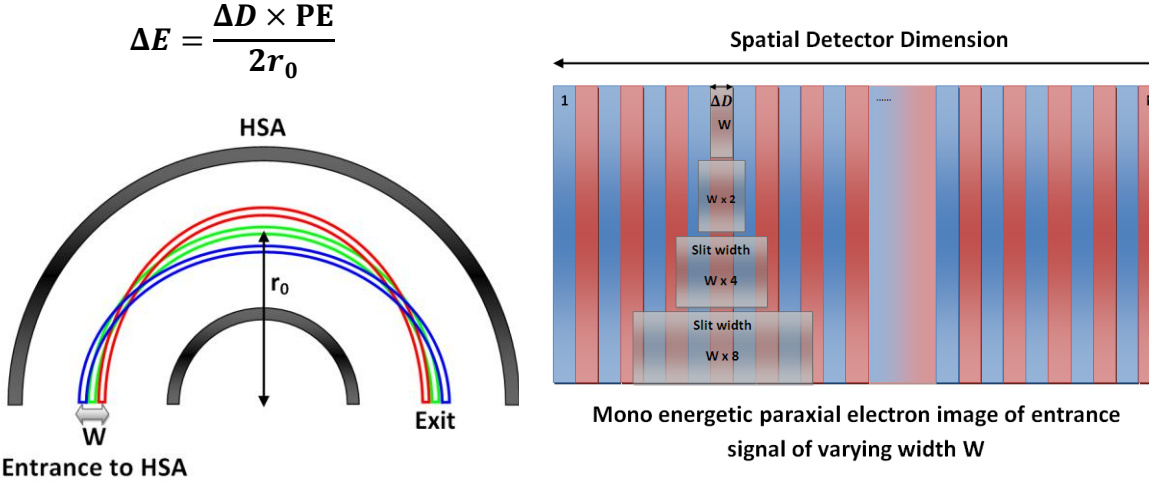

Figure 4. The width of the entrance aperture to the HSA is a factor in the energy resolution achieved for a given pass energy and mean-radius of the HSA. The wider the entrance aperture, the more detector channels located at the exit aperture are potentially impacted by electrons of a specific energy.

Energy resolution is important in the sense other acquisition parameters such as dwell-time per data bin and energy step-size during a scan over an energy interval should match the energy resolution defined by pass energy and entrance and exit aperture widths. If the energy resolution is too good for the energy step-size there is the danger of missing narrow photoemission peaks. Similarly for low energy resolution mismatch with small step-size results in unnecessarily large number of data bins per spectrum without meaningful separation of signal by element and/or chemical state.

The preference in lowering pass energy to improve energy resolution rather than reducing the widths of apertures is explained as follows. Regarding energy resolution for an instrument, there is a difference between lowering pass energy compared to using a narrower entrance aperture, namely, there is a time penalty associated with choosing high pass energies to acquire narrow scan spectra. This time penalty is realised for data acquired for scanned mode spectra. When spectra are acquired using a multi-channel detector system signal is acquired in parallel over an energy interval determined by the mean radius of the HSA, the dimension of the detector in the energy dispersive

direction and the pass energy used to measure signal. For a given instrument the radius of the HSA is fixed. The dimension for the detector has an upper limit, but it is possible for some instruments to limit the set of detectors used to acquire data which allows the energy interval defined by the detector to alter, but such options are seldom available to users of XPS instruments. The parameter available to users is the pass energy. Doubling the pass energy, all else being equal, doubles the energy interval over which electrons are recorded. When a spectrum is acquired by scanning the retarding lens voltages, to avoid relying on a valid detector calibration, the true energy interval acquired for scanned mode spectra is equal to the requested energy interval, for say a C 1s narrow scan, plus the energy interval defined by detector size, HSA and pass energy. A measurement performed at pass energy 160 eV on an instrument with mean HSA radius 165 mm and the dimension for the detector yields an energy interval of 13.94 eV (Figure 5), which is of comparable width to the interval over which a typical C 1s spectrum would be measured. Scanning the retarding voltages avoids the need for precise intensity calibration of data streams by sampling signal from each detector channel for each energy-bin used to construct a spectrum. However, the retarding lens voltages must scan over the requested interval for a spectrum plus the energy interval defined by the pass energy. Hence there is a trade-off between reduced signal for lower pass energies and the decreased dead-time due to ensuring each detector channel samples signal for equal time.

Narrow energy interval spectra acquired without scanning the retarding lens voltages are referred to as snapshot spectra. These snapshot spectra require the calibration of intensities measured using different data streams.

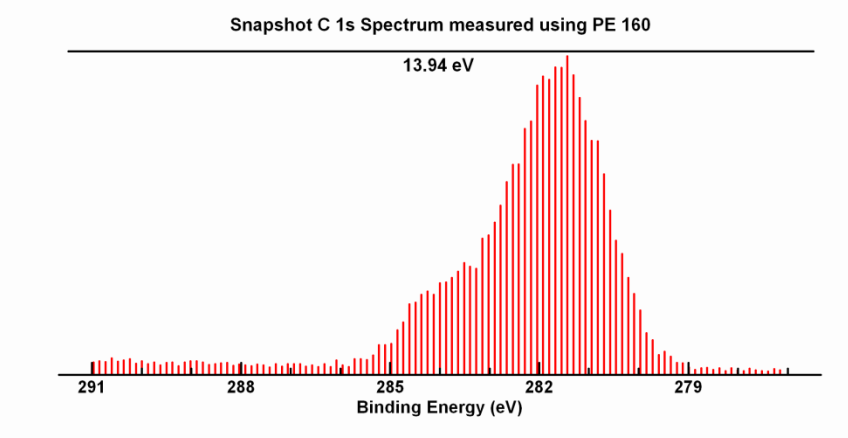

Figure 5. Snapshot spectrum of C 1s photoelectrons measured in parallel by means of a detector array placed at the exit aperture of the HSA (mean radius 165 mm) operating at pass energy 160 eV.

Origin of Photoemission Peaks

Scattering of an electron by a photon creates a hole in a core-level electronic state of an atom forming a singly charged ion. Raising the energy from the atomic ground state to the excited state absorbs a quantum of energy representing the difference between the initial ground state of the atom and the newly created ion in an excited state. This energy is referred to in XPS as the binding energy associated with the creation of a hole in a particular shell. For example, a resonance peak labelled Na 1s indicates a photon excited an atom with the emission of an electron resulting in a vacancy in the K-shell of Na. Ionisation of an atom by a photon of a specific energy results in the recording of an electron with kinetic energy representing the difference between the photon energy

and the quantum of energy required to overcome the binding energy for a given electronic configuration, minus an energy referred to as the work function for an instrument. In practical terms for XPS, the work function energy is the energy required for an electron ejected from a sample that permits the recording of the electron by an instrument. Due to the instrumental work function, there is a lower limit to the kinetic energy for photoemission above zero energy, below which only noise is recorded by the detectors.

The initial scattering of an electron by a photon creating a hole in a core-level has a secondary consequence, namely, the excited state for the system following the photoionization may subsequently relax in energy to a lower energy state with the emission of a photon (fluorescence) or the emission of a further electron via the Auger process (Figure 6). The Auger process represents a change in energy that only depends on the energy of the electronic configuration before and after the Auger electron is emitted and so is independent of the photon energy that created the initial core level hole. In terms of energy spectra, this means Auger peaks always appear with the same kinetic energy regardless of the photon energy used as the source for emission. This is in contrast to photoelectrons which are emitted with a kinetic energy that depends on the photon energy. The binding energy for a core-level is a constant for a given chemical state of an atom so changing the photon energy alters the kinetic energy for photoelectrons.

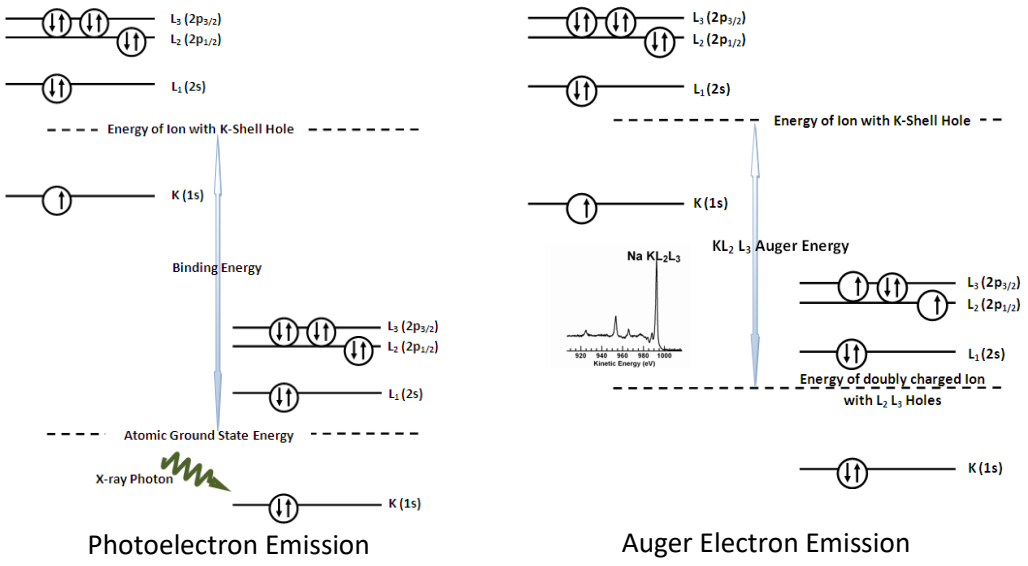

Figure 6. Photoionization of a sodium atom creates a vacancy in the electron configuration of the sodium atom. The resulting ion is created in an excited state with respect to the ground state of the ion, which is unstable and therefore relaxes to a less energetic electron configuration that fills the vacancy. If the relaxation of the electron configuration of the ion liberates energy, the Auger process illustrated results in the emission of a, so called, Auger electron.

In X-ray sources high energy electrons emitted from a filament are accelerated towards the anode which is coated with a specific material. The function of these electrons is to create holes in core-levels of the anode material atoms and thereby stimulate fluorescence (Figure 7) in the form of X-rays with characteristic energy.

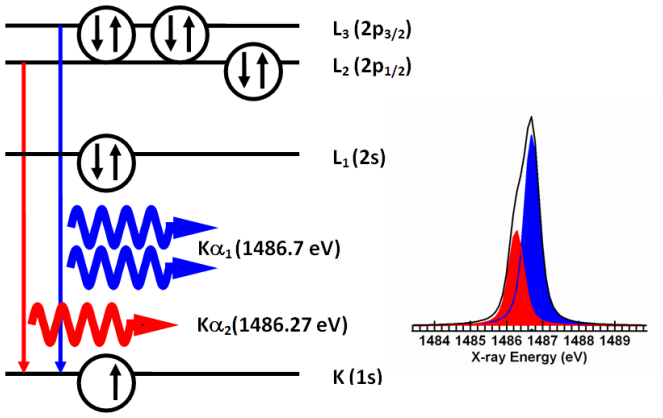

Figure 7. X-ray guns used in XPS are an example of the relaxation of an ion with a core-level vacancy to a lower energetic state that results in emission of energy in the form of fluorescence. For an aluminium anode material, the primary X-ray emission energy is 1486.7 eV.

XPS may be performed using a variety of X-ray sources by making use of different anode materials (Figure 8). A dual anode X-ray gun makes use of resonance peaks in the X-ray spectra of Al and Mg to form an XPS energy spectrum. The X-ray spectra of Al and Mg also include less intense satellite X-ray resonances and extended X-ray intensities to energies greater than the primary X-ray lines that are intended for use by XPS. These X-ray satellite-peaks induce photoemission by XPS too, so dual anode XPS spectra include satellite photoemission peaks of lower intensity, offset from the main photoelectron peaks. Auger emission induced by X-ray satellite peaks appear at the same kinetic energy as Auger emission due to primary X-ray peaks, so satellite signal is present but not observed as energy shifted signal for Auger peaks in XPS spectra. A further consequence of using a dual anode X-ray source is the background to XPS energy spectra is more intense than when a monochromatic source is used owing to the full X-ray spectrum from Al or Mg materials contributing to the XPS signal.

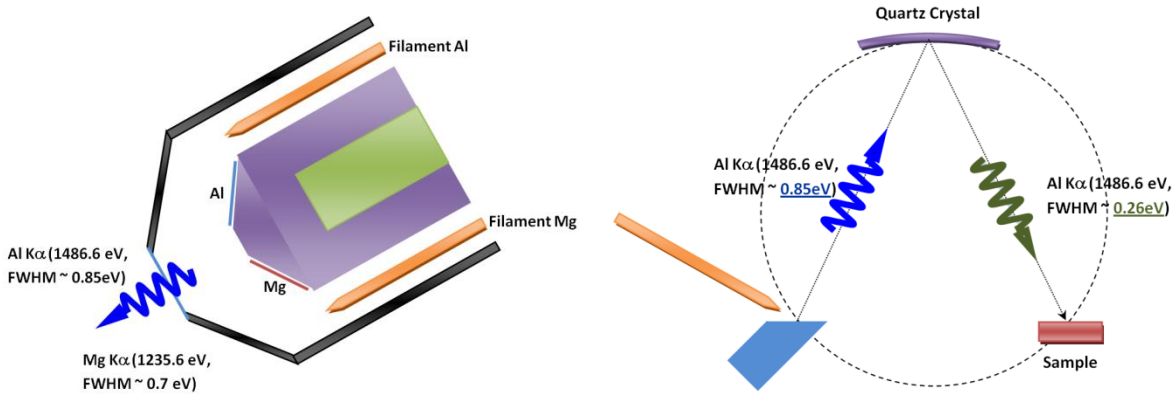

Figure 8. Illustration of a dual anode X-ray source (lefthand diagram) capable of generating photon energies characteristic of aluminium and magnesium coting on a copper anode. The cathode filaments are the source for electrons that are attracted to the anode with sufficient energy to create vacancies in the 1s orbitals of aluminium and magnesium. The righthand diagram illustrates the use of a quartz crystal in a monochromator to create monoenergetic photons from a flux of photons with a range of energies.

The most commonly used X-ray source today is a monochromatic Al anode X-ray gun (Figure 8) although a dual Al and Mg anode X-ray gun is commonly found on laboratory-based instruments. A mono X-ray source provides photon energies in a narrow band of energies determined by the physics of X-ray diffraction via a quartz crystal. An Al anode and an electron emitting cathode filament pair accelerate electrons towards the anode generating X-rays with a range of energies. Al Kα resonance X-ray peak has a FWHM of about 0.85 eV. The width of the photon energy distribution has an impact on the FWHM achieved for XPS energy peaks. A geometric configuration for the anode, the position of the quartz crystal and the location of the sample allows energy filtering of any X-rays emitted from the anode. The quartz crystal diffracts X-rays with energies that are multiples of 1486.6 eV forming a monochromatic spot of X-rays on the sample with a distribution of energies achieving a FWHM of approximately 0.26 eV. The FWHM for the X-ray distribution places a lower limit on the FWHM that is possible for XPS peaks (Figure 9). When using a dual anode X-ray source, based on the FWHM for the X-ray line shapes for Al Kα and Mg Kα, the lower limit for an electron energy spectrum photoemission line width for an Al anode is about 0.85 eV and for Mg anode data the lower limit is about 0.75 eV. In general, other factors involving instrumental, sample and the physics of photoemission prevent achieving these FWHM limits due to X-ray source for XPS peaks.

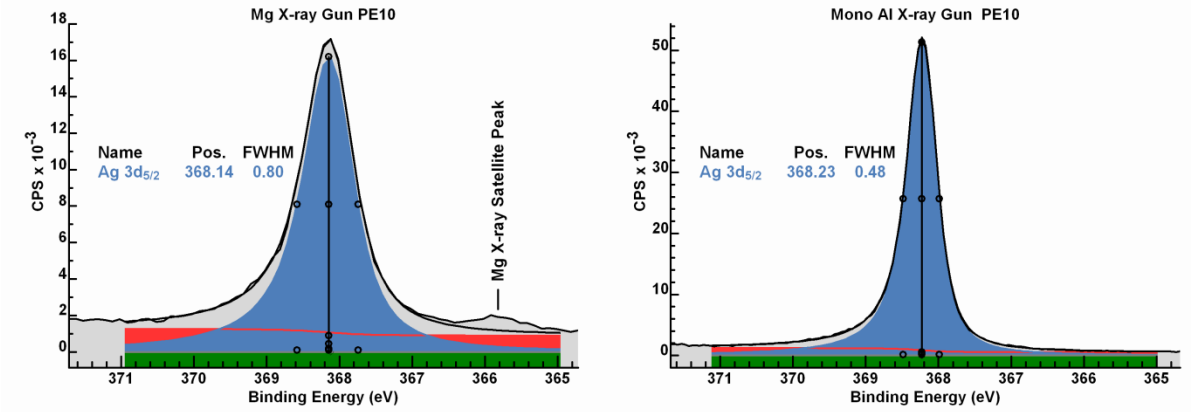

Figure 9. Lefthand spectrum of Ag $3d_{5/2}$ photoelectrons measured using the Mg anode of a dual anode X-ray gun. Note the FWHM for the Ag $3d_{5/2}$ peak measured using pass energy 10 eV is 0.80 eV, which compares less favourably to the FWHM for the same photoelectrons measured using pass energy 10 eV excited by monochromatic X-rays, namely, FWHM 0.48 eV (righthand spectrum).

Transfer Lens System

Arguably the most critical part of an XPS instrument is the transfer lens system (Figure 10). The function of the transfer lens system is to gather electrons emitted from the sample and guide these electrons to the entrance slit of the HSA. Spectral shapes in terms of photoemission peak shapes and overall variation in count rates as a function of kinetic energy for electrons emitted from the sample depend on the design and tuning of lens and apertures within the transfer lens system.

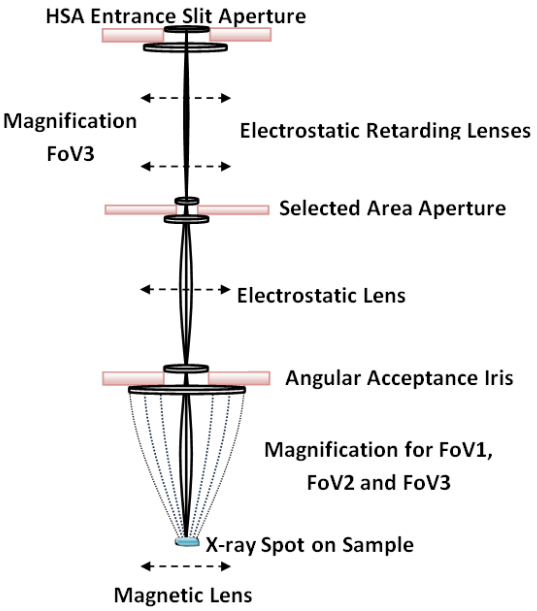

Figure 10. An example of a transfer lens column designed to guide electrons emitted from a sample to the entrance aperture of the HSA. The transfer lens column for other spectrometers may vary, but the essential features illustrated are found in all spectrometers. That is, electrostatic and/or magnetic lenses focus and magnify electron trajectories emanating from the sample and culminating at the entrance to the HSA. En route, these electrons pass through slot or iris apertures, the location and size may vary depending on spectrometer design, but spectrometer performance is highly dependent on tuning of this lens and aperture ensemble.

For ideal spectral shapes the transfer lens system would collimate the trajectories of electrons emitted from the sample so that on entry to the HSA electrons are moving parallel to the axis of the lens column. In practical terms this ideal mode limits the number of electrons entering the HSA resulting in low count rates and measurement times of unacceptable durations. For this reason, design for lens columns lies at the heart of instrument design, where different instruments and operating modes select different compromises to ideal electron trajectories so as to gain sensitivity (enhanced count rates) without inflicting too much damage to spectral shapes.

There are three aspects to tuning a lens system of significance to data analysis, namely, optimising count rates, minimising influences of lens mode on photoemission peak shapes and allowing the characterisation of signal intensity for a wide range of energies used to measure spectra. Optimising count rates is important because chemistry of samples may have a limited lifetime when exposed to X-rays in a vacuum chamber. Peak shapes are important when designing peak models aimed at separating signal into elemental and chemical state for complex data envelopes. Characterisation of count rate to kinetic energy, referred to as instrument transmission, is essential for quantification of samples by XPS. Hence the assertion that the transfer lens system is of critical importance to XPS. The reason XPS instruments offer many operating modes is because optimising for count rate necessarily damages peak shapes and transmission. It is therefore left to the user of XPS instruments to select for a given sample the best compromise for these competing properties for data quality.

While tuning of lens systems is best left to experts, monitoring and verification of instrument performance is the responsibility of the XPS user. Simple routine periodic measurements from clean

gold and silver foils can be used to verify the performance of an instrument. Data analysis for complex and not so complex samples is built on the foundation of repeatability, a necessary condition for which is correctly functioning instrumentation. Hence monitoring the performance of an instrument is an essential part of any scientific investigation by XPS.

Charge Compensation for Photoemission

When electrons are scattered by photons positively charged ions are created within the sample. A build-up of positive charge continues to occur during exposure of the sample to X-rays unless a mechanism is available that returns negative charge to the sample. For this reason, XPS instruments typically include a means of delivering charged particles to the sample in doses that compensate for photoemission. Historically the term charge neutralisation has been used to describe this process, but in more recent times the term charge compensation is used to describe the act of returning charged particles to the sample surface that compensate for photoemission. This change in terminology reflects the fact that the sample is seldom in a neutral state with respect to ground (Figure 11) but rather achieves a stable steady state potential between the sample and ground.

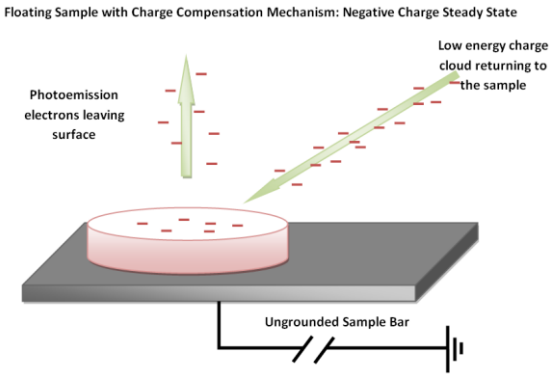

Figure 11. A sample disconnected from ground allows the sample to enter a steady state between the emission of electrons due to photoionization and the return of charged particles to the sample via charge compensation apparatus. Depending on how charge compensation is performed, it is possible that the sample charges negatively before the steady state is achieved.

For conducting samples that permit the free movement of electrons to all parts of a sample, charge compensation is a simple matter of electrically connecting the sample to ground. In the case of insulating samples charge compensation takes the form of actively returning charge to the sample via a cloud of low energy electrons and/or ions. If charge compensation is not performed electrons emitted from the sample would be attracted by a constantly changing positive charge back to the sample and as a consequence photoemission peaks would move in energy to lower kinetic energy as a function of measurement time. The act of charge compensation for an insulator stabilises a static charge on the sample and so the kinetic energy for photoemission peaks is stable with respect to time. Raw data from insulating samples often exhibit photoemission peaks with apparent binding energy lower than expected. This lower binding energy or, alternatively stated, higher kinetic energy for peaks is due to the sample attaining a steady state that is negative. Given stability of peaks in terms of kinetic energy, the energy scale can be calibrated allowing the assignment of binding energy for peaks. The act of calibrating the energy scale is referred to as charge correction and is performed in software.

Since correlating binding energy with photoemission peaks is an indicator of chemical environment for an atom, charge compensation is an essential part of any XPS measurement. Charge compensation is also important for maintaining repeatable and correct peak shapes and therefore confidence in charge compensation is a key requirement for chemical state analysis by fitting of curves to data.

Background Signal

A feature of XPS is background signal representing electrons recorded with kinetic energy different from energies expected as a consequence of quantized photoemission from bound states of atoms or ions. While the origin of these background counts is energy quantized photoemission signal, initially quantized signal is spread to lower kinetic energy due to scattering of electrons by electrons bound to atoms within the sample. The shape and intensity of these inelastically scattered backgrounds depends on material and proximity of material within a sample, and represents valuable information about a sample provided by XPS. A point worth highlighting is that background structures in XPS, on occasion, have the appearance of quantized photoemission peaks. Most notably sequences of loss peaks are evident in spectra from metallic Mg, Al and other materials. Broader loss peaks are also a feature of materials such as ZrO_2 which is an example of where background signal must be accounted for when calculating peak intensity for Zr 3p (Figure 12).

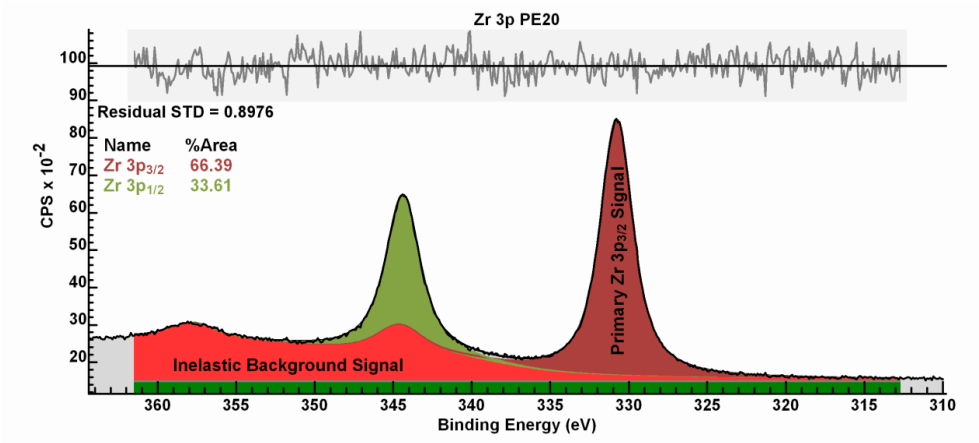

Figure 12. The XPS of Zirconium provides and example of photoelectron signal that is split into two peaks due to electron-spin interaction with orbital angular momentum. Moreover, inelastic scattering of these Zr 3p photoelectron peaks creates electrons with lower kinetic energies, in which peak-like structures (that are correlated to the primary photoelectron signal) are a feature of the spectra. Importantly to quantification by XPS, the background signal beneath Zr $3p_{1/2}$ includes a peak-like structure due to the Zr $3p_{3/2}$ photoelectron peak, the result of which is the theoretical ratio of Zr $3p_{1/2}$ to Zr $3p_{3/2}$ is not achieved unless the contribution of the background (to that part of the spectrum involving Zr $3p_{1/2}$ signal) is included in a peak model used to measure the ratio of these doublet peaks.

Accounting for background signal and separating primary unaltered photoemission signal from background signal is one of the greatest sources for error in peak models and quantification by XPS. This topic is best considered in the context of data treatment of spectra with differing backgrounds and will be discussed later using specific examples to illustrate the influence of these inelastic

scattered backgrounds on XPS quantification and chemical state analysis by modelling data with component peaks.

Photoemission Peaks

Photoemission resonances are either photoelectron or Auger. Auger peaks are complex in nature representing many paths by which an ion can relax into a doubly excited ion of lower energy. Auger peaks are more difficult to interpret than peaks due to excitation by a photon. As a consequence, when interpreting XPS data there is generally a greater focus on photoelectron peaks.

Once a background signal is subtracted from XPS data what remains is signal marking kinetic energies in a spectrum that can be assigned to holes within ions created by photoionisation. The photon energy is fixed, and energy lost by electrons to the work function is assumed fixed, therefore the position of a photoelectron peak in an energy spectrum is determined by the amount of energy required to create the hole in a specific electronic shell of an atom. The set of energy levels for electron configurations within atoms or ions depends on electron spin which, if unpaired electrons are present, serves to split the energy for electron configurations that otherwise would have identical energy. The interaction of spin and orbital angular momentum means that the quantum of energy necessary to create a particular electron configuration in an ion may be numerous and depends on chemical bonds between atoms. As a consequence photoemission varies in complexity between simple individual singlet peaks associated with s-orbitals to simple doublet peaks as well as peaks with complex structures due to multiplicity of energy levels involved in the photoionization process. In particular higher atomic number (Z) elements create photoemission shapes formed from numerous distinct quanta of energy absorbed in creating ions from atoms. Cerium oxide is an example of a material where the creation of a hole in a d-orbital creates a sequence of doublet peaks rather than a simple pair of doublet peaks. Simple doublet peaks can be observed for p-orbitals in sulphur, although this is not always the case for all sulphur compounds (Figure 13).

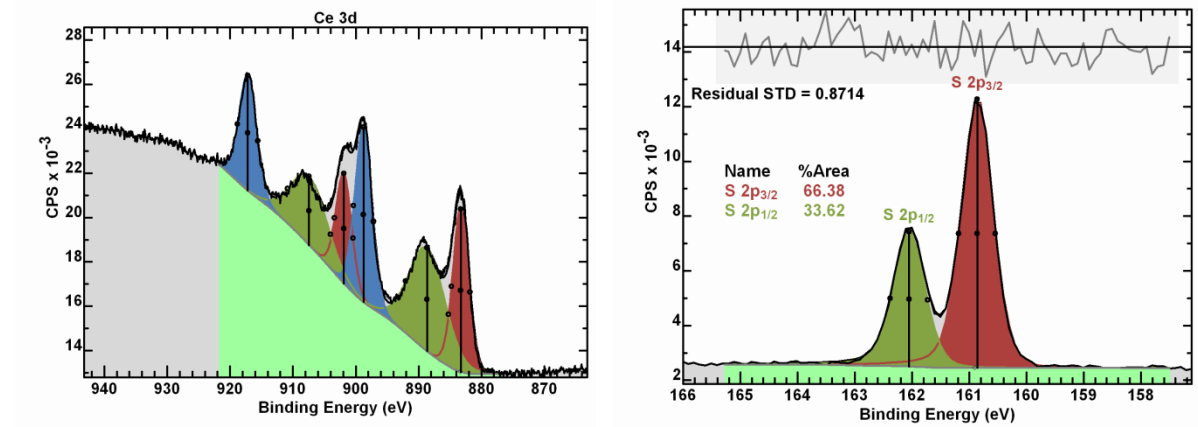

Figure 13. Lefthand spectrum is an example for the XPS of a heavier element in a chemical state where photoionization results in split energy-levels (multiplicity) corresponding to Ce 3d core-level capable of generating peak structures offset in the energy spectrum. By contrast, for lighter elements, the spin-orbit interactions of electrons within an atom and final state ion, are limited to producing either a single peak, in the case of s-orbitals, or doublet peaks for p, d and f orbitals. The righthand spectrum is an example of sulphide doublet peaks created by photoionization. The XPS of a sulphide is an example of a lighter element with well-defined energies for both initial state atom and the final state ion created with a vacancy in the 2p electrons.

The shape of measured photoemission peaks, even when simple in origin, is the result of instrumental factors as well as the underlying shapes dictated by the physics of the photoemission process. There are numerous examples of photoemission peaks from insulating materials, sufficiently broad but still lying within an energy interval in which background intensity variation is negligible, to assert that such peaks are modelled effectively by means of a Lorentzian line shape. The measured shape differs from a pure Lorentzian for the following reasons. If Lorentzian shaped peaks are measured by XPS the shape of the Lorentzian is altered by the integration of signal by a finite width detector aperture (Figure 14). The finite width of an entrance aperture to the HSA similarly alters the shape of signal recorded as too does imperfections in signal trajectories arriving at the entrance aperture to the HSA. These instrumental factors are more obvious for intrinsically narrow photoemission lines. Hence the observation regarding Lorentzian profiles for photoemission is made for sufficiently broad isolated peaks.

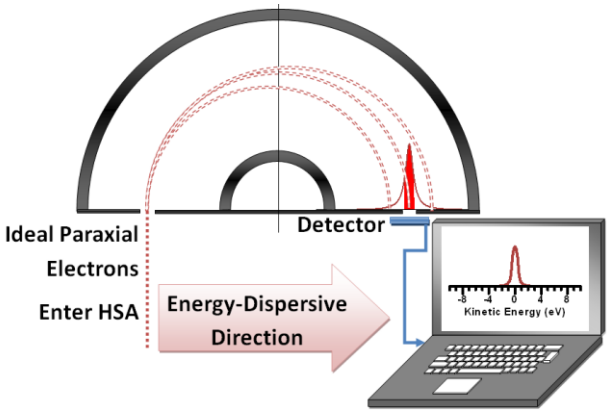

Figure 14. Illustration of how the HSA and exit apertures integrate signal for each energy bin within a scanned spectrum. The width of the exit aperture and the FWHM of the underlying photoelectron peak determines the line shape as it appears in a spectrum. For a narrow exit aperture compared to the width of a peak, the output resembles more closely the line shape of the underlying photoelectron peak. If the photoelectron peak is narrow compared to the exit aperture, then instrumental factors are more dominant in the shapes seen in spectra.

Mathematically, modification of a Lorentzian/Cauchy shape in an attempt to match shapes observed in measured photoemission peaks is performed by a convolution of a Lorentzian with a Gaussian referred to as a Voigt function. The LA line shape in CasaXPS (Figure 15) is a generalised Voigt function offering the special case of LA(1,1,n) to compute a Voigt function with differing Gaussian contribution altered via the parameter n.

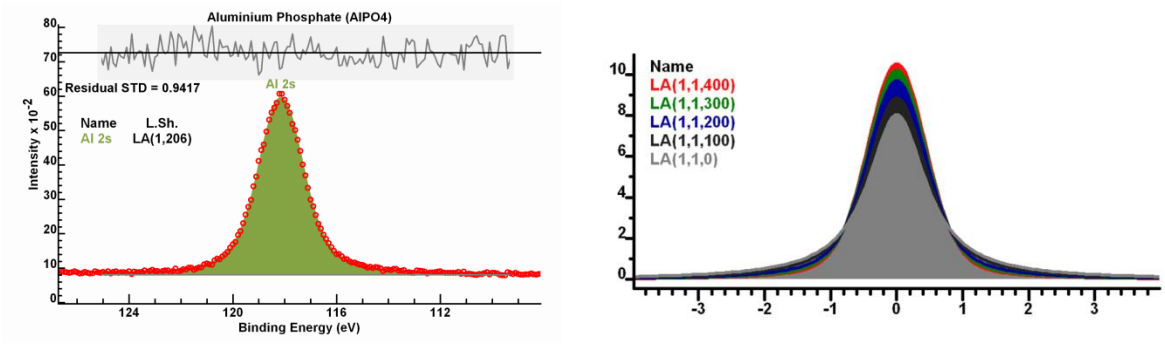

Figure 15. Lefthand spectrum fitted to a peak model consisting of a constant background and a single Voigt line shape. The LA line shape in CasaXPS is polymorphic in the sense that the same Voigt line shape can be obtained by using one of three specifications, namely, one parameter, e.g. LA(50), two parameters e.g. LA(1,701) or three parameters LA(1,1,701). LA(m) is intended to mirror the specification parameter used by the historical pseudo-Voigt line shape GL(m), whereas the three parameters LA(a,b,n) is the basis from which asymmetry can be introduced into the LA line shape. The righthand line shapes are examples of how a Voigt line shape of equal intensity alters from a pure Lorentzian (LA(1,1,0)) by increasing the width of the Gaussian in the convolution integral.

Detection Limit for XPS Photoemission Peaks

Underlying the concept of detection limit for XPS is the assumption that spectral intensity obeys Poisson statistics, which is equivalent to assuming for a data channel containing n counts, any data bin containing counts in the range $n \pm \sqrt{n}$ can be considered to have identical counts with a confidence of 68.3% that these two data bins represent identical intensities. An implication of this statement is that as n increases, the range of values we consider to be identical measurements increases at a slower rate than the signal. Thus measuring for longer time favours systematic signal such as a photoemission peak which increases compared to noise at a rate proportional to the $\sqrt{n}$.

For XPS the nature of Poisson behaviour has implications for photoemission peaks superimposed on background signal resulting from inelastic scattering of photoemission within a sample. During a fixed period, photoemission from a core level contributes to a data bin within the recorded spectrum n counts while the inelastic background contributes m counts to the same data bin. The noise level we expect for the data bin containing $n + m$ counts will be $\sqrt{n + m}$. However the counts of interest are n so the uncertainty in these n counts will be equal to $n \pm \sqrt{n + m}$, thus the background signal alters the ability to detect photoemission peaks. A low intensity peak may be available for detection if located in a spectrum where the background is low, but the same peak intensity superimposed on an intense background may not be detectable.

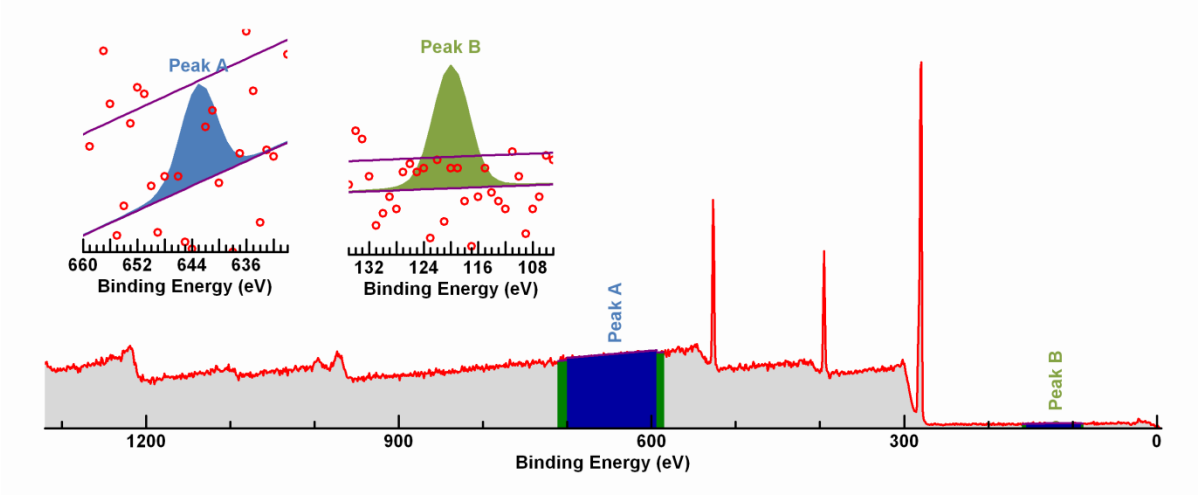

Figure 16. Illustration of how background signal alters the detectability of a photoelectron peak. In this example, two synthetic line shapes defined with equal intensity and FWHM, but placed on the survey spectrum at different energies with different intensity of background signal are not equally as detectable due to the increase in noise in the background as shown.

To illustrate this point, consider two synthetic component peaks (Peak A and Peak B in Figure 16), with the same area (CPSeV) and FWHM, placed on background signal resulting from the accumulation of inelastic scattering of photoemission to higher kinetic energy. These two peaks are summed with a linear background-type ***Regression***. A second region is used to display one standard deviation in signal variation plotted relative to the linear background. The background-type used for these second regions is ***Limit of Detection***. Note how Peak A, while exactly the same as Peak B in CPSeV and FWHM, fails to rise above the line representing one standard deviation in intensity due to Poisson noise. Peak B however, due to the lower background signal, is easily identified.

Basics of Quantification by XPS

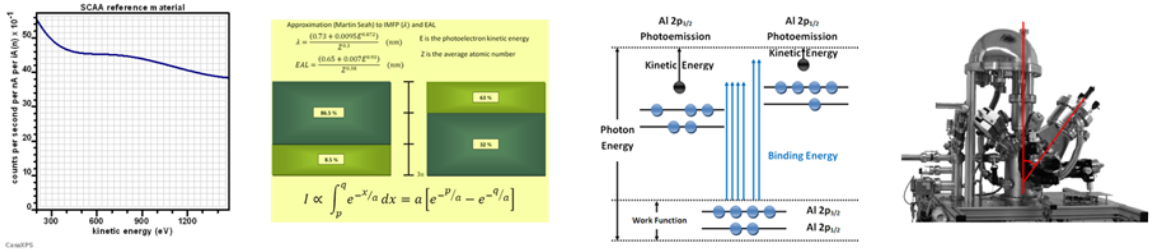

$$S_k = transmission \times escape\ depth \times cross\ section \times angular\ distribution\ correction$$

Figure 17. Illustration of the four (minimum) requirements for the correction of as-recorded photoelectron peak intensity when converting peak intensity into atomic concentration at the surface of a sample.

Percentage atomic concentration B_i for an element is computed from n peak areas $\{A_k : k = 1, n\}$ with corresponding total sensitivity factors $\{S_k : k = 1, n\}$ (Figure 17) using the formula

$$B_i = 100 \times \frac{\frac{A_i}{S_i}}{\sum_{j=1}^{n} \frac{A_j}{S_j}}$$

An element library is a file containing information necessary when computing B_i and take different forms depending on instrument and philosophy followed by a particular instrument manufacturer.

Element Library and Relative Sensitivity Factors

The element library in CasaXPS is an ASCII file containing information relating to the identification of photoemission peaks and for use when quantification is performed based on computed photoemission signal after an inelastic scattered background signal is removed. The essential information within the element library for both these purposes is:

1. Element and photoelectron assignment for the emitted electron from a ground state electron configuration (e.g. Na 1s or Cu $2p_{1/2}$).

2. Approximate energy for photoemission corresponding to each photoemission process and each element in the periodic table.

3. Relative Sensitivity Factors (RSFs) for each photoemission process and each element.

The first two allow identification while the third is the means by which quantification is performed.

Characterising photoemission by these three entities is an over simplification for both identification of photoemission peaks within an XPS spectrum and for calculating amount of substance by XPS. Photoemission peaks described by an idealised symmetric bell-shaped peak at a fixed energy with area proportional to sample composition is only possible for a small number of materials. Chemical state and complex interactions in final state electron configuration result in photoemission spectral shapes that do not follow a simple peak model, and signal can be spread over many electron volts. Nevertheless, these element library essentials are the starting points from which sample analysis by XPS begins and as such an element library based on these three sets of information is a required part of quantification by XPS. It is, however, important to understand how these values are compiled for a given instrument and the limitations of such information for different materials when analysed by XPS.

Relative sensitivity factor is the name given to a scaling factor used to convert peak area into an amount of substance. Historically the term RSF had and still has at least two meanings, namely, empirical RSF or theoretical RSF.

Photoelectrons from a bulk solid-state material are scattered by inelastic interactions with the sample material and so photoemission from a bulk material alters the relative intensity for photoemission peaks as a function of the scattering rate, which in turn varies as a function of kinetic energy for photoelectrons. These influences are referred to as escape depth corrections. Relative intensities for measured photoemission peaks will include the influence of inelastic scattering.

Empirical RSFs are the basis for element libraries used by the more established instrument manufacturers. By way of example, a paper by Wagner et al reported a set of sensitivity factors that were determined from a set of standard materials using specific XPS instruments. Measured relative peak intensity RSFs represent empirical scaling factors that necessarily include instrumental factors commonly referred to as transmission characteristics, instrument geometry relating to intensity dependency on sampling direction with respect to the X-ray source direction and also escape depth differences for the materials used to calculate sensitivity factors. These empirical factors are therefore specific to both instrument and material composition. One essential consideration for empirical RSFs is the material used as a standard must be homogeneous in both area and depth (for a depth significantly greater than the sampling depth by XPS). Empirical RSFs therefore tend to be obtained for bulk materials.

It is possible to process empirical RSFs to remove transmission and angular distribution contributions to empirical RSFs resulting in RSFs that can be used for different instruments. The use of such RSFs for a range of instruments relies on a good knowledge of the transmission function for instruments making use of these processed empirical RSFs. An example of processed empirical RSFs is Ulvac PHI sensitivity factors that represent magic angle RSFs which can be applied, with appropriate corrections, to other PHI instruments with angles of 45^{o} and 90^{o} (two common arrangements for the angle between the direction for X-rays and sampling direction for photoemission on Ulvac PHI instruments).

The alternative to empirical RSFs is theoretical RSFs in the form of photoionization cross-sections calculated for specific photon energies. Scofield reported theoretical photoionization cross-sections

for photon energies corresponding to X-ray energies for anode materials aluminium (1486.6 eV) and magnesium (1253.6 eV). These theoretical cross-sections are effectively relative sensitivity for photoemission intensities from an infinitely thin layer of a given element measured using polarized X-rays at the, so called, magic angle to the direction of the analyser. These Theoretical RSFs can therefore be considered a more fundamental entity and are related to empirical RSFs by adjusting these theoretical RSFs for angular distribution, escape depth and instrumental response.

Escape Depth Correction

The discussion that follows assumes the measurement is performed using an instrument with a flat transmission response to kinetic energy for photoemission intensity.

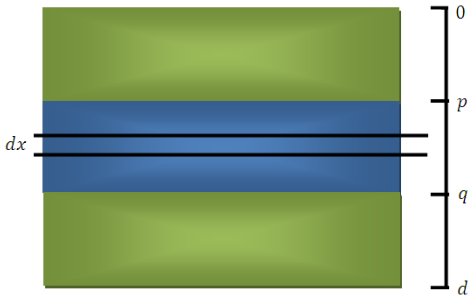

Figure 18. Depth representation of a sample where 0 represents the interface of the sample with the vacuum.

The intensity emitted at the surface I from a layer of material between the depths of p and q (Figure 18) is proportional to the integral:

[1] $$I \propto \int_p^q \exp\left(-\frac{x}{\lambda(E_{Z_{nl}})}\right)dx = \lambda(E_{Z_{nl}})\left[\exp\left(-\frac{p}{\lambda(E_{Z_{nl}})}\right) - \exp\left(-\frac{q}{\lambda(E_{Z_{nl}})}\right)\right]$$

An element library containing Scofield cross-section $S_{Z_{nl}}$ (atomic number Z, principal quantum number n and orbital angular momentum quantum number l) represents a set of sensitivity factors assuming electron emission occurs at the precise interface between a material and the vacuum, assuming photons arrive at the surface with the magic angle with respect to the direction for which electrons are recorded by the analyser. The measured photoemission intensity $I_{Z_{nl}}$ forming the basis for a measure of the amount of substance assuming a lamina associated with an element with atomic number Z must be scaled using Scofield cross-section $S_{Z_{nl}}$, namely, $\frac{I_{Z_{nl}}}{S_{Z_{nl}}}$, however if rather than a lamina the material is of thickness d, then the bulk equivalent amount of substance intensity $I^B_{Z_{nl}}$ is obtained as follows,

[2] $$I^B_{Z_{nl}} = \frac{I_{Z_{nl}}}{S_{Z_{nl}} \times \lambda(E_{Z_{nl}}) \times \left(1 - \exp\left[-\frac{d}{\lambda(E_{Z_{nl}})}\right]\right)}$$

The expression $\lambda(E_{Z_{nl}}) \times \left(1 - \exp\left[-\frac{d}{\lambda(E_{Z_{nl}})}\right]\right)$ derives from the escape depth correction assuming an exponential decay dependent on the effective attenuation length $\lambda(E_{Z_{nl}})$ due to inelastic scattering of electrons within the sample prior to electrons emerging into the vacuum. If the

material is of thickness d is greater than $3 \times \lambda\left(E_{Z_{nl}}\right)$ for all photoelectron energies $E_{Z_{nl}}$, then $\exp\left[-\frac{d}{\lambda\left(E_{Z_{nl}}\right)}\right] \approx 0$ therefore the corrected intensity used in an atomic concentration calculation that accounts for escape depth is given by:

[3] $$I^{B}_{Z_{nl}} = \frac{I_{Z_{nl}}}{S_{Z_{nl}} \times \lambda\left(E_{Z_{nl}}\right)}$$

Escape depth has a profound influence on quantification by XPS for sample of a heterogeneous nature. The consequence of inhomogeneous depth distributions with very simple layer structure is illustrated by two scenarios for two materials measured using emission electrons with similar kinetic energy. Carbon and ruthenium measured using C 1s and Ru 3d emission peaks are two such materials.

Ru 3d and C 1s are emitted with the same kinetic energy. Assuming the same effective attenuation length $\lambda\left(E_{Z_{nl}}\right)$ for both materials (which is not necessarily true), applying the exponential attenuation model then the following statements are true:

a) 95% of signal originates from $3\lambda\left(E_{Z_{nl}}\right)$ depth.
b) 63% of signal originates from $\lambda\left(E_{Z_{nl}}\right)$ depth.
c) 86.5% of signal originates from $2\lambda\left(E_{Z_{nl}}\right)$ depth.
d) Only 8.5% of the signal originates from between $2\lambda\left(E_{Z_{nl}}\right)$ and $3\lambda\left(E_{Z_{nl}}\right)$ depths.

The following two depth distributions for carbon and ruthenium would result in very different atomic concentration values obtained by XPS.

Scenario 1: A layer of carbon of thickness $\lambda\left(E_{Z_{nl}}\right)$ nm on top of a layer of ruthenium of depth $2\lambda\left(E_{Z_{nl}}\right)$ nm measured using Al anode X-rays (Figure 19).

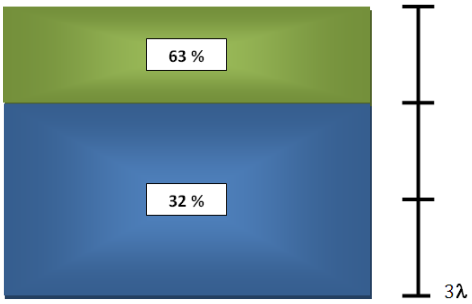

Figure 19. Layered structure of a sample containing carbon and ruthenium. C 1s and Ru 3d photoelectron binding energies are very similar and therefore experience similar inelastic scattering en route to the vacuum from within the sample and therefore equivalent attenuation lengths λ nm. Carbon forms a layer of thickness λ nm closest to the vacuum, while ruthenium is located below the carbon layer and is of thickness 2λ nm.

Given a model with ratio Ru:C = 2:1, XPS RSF corrected intensity ratio 32:63 is approximately 1:2. Thus the ratio is the exact opposite of the true value for the amount of Ru to C.

Scenario 2: A layer of carbon of thickness $\lambda(E_{Z_{nl}})$ nm below a layer of ruthenium of depth $2\lambda(E_{Z_{nl}})$ nm measured using Al anode X-rays (Figure 20).

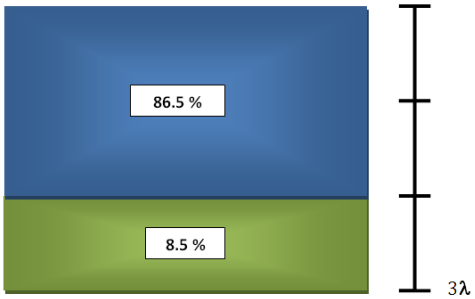

Figure 20. Layered structure of a sample containing carbon and ruthenium. C 1s and Ru 3d photoelectron binding energies are very similar and therefore experience similar inelastic scattering en route to the vacuum from within the sample and therefore equivalent attenuation lengths λ nm. Carbon forms a layer of thickness λ nm furthest from the vacuum, while ruthenium is located above the carbon layer and is of thickness 2λ nm.

Given a model with Ru:C in the ratio 2:1 within the first $3\lambda(E_{Z_{nl}})$ nm, measured by XPS the RSF corrected intensity ratio would be 86.5:8.5 approximately 10:1.

The surface sensitivity of XPS provides remarkable information about the top 10 nm of material, but unless a sample is prepared to be homogeneous in depth and without contamination, the atomic concentration reported by XPS is not a representation of the sample composition in terms of proportions of elements.

Angular Distribution Correction

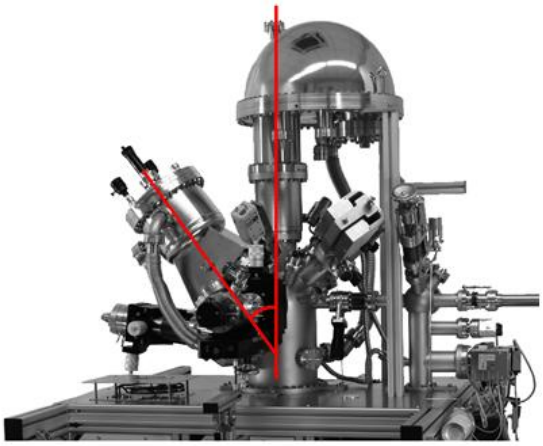

Figure 21. An XPS instrument design, where the red lines indicate the angle between the monochromatic X-ray source and the direction electrons emitted from the sample must travel to be available for detection by the spectrometer.

Scofield cross-sections do not account for angular distribution variation in intensity as a consequence of instruments detecting electrons in a specific direction relative to the photon source (Figure 21). Angular distribution correction to RSFs based on a given instrument geometry are

applied resulting in total sensitivity values appropriate for a given X-ray source and the angle between the X-ray source and the direction defined by the electron energy analyser. Total sensitivity factors are corrected for angular distribution using the factor $1 - \frac{\beta}{4}(3\cos^2\theta - 1)$. Where θ is the angle between an X-ray source and the axis defined by the transfer lens system for an electron analyser angle and the value for β is computed for the element in question. Variation in intensity as a consequence of an instrument with $3\cos^2\theta - 1 \neq 0$ is performed at the time RSFs are extracted from the element library. Corrections due to angular distribution are applied to RSF values relative to s-orbital electron configurations which all respond identically in terms of direction, so RSFs are modified due to angular distribution correction for p, d and f photoemission lines only. These corrections appear as adjustments to element library RSFs when extracted from the element library and entered into quantification regions or component peaks RSF fields.

Instrumental Transmission Correction

The number of electrons recorded by an instrument at a specific kinetic energy for the detected electrons deviate from the number of electrons emitted from the sample. The ratio of electrons leaving the sample to the number of electrons recorded at the detector varies as a function of the kinetic energy for the emitted electrons. To adjust for these variations in collection efficiency an instrument transmission function is measured. A transmission function is prepared for each operating mode for a given instrument. Differences in operating mode may include specific settings for the pass energy, electron optical lens modes, aperture settings and detector settings.

Relative Transmission Functions

The primary objective in computing transmission functions that correct spectra to allow for differing intensity response to different kinetic energy of photoelectrons, is to remove in software all instrumental artefacts from spectra. There is a secondary motivation for transmission correction, namely, flexibility in the use of pass energy to select an appropriate sensitivity for each photoelectron peak used during quantification by XPS. If the method used to calculate the transmission correction is successful, then both primary and secondary objectives are achieved. However, there is another school of thought that, rather than computing the true (absolute) transmission response to kinetic energy of photoelectrons, quantification is achieved by constructing tables of RSFs for each photoelectron peak and then applying a method to convert all spectra as-measured, to processed spectra that allow the use of a common table of RSFs. Transmission correction designed to allow quantification based on empirically determined RSFs, is described herein as relative transmission correction. Historically, transmission correction in an absolute sense was seldom available. Consequentially, tables of RSFs were used to create percentage atomic concentration of elements by XPS. These RSFs were a combination of multiple factors, which include photoionization, instrumental and sample dependent factors. When used, transmission correction seldom achieved the absolute adjustment to intensities that fully eliminates instrumental artefacts from tables of RSFs. Thus, these table of RSFs were dependent on the choice made for the method used to construct a relative transmission correction for an instrument.

The absolute transmission response of an instrument alters with lens mode and pass energy. However, provided the transfer lens column and the hemispherical analyser operate with a systematic response to the retard ratio, a single transmission curve can be computed for a lens mode that is used to generate all the transmission functions for the lens mode operated at different

pass energies. The caveat is that transfer lens columns include apertures and imperfections that may prevent the computation of an absolute transmission response. Nevertheless, if the target for transmission correction is to correct for variation in spectra due to pass energy by converting spectra to a spectrum that allows for the use of tabulated empirical RSFs, then quantification may proceed without the absolute transmission correction of spectra via calculating a single transmission curve per lens mode.

The aim of computing a single transmission curve per lens mode, for most operating modes of practical use, is a reasonable target. There are clear advantages to relaxing the requirement to convert spectra from any spectrometer to a spectrum that is independent of spectrometer. Namely, if spectra can be converted to spectra that are independent of pass energy, then the analyst may choose high-sensitivity modes for low-intensity peaks while reserving the low-sensitivity, high energy-resolution modes for photoelectrons with chemical state. Essentially, acquisition-times and signal-to-noise in spectra are best served if spectra are measured according to the need to discriminate between photoelectrons chemically shifted in binding energy (that require peak models to partition signal into chemical state) and photoelectrons that are of consequence to element composition only.

The concept of relative transmission functions is the method used by Kratos Analytical Limited. The element library containing the RSFs for use with Axis spectrometers (Axis 165, Axis Ultra, Axis Nova, Axis Supra) were developed to yield acceptable quantification for data measured using the initial Axis Ultra spectrometers. The requirement to obtain the same quantification for all operating modes, for all Axis spectrometers from the same sample motivated the introduction of relative transmission functions for each lens mode and pass energy, where the transmission function is computed to align gold spectra measured from subsequent instruments with a gold spectrum measured from a specific Axis Ultra. The specific Axis Ultra used to create the reference spectrum returned quantification results correctly for bulk homogeneous materials by applying the Kratos RSF tables to photoelectron peak intensity and no other means to correct for transmission or escape depth. That is, the table of RSFs were empirically determined to include these instrumental and sample considerations. Hence, the relative transmission functions constructed for other instruments do not attempt to remove instrument artefacts, but are designed to compensate for differences in performance of instruments delivered to customers.

Thermo Fisher Scientific and Ulvac PHI provide transmission curves that are designed to calibrate spectra to ensure for a given lens mode, spectra acquired using different pass energies return corrected peak area that are equivalent. That is, quantification becomes possible based on spectra measured using different pass energies. The method used to compute these transmission curves per lens mode have an added advantage to simply aligning spectra in intensity for different pass energies, namely, if the spectrometer is tuned well and is not limited within the transfer lens column by apertures, and the internal scattering of photoelectrons within the HSA is acceptable, then the transmission curve is a class of transmission functions that includes the absolute transmission function for the spectrometer. Thermo Fisher Scientific spectrometers include instruments capable of measuring spectra at pass energies under the control of the user. This design of spectrometer allows data sets to be obtained that lend themselves to the construction of transmission curves. For this reason, Thermo Fisher Scientific spectra are used to explore the transmission correction of XPS instruments.

Case Study: Thermo Fisher Scientific NEXSA G2 (Edinburgh University)

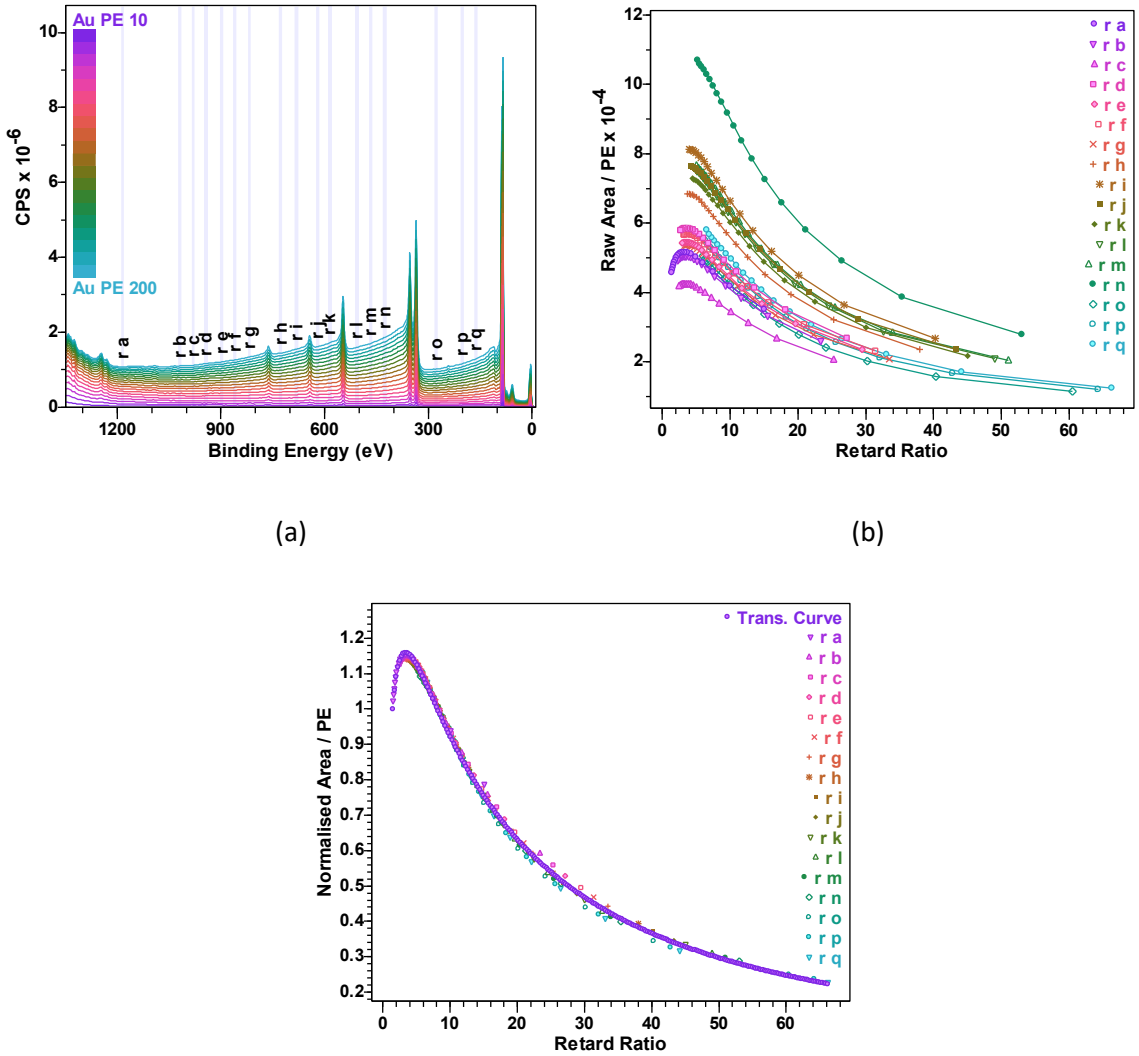

(a) (b)

(c)

Figure 22. a) Survey spectra measured from the NEXSA G2 internal gold standard using pass energy ranging from 10 eV to 200 eV in steps of 10 eV. The regions labelled r a to r q indicate the intervals in energy used to estimate the intensity of the background for a specific kinetic energy providing the data used to compute transmission curves shown in Figure 22b. b) Transmission curves constructed from the spectra in Figure 22a plotted using the estimated intensity as a function of retard ratio before alignments and normalisation is performed. c) Transmission curves shown in Figure 22b following alignment in intensity in preparation for computing the transmission curve for NEXSA G2 Standard lens mode.

The analysis of the transmission for the NEXSA G2 involves a comparison of spectra to spectra collected from an ESCALAB 250Xi. Therefore, it is necessary to explain why the ESCALAB 250Xi spectra are appropriate as a reference standard. If the same procedure that is described below for computing transmission curves for the NEXSA G2 is applied to spectra from the ESCALAB 250Xi, the results for the ESCALAB 250Xi are equivalent to the results obtained by using the NPL transmission correction procedure. Therefore, the assumption made herein is that the transmission corrected

gold spectrum obtained for the ESCALAB 250Xi is a good estimate for an instrument with perfectly flat transmission response to varying kinetic energy. Even if this assumption is false, a comparison between these two instruments provides evidence for the use of relative transmission functions. That is, the results presented in Figure 22 and Figure 23 show that the transmission correction procedure discussed below returns similar transmission corrected spectra between these two instruments, but not exactly the same.

The procedure used to calculate relative transmission curves for the NEXSA G2 makes use of the spectra in Figure 22a. Integration regions, from which an intensity in counts per second (CPS) electron Volts (eV) is computed, are marked on the spectra in Figure 22a. Each region allows an intensity to be identified with a kinetic energy for each spectrum acquired using pass energy for the HSA between 10 eV and 200 eV. A set of transmission curves calculated from the spectra and regions in Figure 22a are plotted in Figure 22b. These transmission curves, in theory, should be identical other than the obvious offset in intensity, which is a consequence of variation in the inelastic background intensity. Therefore, the data set to which a closed-form is fitted is constructed from these data in Figure 22b by normalising these transmission curves in Figure 22b at a specific retard ratio, namely the retard ratio of 8.3. The normalised set of transmission curves and the closed-form fitted to these data are shown in Figure 22c. Once the transmission curve is available, it is possible to construct spectra for which the transmission variation is removed. Figure 23a is a set of survey spectra measured from a standard silver sample using pass energies identical to the gold spectra in Figure 22a. Transmission corrected spectra displayed in Figure 23a all align in terms of background signal, however, due to differences in energy resolution at these pass energies, these spectra differ in terms of photoelectron peak shape. Nevertheless, the corrected area for these peaks should all be equivalent.

An alternative to computing a single transmission curve per lens mode is computing transmission functions for each lens mode and pass energy. The advantage of computing transmission functions for each operating mode is that the closed-form fit to data for each operating mode is performed as independent calculations. Figure 23b is a set of normalised transmission functions calculated by fitting a polynomial of degree nine to the selected intervals in energy extracted from the ratio of NEXSA G2 spectra in Figure 22a and the reference ESCALAB 250Xi gold spectrum. The transmission functions correspond to the normalised curves in Figure 23b, when applied to the spectra in Figure 22a are displayed in Figure 23c. These corrected spectra in Figure 23c are designed to be identical to the reference ESCALAB 250Xi gold spectrum. While ideally, the transmission functions in Figure 23b should be equivalent to the transmission functions calculated from Figure 22c, taking the ratio of gold spectra in Figure 22a corrected for transmission based on Figure 22c and the reference ESCALAB 250Xi gold spectrum results in Figure 23d. Ideally, these ratio spectra in Figure 23d would be flat. However, the ratio spectra all exhibit a positive gradient, thus demonstrating that quantification based on the transmission curve approach will only yield identical atomic concentrations for the identical sample if these differences are accounted for by different RSFs, say. Hence, in the case of the NEXSA G2, the transmission curve approach results in a relative transmission curve, whereas there is evidence (not shown here) to support the hypothesis that the same transmission curve approach applied to ESCALAB 250Xi spectra yields absolute transmission curves.

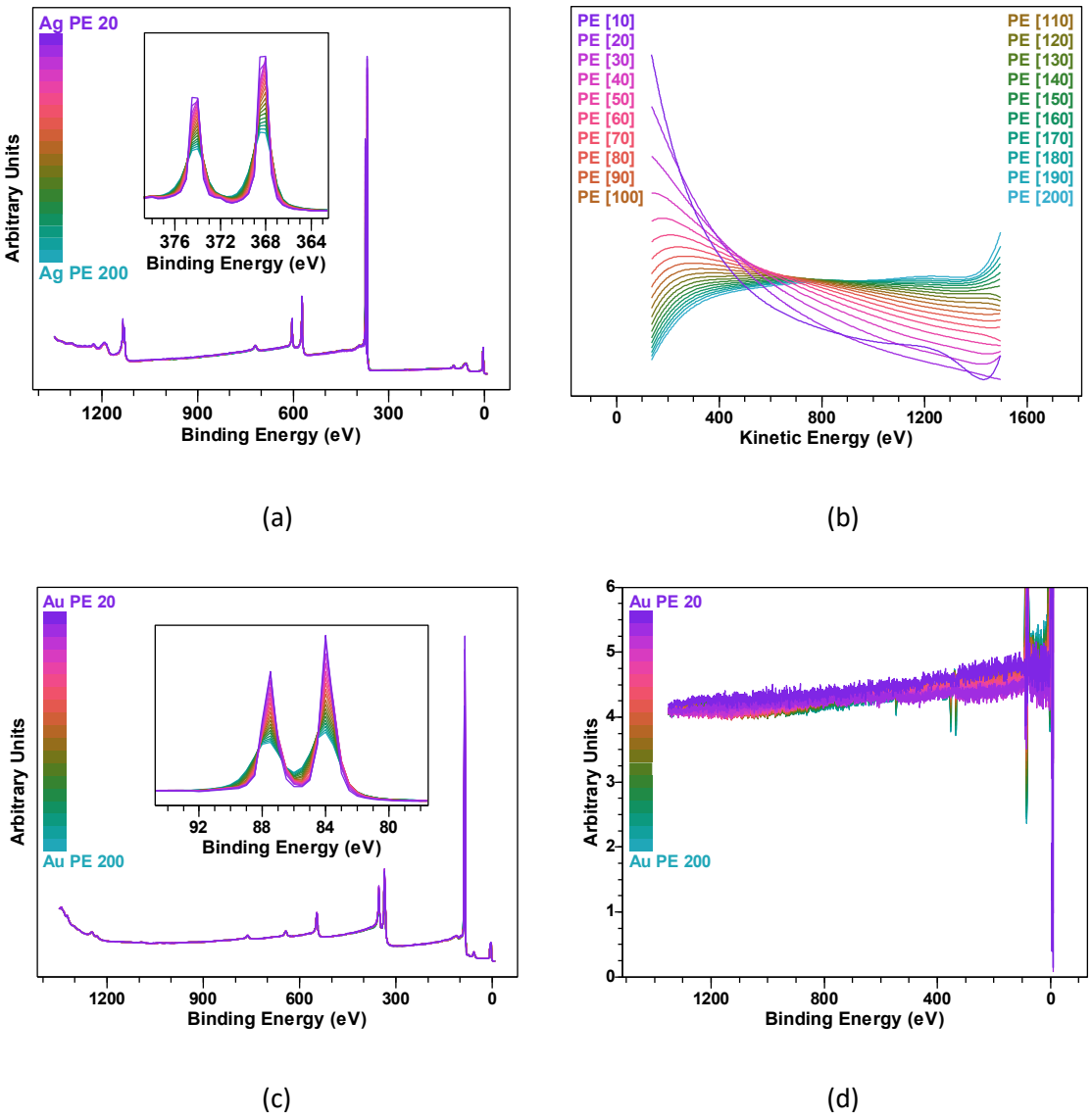

Figure 23. a) An example of survey spectra corrected for transmission using the transmission curve in Figure 22c. Note that the alignment of these spectra is an indication that quantification is precise, but not necessarily accurate. That is, the transmission curve in Figure 22c is a relative transmission curve rather than an absolute transmission curve. b) Normalised transmission functions calculated relative to a reference gold spectrum measured on an ESCALAB 250Xi and corrected for the transmission of the ESCALAB 250Xi. The variation in transmission of the NEXSA G2 relative to the ESCALAB 250Xi required a fit of a polynomial of degree nine to the ratio of NEXSA G2 spectra and the reference spectrum obtain from the ESCALAB 250Xi. c) Application of the transmission functions in Figure 23b to the spectra in Figure 22a. These NEXSA G2 spectra, after correction, all have the same shape as the reference spectrum from the ESCALAB 250Xi, with the exception of the photoemission peaks, which alter in FWHM and maximum intensity depending on pass energy. d) Ratio of NEXSA G2 gold spectra after transmission correction using the transmission curve in Figure 22c to the reference gold spectrum obtained for the ESCALAB 250Xi by correcting the ESCALAB 250Xi gold spectrum for the transmission curve computed identically to the NEXSA G2 transmission curve in Figure 22c.

Escape Depth and Layered Materials

Quantification by XPS assumes homogeneous sample composition. However, there are many examples of materials with variation in composition as a function of depth for which XPS provides useful information. While true atomic concentrations for elements in layered materials are not always possible, changes in relative photoemission peak intensities are an indication of sample structure as well as chemistry. Burying silicon dioxide beneath a thin film layer of a hydrocarbon changes the ratio of Si 2p photoemission with respect to O 1s depending on thickness of the hydrocarbon overlayer (Figure 24).

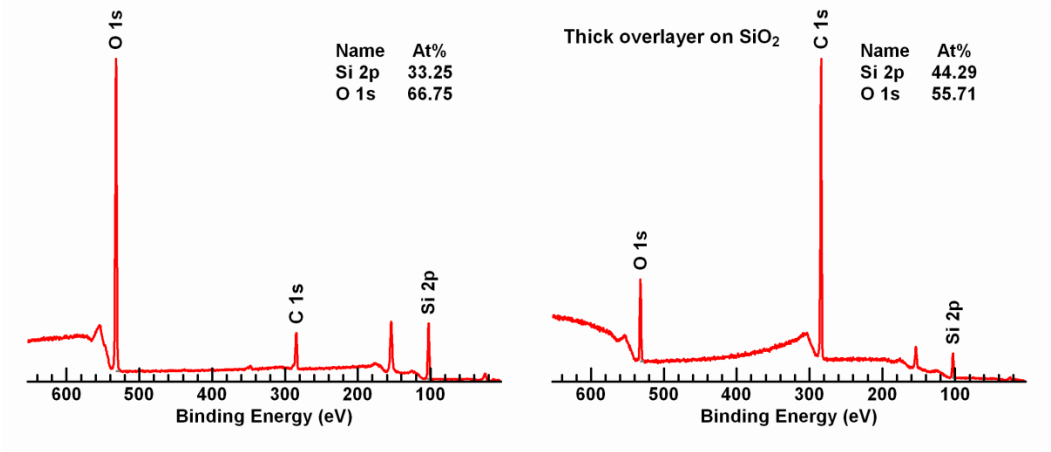

Figure 24. Lefthand spectrum is measured from silicon dioxide. The C 1s peak marked on the silicon dioxide spectrum is adventitious in origin and is unlikely to form a uniform film across the surface of the SiO_2. Consequentially, the relative amount of Si 2p to O 1s is obtained by XPS close to the expected ratio for silicon dioxide. The righthand spectrum originates from a silicon dioxide sample prepared with an overlayer of plasma polymerized hexane (ppHex). The intensity of the C 1s peak is consistent with a thick film coverage of the silicon dioxide substrate. Attempting to measure by XPS without consideration that the silicon dioxide is covered by ppHex results in the proportions of silicon and oxygen from the substrate that are incompatible with the sample true composition.

The reason the percentage of Si to O changes with overlayer thickness is the overlayer attenuates lower kinetic energy photoemission more than photoemission with higher kinetic energy. O 1s signal is emitted with lower kinetic energy than Si 2p signal and therefore the ratio for these two photoemission peaks from a substrate increases in favour of silicon with film thickness.

These changes in photoemission intensity are understood in terms of an exponential decay of signal with respect to depth within a material from which electrons originate. This same exponential decay of signal is the reason XPS is surface sensitive, and has implications for quantification of materials where electrons are emitted from a thin film rather than a bulk material. The relationship between O 1s and Si 2p measured intensities from SiO_2 would reverse for thin films of SiO_2. That is, for films of materials of less than three EAL measured by XPS, assuming these films are uniform for more than three EAL, that is correcting intensities as if the sample is a bulk material results in incorrect quantification.

This point is now illustrated making use of data collected from a layer of Poly (vinyl ethyl ether) PVEE on Poly (styrene) PS. PVEE contains oxygen whereas PS only contains C and H. As a consequence,

oxygen signal originates from a film of PVEE at the surface only. XPS of these polymers results in photoelectrons due to the creation of holes in the K-shell in the electronic configuration of oxygen. A dominant path for these ions to relax to a lower energy level filling the K-shell in the process is via the O KLL Auger process. The number of K-Shell holes created by photoionization and the number of relaxation events leading to O KLL are proportional and these two photoemission events result in the emission of electrons with different kinetic energies. It is therefore possible to examine the consequences for photoemission from thin films by considering the ratio of O 1s to O KLL signal measured from PVEE on PS with different depths of PVEE.

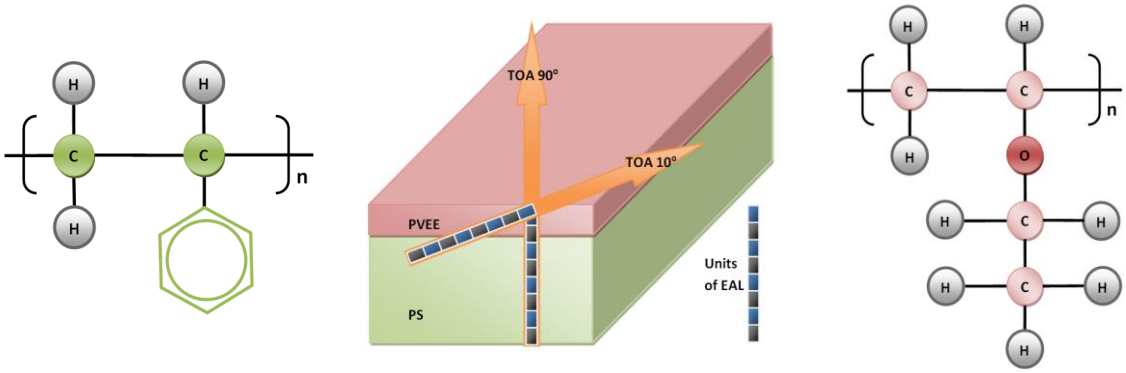

Figure 25. Schematic of a sample prepared with an overlayer of PVEE upon a PS substrate. Tilting the sample to obtain two angles between the sample surface and the direction of the spectrometer transfer lens system (take-off angle (TOA)) alters the proportions of the photoelectrons recorded by the spectrometer from these two polymers.

Two measurements from the same sample using take-off angle (TOA) 90° and 10° change the effective film thickness for PVEE by a factor of 5.76. TOA 90° adjusted assuming a bulk material over compensates for escape depth thus O KLL is reported as a more intense signal compared to O 1s. TOA 10° by contrast, mostly due to sampling a factor of 5.76 more within the PVEE film, behaves as a bulk PVEE material and therefore favours O KLL and O 1s equally.

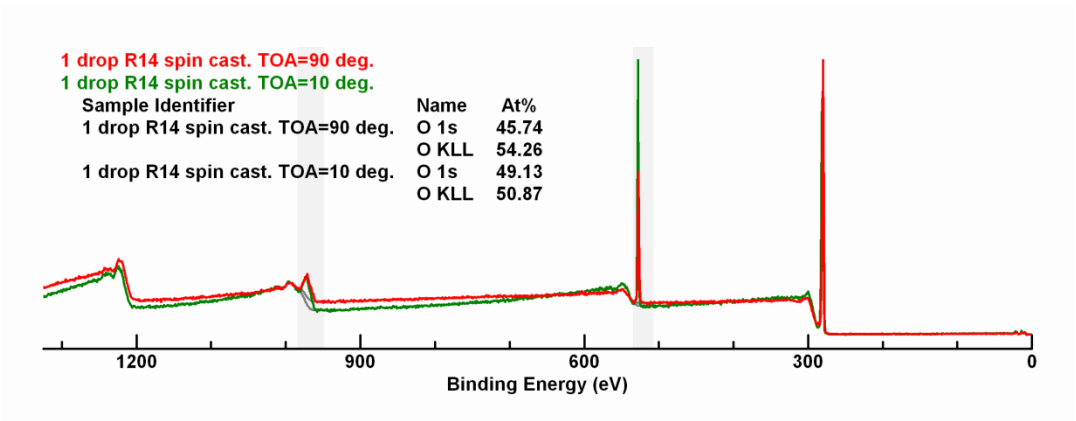

Figure 26. Overlay of survey spectra measured from the sample and TOCs illustrated in Figure 25.

The total sensitivity factor for a photoemission line is the product of four factors. These four factors are corrections for instrument transmission, photoionization cross-section, angular distribution and escape depth. For a bulk material the escape depth correction is performed by use of the following

factor defined in terms of the effective attenuation length $\lambda(E_{Z_{nl}})$ calculated at a kinetic energy $E_{Z_{nl}}$ using the depth of material $d = \infty$.

$$escape\ depth\ correction\ factor = \lambda(E_{Z_{nl}}) \times \left(1 - \exp\left[-\frac{d}{\lambda(E_{Z_{nl}})}\right]\right)$$

If the PVEE film measured at TOA 10° is assumed to be bulk PVEE then $d = 4.4\ nm$ would align quantification obtained for both TOA 10° and TOA 90°.

A film thickness estimate is therefore possible by these means, but does require a sample to match precisely the model proposed of an overlayer of uniform thickness entirely covering a substrate without photoemission from the element in the overlayer used to calculate thickness. Any contamination layer would attenuate O KLL relative to O 1s resulting in significant errors to a film thickness estimate for PVEE by this means.

PVEE Film on PS Substrate: Hill Equation

The problem of estimating a film thickness is illustrated using data from a sample prepared with a film of PVEE on as substrate of PS and making use of a C 1s spectrum only. The C 1s spectrum includes signal deriving from both polymers and therefore a peak model is required that separates these distinct sources for C 1s signal. Identifying PVEE and PS C 1s intensity is performed here by fitting components computed from data and integrating intensity above a Tougaard polymer background using quantification regions computed for each component spectrum (Figure 27).

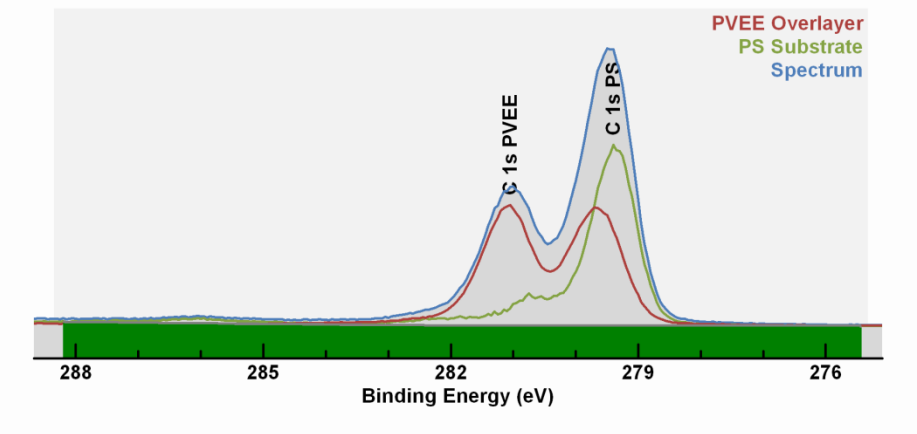

Figure 27. Separation of C 1s signal originating from PVEE and PS is performed by fitting to C 1s spectra two spectral components derived from data. These two component-spectra are illustrated in proportions that when summed fit the as-recorded spectrum for C 1s.

A film thickness estimate assumes the emission depth distribution function is exponential in form:

$$\boldsymbol{N(t) = N_0 e^{-\left(\frac{t}{a}\right)}}$$

The parameter t is the depth beneath the surface from which photoemission originates and the constant a is characteristic of the material from which the zero-loss electrons must emerge. The value used for a is the effective attenuation length (EAL). The intensity of electrons emitted by the

overlayer I_o of thickness $d = t \times cos\theta$ for a measurement performed at an angle θ to the sample normal is proportional to:

$$\frac{1}{a}\int_0^t e^{-\left(\frac{p}{a}\right)}\,dp = 1 - e^{-\left(\frac{t}{a}\right)}$$

Similarly, the intensity I_s from the substrate is proportional to:

$$\frac{1}{a}\int_t^\infty e^{-\left(\frac{p}{a}\right)}\,dp = e^{-\left(\frac{t}{a}\right)}$$

The constant of proportionality in either case is the signal intensity expected for infinitely thick homogenous samples for the overlayer and substrate materials. Thus

$$\frac{\left({I_o}/{I_o^\infty}\right)}{\left({I_s}/{I_s^\infty}\right)} = \frac{1 - e^{-\left(\frac{t}{a}\right)}}{e^{-\left(\frac{t}{a}\right)}} = e^{+(t/a)} - 1$$

On solving for t the equation becomes:

$$\frac{t}{a} = ln\left(1 + \frac{\left({I_o}/{I_o^\infty}\right)}{\left({I_s}/{I_s^\infty}\right)}\right)$$

If the measurement is made at an angle θ to the sample normal, the Hill Equation for an overlayer of thickness d becomes:

Hill Equation:

$$d = a \times \cos\theta \times ln\left(1 + \frac{\left({I_o}/{I_o^\infty}\right)}{\left({I_s}/{I_s^\infty}\right)}\right)$$

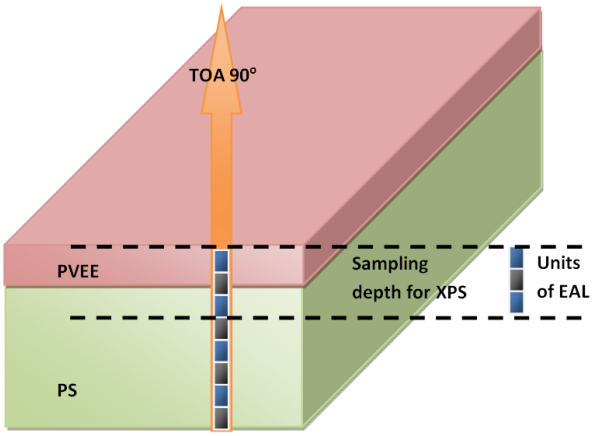

Figure 28. Schematic of sample showing the trajectory for photoelectrons contributing to the spectrum illustrated in Figure 27. The spectrum in Figure 27 is due to photoelectrons emerging from the sample without loss of energy, which is probable for the top three EAL only.

Applying the Hill equation to estimate the thickness for PVEE is obtained by computing the ratio

$$\left(I_{PVEE}/I^{\infty}_{PVEE}\right)/\left(I_{PS}/I^{\infty}_{PS}\right)$$

PVEE and PS both include two carbon atoms in the polymer backbone differing only in the number of carbon atoms attached to these backbones. For PVEE there are two additional carbon atoms while for PS there are six additional carbon atoms in the form of a ring. The density for PVEE and PS are similar therefore the estimate will be computed assuming $I^{\infty}_{PVEE}/I^{\infty}_{PS} = 4/8$ corresponding to the number of carbon atoms for these two polymers. The effective attenuation length for PVEE is computed from the Universal EAL formula defined by Martin Seah which estimates EAL equal to 3.8 nm. The take of angle is 90° (Figure 28) therefore the angle with respect to the sample-normal in the cosine term of the Hill equation is unity. Applying the Hill equation based on these assumptions estimates the thickness for PVEE to be 4.7 nm.

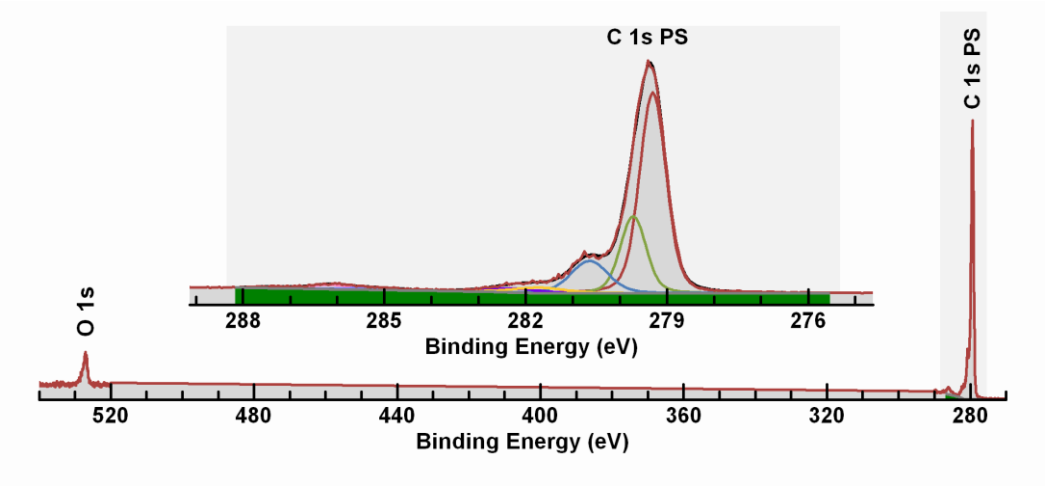

Figure 29. The component-spectra used in Figure 27 are derived from spectra measured from the sample in Figure 28. The component-spectrum for PS differs from the expected spectrum for PS, however, the derivation of the component-spectrum for PS coupled the C 1s photoelectrons with some oxygen as shown. PS does not contain oxygen, therefore the derived component-spectrum is thought to be closer to the sample chemistry than if a standard PS sample were used to obtain the shape for C 1s signal.

A note regarding the spectral shape computed representative of PS is as follows. The component spectrum computed from data (Figure 29) representing PS is not exactly the C 1s spectrum expected for pure PS. Beamson and Briggs XPS of Polymer database includes spectra with characteristics similar to these computed data where OH or OCH_3 is added to the structure of PS (Figure 30).

Figure 30. Possible modifications to PS that might explain the existence of O 1s signal seen in Figure 29.

The film estimate made using these computed spectra assumes these processed data are more representative of sample chemistry than assuming spectral shapes measured from standard materials for PVEE and PS as separate samples. Observing the peak structure for the computed substrate, judging by the binding energy offset from the CH component for additional peaks to PS, these deviations from pure PS are assumed to be predominantly a form with number of carbon atoms also equal to eight. When computing spectral shapes from data the outcomes are not unique and it could also be argued the interface between PVEE and PS is formed by an arrangement with a different number of carbon atoms from eight. These types of assumptions alter the computed film thickness need careful consideration and confirmation by other approaches to measuring film thickness. Results from the Hill equation for other sample preparations are shown in Figure 31.

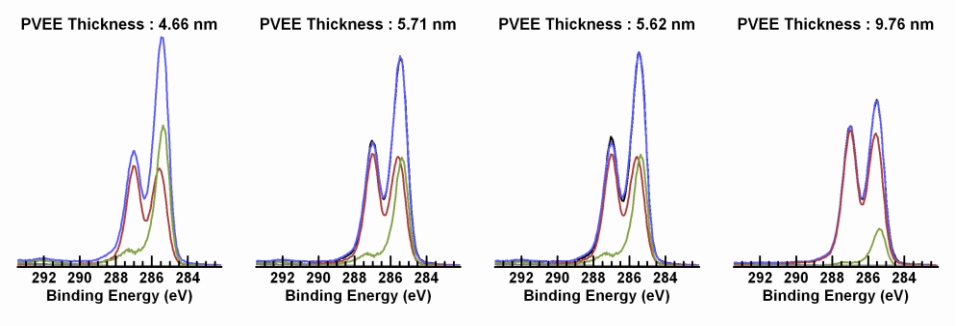

Figure 31. Film thickness estimates for different sample preparations resulting in a PVEE overlayer and PS substrate.

Quantification from Narrow Scan Spectra

A VAMAS file contains VAMAS blocks, where each VAMAS block holds data. When a VAMAS file is opened in CasaXPS (Figure 32), data are read and displayed in an experiment frame which is a window divided into two panes. The lefthand-pane displays data such as spectra or images, while the righthand-pane displays a logical arrangement of VAMAS blocks within the VAMAS file. Before quantification is performed, a VAMAS file when displayed in CasaXPS must appear with a specific format for VAMAS blocks when visualised via the righthand-pane of an experiment frame. The arrangement of VAMAS blocks allows quantification information to be gathered from different spectra all acquired as part of an experimental unit aimed at characterising a sample surface.

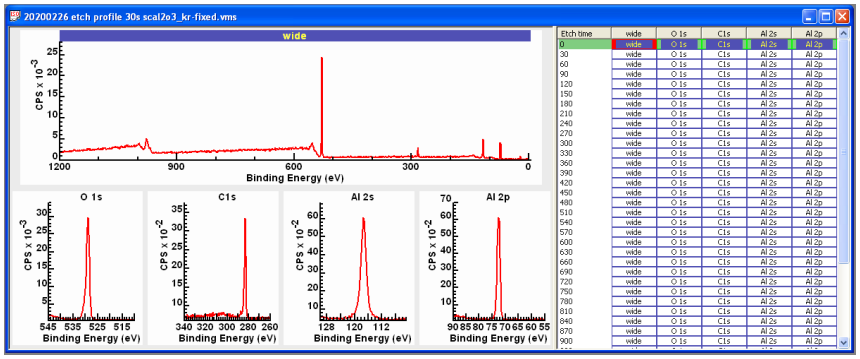

Figure 32. An experiment window of CasaXPS displays data in the lefthand pane while the righthand displays the logical structure of the VAMAS blocks within a VAMAS file. VAMAS blocks are arranged in the righthand pane into rows and columns of selectable items labelled by the VAMAS block identifier string.

When a VAMAS file is loaded into CasaXPS, the righthand-pane arranges VAMAS blocks making use of the experimental variable VAMAS block field to align rows of VAMAS blocks. The experimental variable is a value assigned to spectra acquired from a sample in a given state during the course of an experiment. For example, a sample that is repeatedly etched using an ion beam followed by a sequence of XPS measurements, the state of the sample surface following an etch cycle can be defined by specifying the elapse time for ion beam sputtering. Columns of VAMAS blocks are formed based on a string constructed from two VAMAS block fields, namely, the element string and the transition string which together specify the origin of spectra held within the VAMAS block.

For each VAMAS block within a VAMAS file that is intended for use in computing percentage atomic concentration, quantification items must be defined, meaning regions defining an energy interval and background and/or component peaks fitted to data are available to compute signal intensity for photoemission peaks. VAMAS blocks organised into rows in the righthand-pane link together data acquired at the same time from the same state of the sample surface. Selecting VAMAS blocks in the righthand-pane in the same row specifies a subset of spectra that are appropriate for computing percentage atomic concentration for a specific measurement.

The example of a VAMAS file used here contains a sequence of XPS measurements interleaved by sputter cycles designed to remove adventitious carbon. Each XPS measurement includes a survey spectrum and four narrow scan spectra. The narrow scan spectra include data collected over energy intervals corresponding to O 1s, C 1s, Al 2s and Al 2p. Two of these narrow scan spectra are acquired using energy intervals recording signal from Al atoms. When quantification in terms of elemental composition is performed only one of these Al spectra per row should be selected together with O 1s and C 1s spectra.

Survey spectra also include photoemission signal measured from O1s, C 1s, Al 2s and Al 2p. However, these photoemission peaks are measured as part of survey spectra using different acquisition conditions from the equivalent energy intervals measured using narrow scan spectra saved as separate VAMAS blocks. Therefore, these survey spectra should not be used as part of an atomic concentration calculation involving narrow scan spectra of different energy resolution. While it is possible mixed-operating mode data can be used to quantify a sample, an instrument used in this way would need careful characterisation to ensure the same analysis area and angular acceptance at the sample are measured for all operating modes used to collect spectra assumed to be equivalent.

In this example, quantification regions will be used to define photoemission for each narrow scan spectrum. Peak models defined in terms of components representing chemical state signal could equally well be used to measure photoemission intensity, but for simplicity in terms of discussing quantification of narrow scan spectra, regions alone will be used in this discussion.

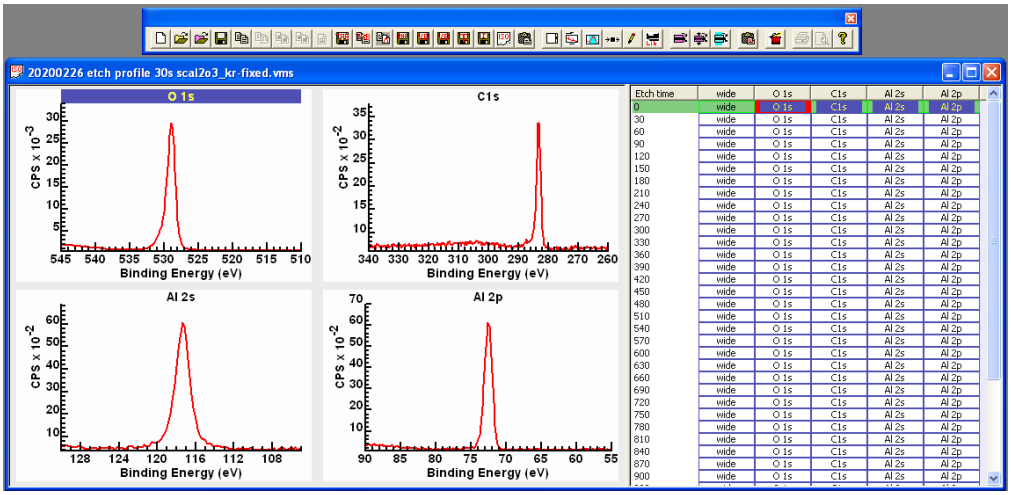

Figure 33. CasaXPS toolbars are used to display in the lefthand-pane VAMAS blocks selected in the righthand-pane. Toolbar buttons are also used to process spectra and, provided the VAMAS block fields for the element and transition are assigned correctly, to create quantification regions on narrow scan spectra populated with RSFs from the element library. The VAMAS file displayed is in a state where four VAMAS blocks in the righthand-pane are selected and displayed in the lefthand-pane. The selected VAMAS blocks will be the VAMAS blocks affected by pressing a toolbar button.

Regions can be added to spectra for which the correct element/transition fields are used within the VAMAS blocks representing narrow scan data (Figure 33). Each of these four narrow scan data are correctly assigned therefore selecting VAMAS blocks before pressing the toolbar button indicated in Figure 34 creates regions for each spectrum so indicated. The element/transition VAMAS block fields allow the creation mechanism to extract appropriate RSFs from the current element library.

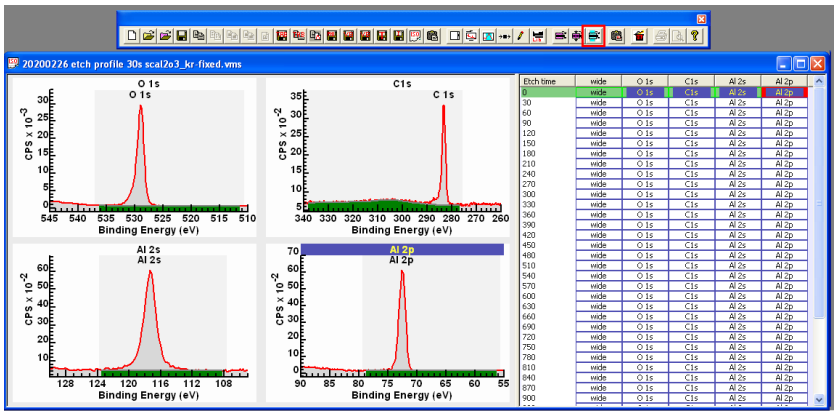

Figure 34. Given the selection of VAMAS blocks and the state of the VAMAS file shown in Figure 33, pressing the toolbar button indicated by the red box results in the creation of quantification regions for each of the four selected VAMAS blocks. Only the selected VAMAS blocks (provided the corresponding string to the element/transition strings appears in the element library) will have newly created regions with RSFs extracted from the element library.

The same toolbar button would not work for survey data. Survey data, by definition, is not specific to an element or transition therefore it is not possible to use element/transition VAMAS block field information to link RSFs from the element library with newly created regions via the toolbar button.

Options on the Element Library dialog window are used to manage the creation of regions on survey data.

The background type used to create these regions is the last-used background type. In this example a Tougaard background was the default background type specified in the ParameterFile.txt configuration file found in the directory CasaXPS.DEF. The specific Tougaard background makes use of cross-section parameters defined by Tougaard for polymer data. Since these data selected include adventitious carbon, there is at least some consistency in adopting a hydrocarbon type background approximation for these photoemission peaks. The Tougaard background is also used for the Al and O photoemission peaks on the basis adventitious carbon is an overlayer and so O and Al photoemission are attenuated by the hydrocarbon, coupled with assuming Al_2O_3 has a sizeable band gap.

These regions defined for the first row of VAMAS blocks need further adjustments to the energy interval limits, after which these can be propagated via Browser Operations to VAMAS blocks with identical element/transition fields.

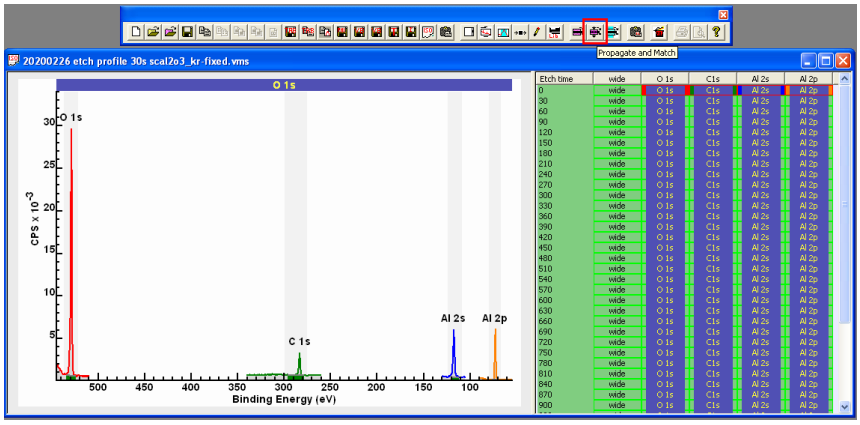

Figure 35. The state of the display in the lefthand-pane coupled with the selection of VAMAS blocks in the righthand-pane is established in preparation for using the indicated (red box) toolbar button.

The four VAMAS blocks with regions are overlaid in the active tile (Figure 35). A selection of VAMAS blocks in the righthand pane provides the target VAMAS blocks for the Propagate and Match toolbar button indicated in Figure 35.

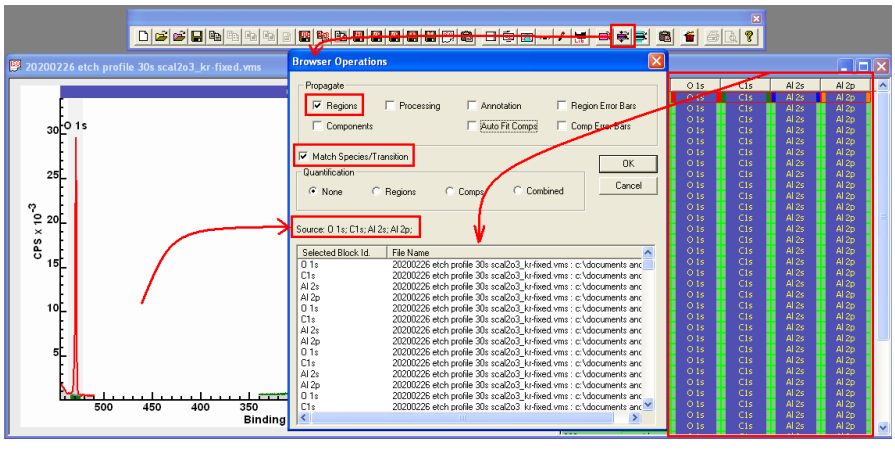

Figure 36. Given the display state of the active display-tile in Figure 35 and the corresponding selection of VAMAS blocks in the righthand-pane, pressing the indicated toolbar button invokes the Browser Operations dialog window in the state indicated by the red rectangles as marked.

Following propagation each narrow scan VAMAS block includes a region appropriately defined (Figure 37) to allow the computation of atomic concentration for oxygen, carbon and aluminium.

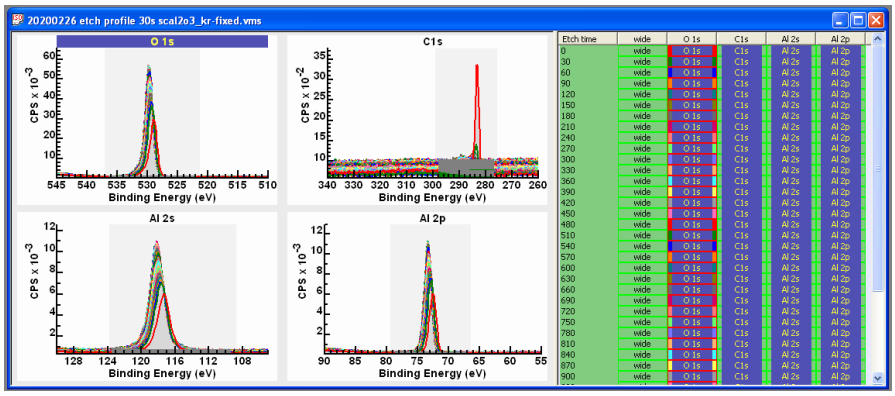

Figure 37. CasaXPS experiment window where each column of selected VAMAS blocks is displayed overlaid in four display tiles, one display tile for each column of selected VAMAS blocks.

A text report generated from these regions is defined in terms of the region names fields, peak areas calculated from integrated signal after background subtraction from raw data and adjustments to integrated peak areas to allow amount of substance to be computed. These corrections involve relative sensitivity for different photoemission using RSFs, instrumental response via transmission functions included in VAMAS blocks and escape depth correction to account for sampling depth variation with energy. The instrument in question is designed using the magic angle for angular distribution correction.

The Standard Report option Regions makes use of a configuration file to create a report from regions defined on selected VAMAS blocks (Figure 38).

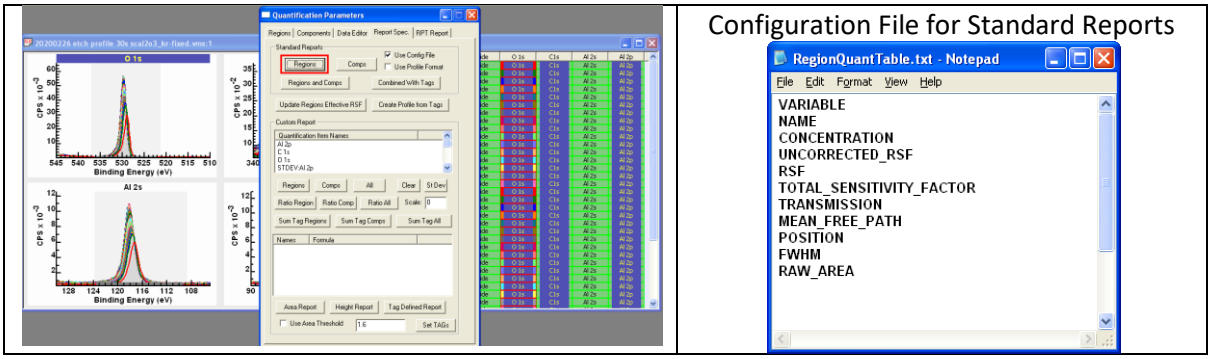

Figure 38. The Report Spec property page of the Quantification Parameters dialog window allows the creation of configurable report tables via the buttons within the Standard Report section. Each row of the report is specified using keywords listed in a configuration file. When the Regions button indicated by the red box is pressed, a report is constructed from regions defined on the selected VAMAS blocks.

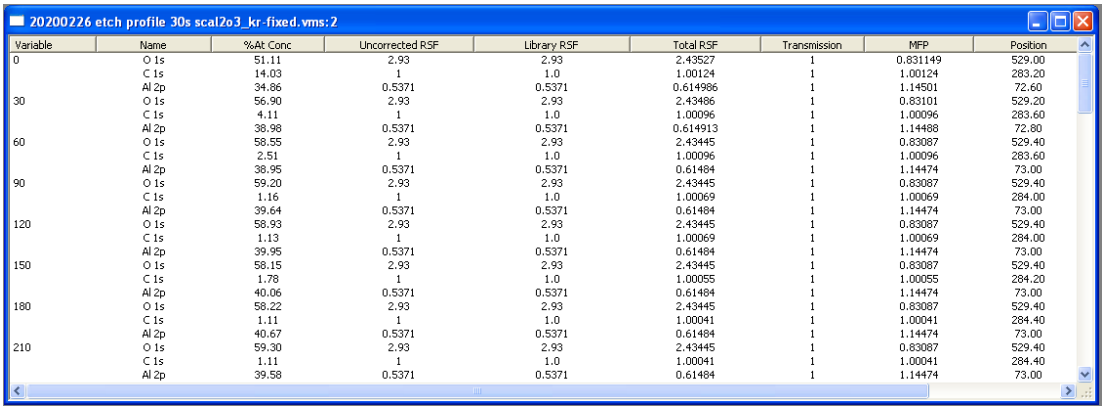

20200226 etch profile 30s scal2o3_kr-fixed.vms:2

Variable	Name	%At Conc	Uncorrected RSF	Library RSF	Total RSF	Transmission	MFP	Position
0	O 1s	51.11	2.93	2.93	2.43527	1	0.831149	529.00
	C 1s	14.03	1	1.0	1.00124	1	1.00124	283.20
	Al 2p	34.86	0.5371	0.5371	0.614986	1	1.14501	72.60
30	O 1s	56.90	2.93	2.93	2.43486	1	0.83101	529.20
	C 1s	4.11	1	1.0	1.00096	1	1.00096	283.60
	Al 2p	38.98	0.5371	0.5371	0.614913	1	1.14488	72.80
60	O 1s	58.55	2.93	2.93	2.43445	1	0.83087	529.40
	C 1s	2.51	1	1.0	1.00096	1	1.00096	283.60
	Al 2p	38.95	0.5371	0.5371	0.61484	1	1.14474	73.00
90	O 1s	59.20	2.93	2.93	2.43445	1	0.83087	529.40
	C 1s	1.16	1	1.0	1.00069	1	1.00069	284.00
	Al 2p	39.64	0.5371	0.5371	0.61484	1	1.14474	73.00
120	O 1s	58.93	2.93	2.93	2.43445	1	0.83087	529.40
	C 1s	1.13	1	1.0	1.00069	1	1.00069	284.00
	Al 2p	39.95	0.5371	0.5371	0.61484	1	1.14474	73.00
150	O 1s	58.15	2.93	2.93	2.43445	1	0.83087	529.40
	C 1s	1.78	1	1.0	1.00055	1	1.00055	284.20
	Al 2p	40.06	0.5371	0.5371	0.61484	1	1.14474	73.00
180	O 1s	58.22	2.93	2.93	2.43445	1	0.83087	529.40
	C 1s	1.11	1	1.0	1.00041	1	1.00041	284.40
	Al 2p	40.67	0.5371	0.5371	0.61484	1	1.14474	73.00
210	O 1s	59.30	2.93	2.93	2.43445	1	0.83087	529.40
	C 1s	1.11	1	1.0	1.00041	1	1.00041	284.40
	Al 2p	39.58	0.5371	0.5371	0.61484	1	1.14474	73.00

Figure 39. For each row of VAMAS blocks selected in Figure 38, the information defined by the configuration file shown in Figure 38 is gather from the quantification regions prepared as shown in Figure 37. A window in CasaXPS is created and a summary of the quantification is displayed.

After a text report is created (Figure 39), the Copy toolbar button is used to place text reports onto the clipboard so that results can be pasted via Ctrl + V into a spreadsheet or other programs (Figure 40). While a summary of the report is shown in CasaXPS, the clipboard is populated by the information shown in CasaXPS using a variety of table formats. Pressing the Copy All button shown in Figure 40 will place all the different formatted tables on the clipboard and therefore made available to a spreadsheet program (Figure 41).

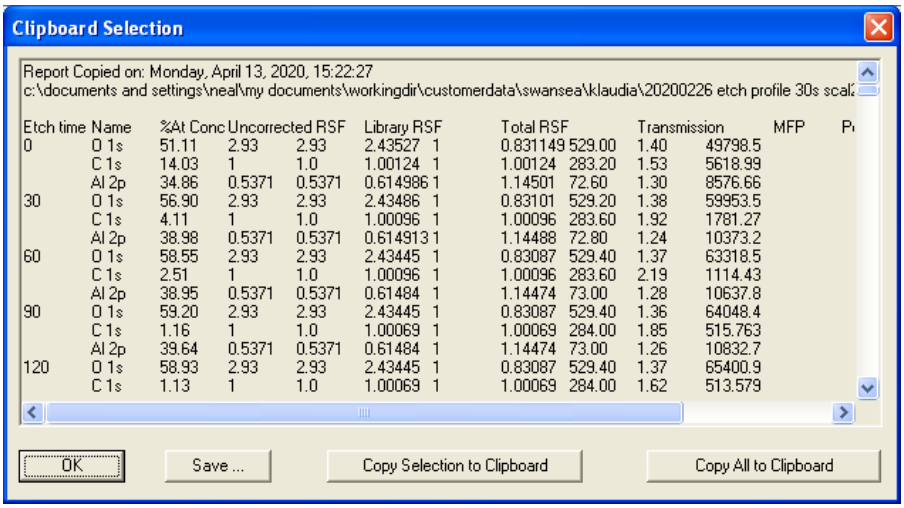

Figure 40. Clipboard selection dialog window that appears once the Copy toolbar button (Ctrl + C) is invoked. The report seen in CasaXPS is one of many formats listed on this dialog window as TAB spaced tables. The full range of tables is best viewed within a spreadsheet program.

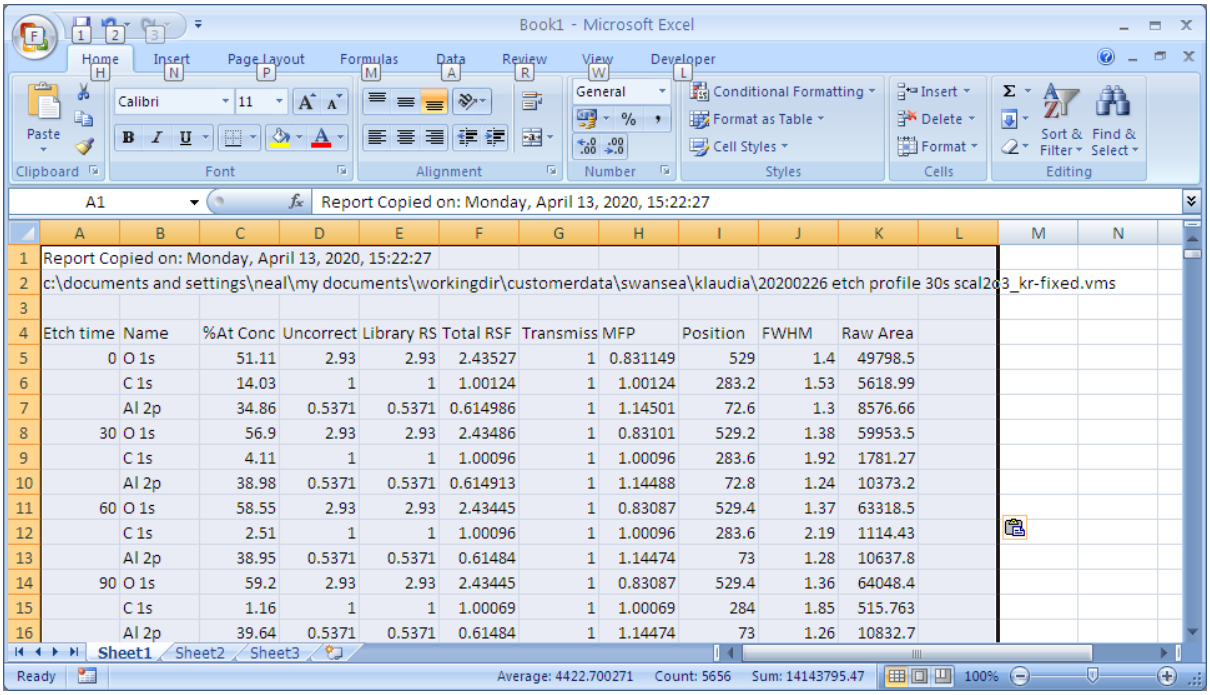

Figure 41. The state of Microsoft Excel following Ctrl + V places the full set of table formats placed on the clipboard by the dialog window shown in Figure 40.

Data Analysis by Example

The first step in understanding samples of scientific interest is to develop strategies for the measurement and analysis of these samples using samples with known composition similar in character to the samples of interest. The objective when measuring samples of lesser interest but of known substance is to evaluate different measurement protocols and data treatment options that will be of use when considering samples of greater scientific interest.

The data set considered here (Figure 42) is part of a preliminary study considering chemistry related to aluminium oxide. A sequence of measurements was performed using a sample prepared as Al_2O_3. Each measurement consists of a survey spectrum (meaning data are acquired over an energy interval equivalent to photoemission peaks accessible by mono Al Kα X-ray source) and a set of spectra measured over narrow energy intervals focused on photoelectron peaks of significance to Al_2O_3. The function of a survey spectrum is to monitor photoemission not included in narrow scan spectra and just as importantly provides information about trends in background signal. Shapes within the background can indicate changes in in-depth distribution of material and in this case supports the assumption the material remains, despite repeated sputtering with an ion beam, essentially homogeneous in depth. Narrow scan spectra form the basis for chemical state analysis and are collected using smaller energy steps and increased dwell-time compared to the survey measurement to improve quality of curve shapes in data and signal-to-noise.

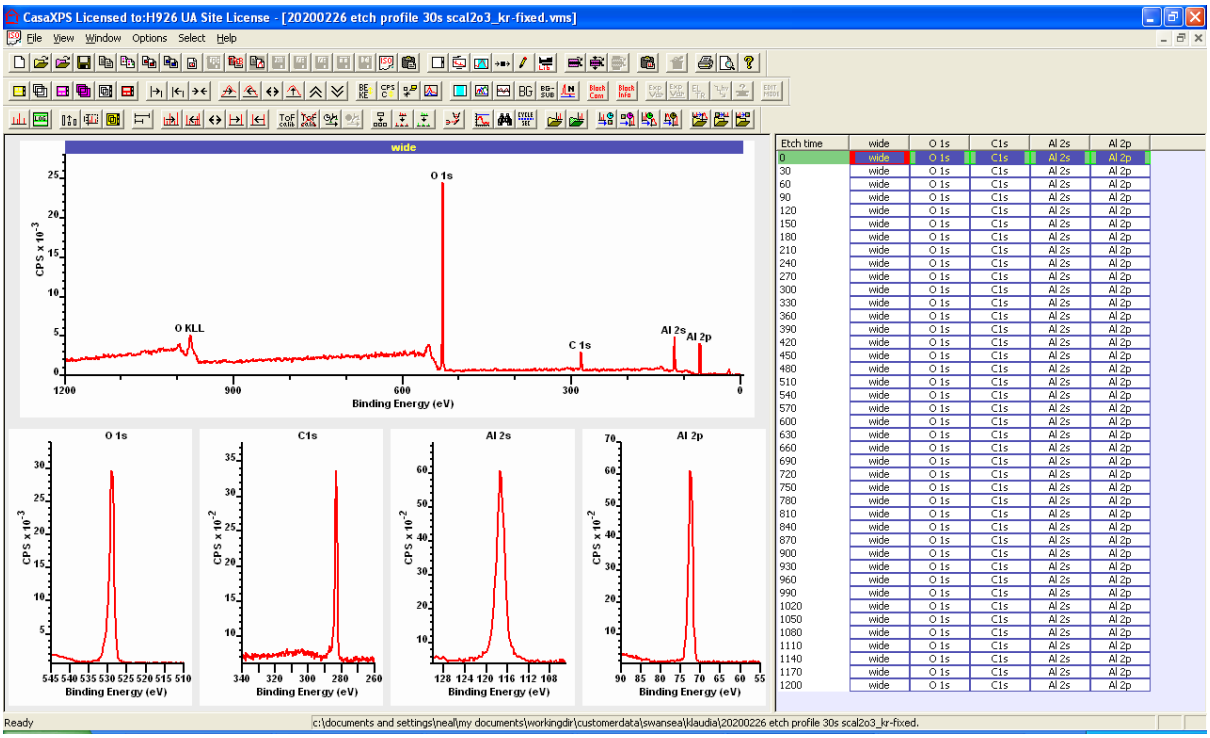

Figure 42. CasaXPS experiment window illustrating the first row of spectra in a sputter depth-profile experiment. The main photoelectron and Auger peaks within the survey spectrum are annotated using the Peak Label property page on the Annotation dialog window of CasaXPS. The format for the page of display tiles is specified using the Page Tile Format dialog window. Each of the five display tiles may be independently designed using the Tile Display Parameters dialog window. These dialog windows are available from the Options menu on the top menu bar of the CasaXPS main window.

The data set measured from the same location on the same sample of Al_2O_3 is acquired by measuring spectra followed by sputtering the sample with relatively low energy argon ions. The purpose of sputtering the surface with an ion beam is to gently remove contamination from the Al_2O_3 surface. Evidence of ion beam sputtering includes changes to C 1s narrow scan spectra (Figure 43). Also, charge state alters with ion beam etch time which further indicates changes have occurred to the surface measured by XPS as a consequence of sputtering with the ion gun. These changes in charge state with etch time requires the use of charge correction to align spectra throughout the data file.

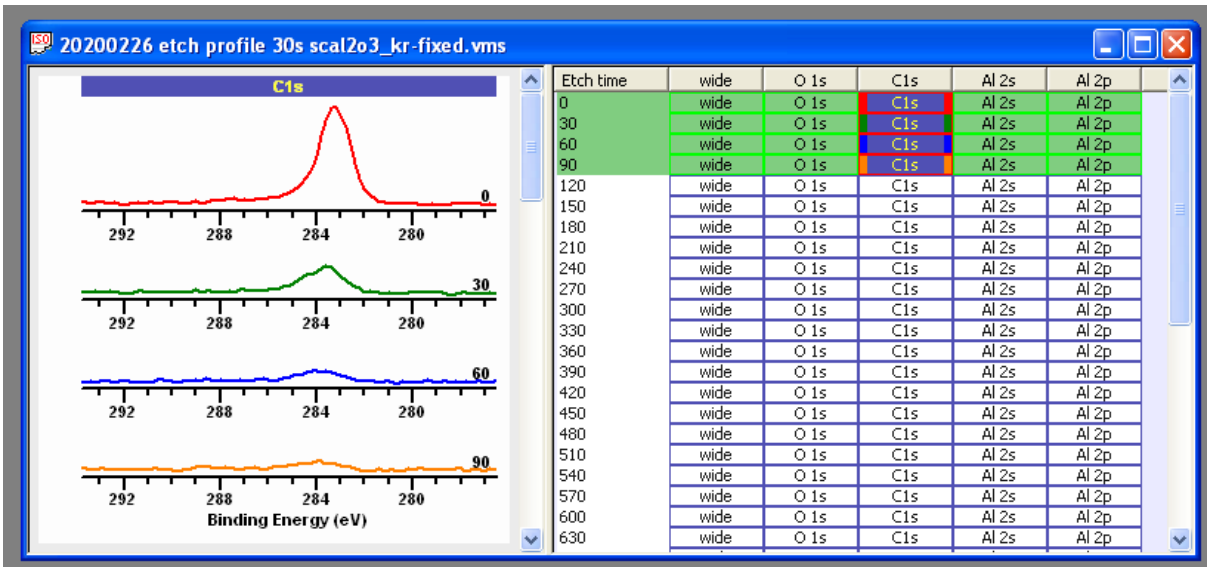

Figure 43. The display tile visible in the scrolled list of display tiles is displaying C 1s narrow scan spectra overlaid. The colours used to plot each spectrum is used to mark the VAMAS blocks in the righthand-pane to indicate the source for the spectra that appear overlaid in the lefthand-pane. Each row of the VAMAS blocks corresponds to the etch time the sample has been exposed to an ion beam. The spectra, as displayed, are stacked with an offset that is adjusted using the Y Axis property page of the Tile Display Parameter dialog window. The etch time is added to the display using an option also on the Y Axis property page. The use of energy axes displayed for each spectrum when overlaying stack spectra is controlled by options on the X Axis property page of the Tile Display Parameter dialog window.

Charge Correction

Data recorded from an insulating material such as Al_2O_3 requires the use of charge compensation, the mechanism by which a steady state charge distribution is established by returning electrons to the sample to compensate for the emission of electrons from the sample due to irradiation by X-rays. For an experiment involving sputtering with an ion beam or even simply small changes in analysis conditions and/or sample chemistry with exposure to X-rays may result in changes to the steady state charge on the sample for each XPS measurement. As a consequence, each measurement in the Al_2O_3 data set represents a different charge compensation state and requires calibration in terms of binding energy scale to align signal with respect to energy.

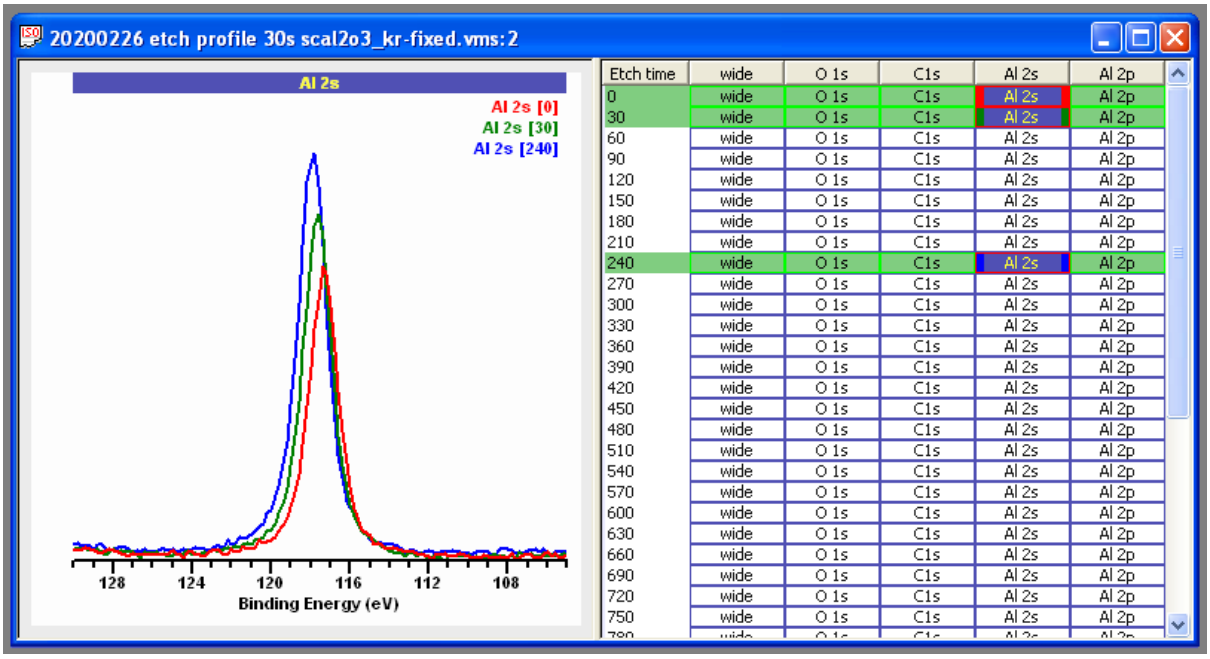

Figure 44. An experiment window displaying three Al 2s narrow scan spectra overlaid in the lefthand-pane. The as-recorded spectra do not appear with peaks aligned in binding energy. The assumption used herein is that these Al 2s peaks are shifted in apparent binding energy due to differing potential of the sample with respect to ground for different cycles in the sputter profile. The spectra used in this illustration are indicated by the key (lefthand-pane display tile) and the coloured VAMAS blocks in the righthand-pane. A legend or key is added to the display of spectra using options on the Display property page of the Tile Display Parameters dialog window.

Binding energy is calibrated by applying a shift in energy to each spectrum considered to be acquired under identical charge compensation conditions. An appropriate shift is calculated using a peak of known binding energy and shifting the measured spectra to position the peak maximum at the known energy. The common practice of calibrating spectra using C 1s as the reference peak has in recent times been called into question. Traditionally spectra are aligned to place the lowest binding energy C 1s component peak, established by fitting a model to adventitious C 1s data, at a binding energy of 285 eV. Such an approach has merit in providing improved precision for aligning photoemission peaks with binding energy but lacks accuracy due to carbon potentially being part of the sample chemistry and the assumption that adventitious carbon is a uniform layer over the sample surface. The latter point is relevant for samples with islands of contamination, in which case charge compensation state for such islands may not be the same as for fully exposed substrate. Charge compensation in the case of sputtered Al_2O_3 is a particular problem for binding energy calibration based on adventitious carbon since the cleaning action of the ion beam is intended to remove adventitious carbon. For this reason charge correction for each row in the Al_2O_3 data set will be calibrated using the Al 2s to align spectra in binding energy rather than making use of C 1s (Figure 44).

Al 2s is a broad peak with Lorentzian character. Both these characteristics can be exploited to provide a precise systematic tool for identifying the maximum intensity for photoemission from Al 2s. While aluminium chemistry is the reason for making these XPS measurements, the chemical differences within these spectra result in relatively minor changes to Al 2s and Al 2p compared to

changes in C 1s and O 1s spectra. Hence the use of Al 2s to calibrate binding energy for each measurement is seen as preferable to the use of C 1s data for charge correction. The approach adopted here is to use a synthetic component representative of Al 2s fitted to the Al 2s spectrum in each row of VAMAS blocks within the VAMAS file and shift each row of VAMAS blocks representing spectra acquired under identical charge compensation conditions by aligning these Al 2s synthetic components throughout the sputter sequence.

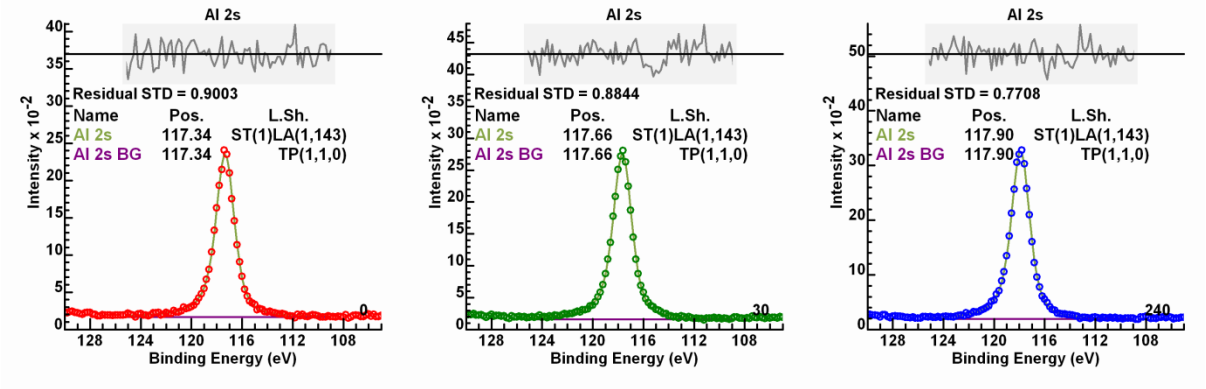

Figure 45. Application of the peak model making use of the asymmetric line shape ST(1) LA(1,143) to model the Al 2s photoelectron peak and TP(1,1,0) to model inelastic background signal beneath the Al 2s peak. The residual plot showing the variation between the peak model fitted to each spectrum and the spectrum is enabled for display using options on the Display property page of the Tile Display Parameters dialog window. Plotting data using symbols is similarly enabled and disabled on the Display property page. Options used to colour spectral data and the shape of symbols used to mark spectral intensities are adjusted using the Colours property page on the Tile Display Parameters dialog window. The tables constructed from components to the peak model in use is added to the display using the Components property page on the Annotation dialog window.

These Al 2s peaks include extended tails that can be modelled using the line shape LA(1,143) modified by asymmetry using the prefix ST(1) to the LA line shape. The objective is to fit each Al 2s spectrum with a precision consistent with a residual standard deviation of close to 0.9 (Figure 45 and Figure 46). A value for the residual standard deviation of 0.9 is expected for pulse counted data combined from multiple detector streams to form data fitted by the line shape ST(1)LA(1,143). The Test Peak Model option on the Quantification Parameters, Components property page (Figure 47) is used to obtain the line shape selected for use with the Al 2s spectra. The model fitted to these Al 2s data includes the use of TP(1,1,0) line shape representing a trapezium (TP) of equal height to both sides, that is, in this case a rectangle. The TP(1,1,0) provides a constant offset to the ST(1)LA(1,143) bell-shaped curve with Lorentzian character that is determined as part of the optimisation steps for each spectrum. Owing to a significant band gap for Al_2O_3 the background trend can be modelled using a constant background set to zero. Thus TP(1,1,0) is the means by which background signal is accounted for when fitting Al 2s photoemission.

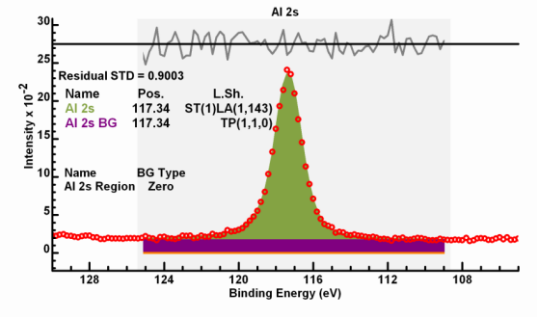

Figure 46. The different aspects of the peak model used to fit spectra in Figure 45 are illustrated using annotation tables created via the Regions and Components property pages of the Annotation dialog window. Annotation tables are repositioned on the display by adjusting the position of marker boxes that appear on the display of spectra whenever the Annotation History property page is topmost of the property pages on the Annotation dialog window. These tables are constructed from information gathered from quantification regions and components to peak models that are defined using the Quantification Parameters dialog window. Regions defined on a VAMAS block and similarly components to a peak model are edited on the corresponding property pages of the Quantification Parameters dialog window (Figure 47).

Charge correction for a data set arranged so that each measurement cycle is organised as a row of VAMAS blocks is performed by creating a peak model for a specific column of VAMAS blocks corresponding to particular spectra. In the current example the spectra used for calibrating the data file are the Al 2s spectra. The peak model for Al 2s is arranged such that the component defined in Column A in the list of components on the Component property page corresponds to the energy entered on the Spectrum Processing, Calibration property page in the text-field labelled True.

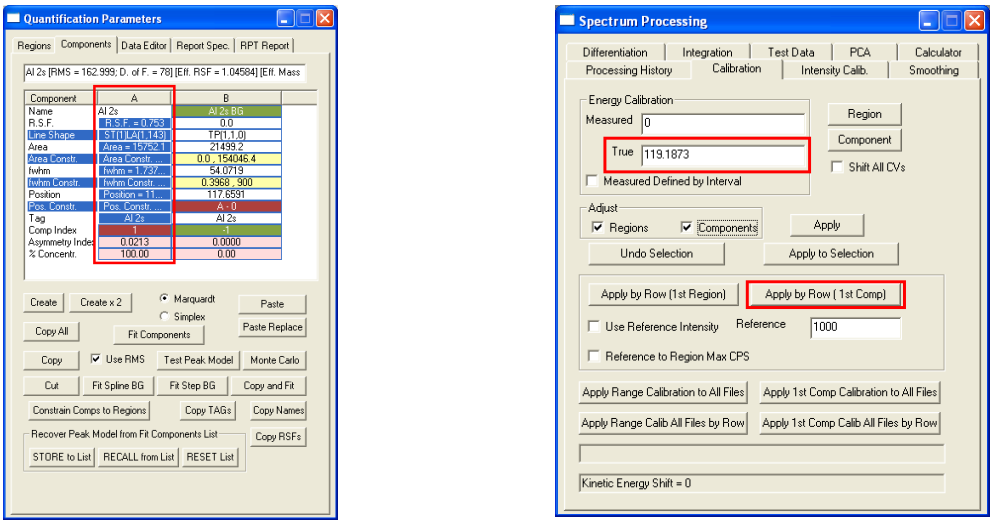

Figure 47. Dialog windows invoked from the Options menu on the CasaXPS main window used to specify quantification regions and components (Quantification Parameters dialog window, lefthand dialog) and the Spectrum Processing dialog window (righthand dialog). Property pages are selected using the tabs at the top of each dialog window. These two dialog windows are prepared in anticipation for charge correcting the spectra in Figure 48. The red boxes highlight the information used by the **Apply by Row (1st Comp)** button on the Calibration property page of the Spectrum Processing dialog window to calibrate the energy scale for the spectra in Figure 48.

Calibration of all VAMAS blocks in the VAMAS file is performed by selecting the column of VAMAS blocks for which the peak model is defined and only that column of VAMAS blocks (Figure 48), then pressing the button on the Spectrum Processing, Calibration property page labelled **Apply by Row (1st Comp) (Figure 47)**. The action of the **Apply by Row (1st Comp)** button causes an offset to be calculated using the Al 2s peak model and the value entered in the True text-field of the Calibration property page. The offset so computed is designed to align the component in Column A of the Components property page so that the energy for components in Column A matches the value in the True text-field in each row of VAMAS blocks. For each row of VAMAS blocks the offset calculated using the Al 2s spectrum is applied to these spectra in the same row of VAMAS blocks.

Before calibration is performed, an overlay of each column of VAMAS blocks in separate display tiles, one for each column of spectra with the same element/transition labels clearly demonstrates offset peaks for O 1s, C 1s, Al 2s and Al 2p (Figure 48).

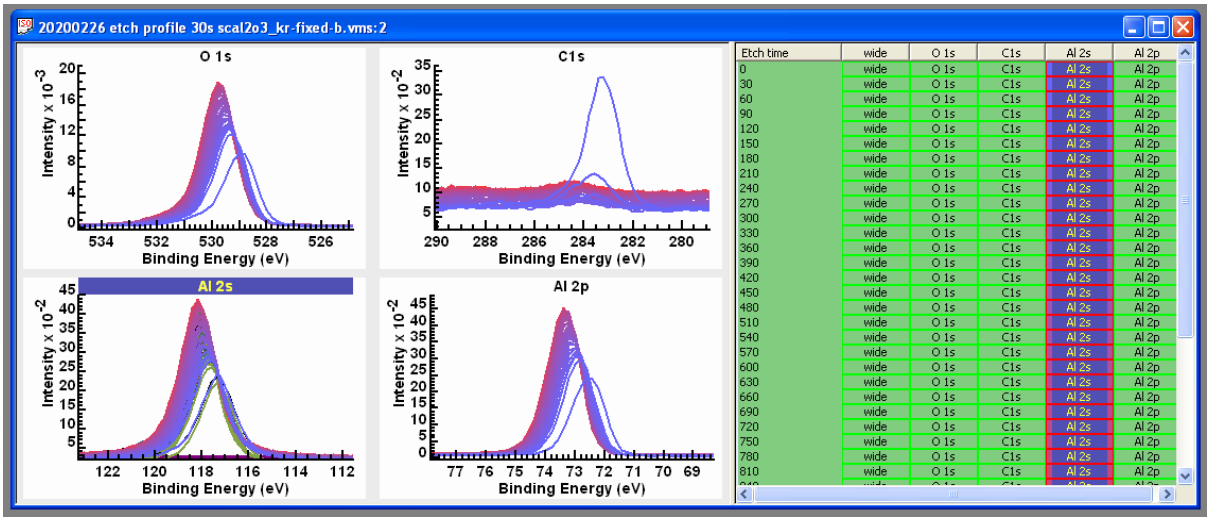

Figure 48. CasaXPS experiment window illustrating the selection of Al 2s spectra, all of which are prepared with the peak model shown in Figure 46 in preparation for charge correction. The selection of Al 2s VAMAS blocks indicates the source for the peak model for each row that will be used to compute the apparent binding energy for the Al 2s component. The desired binding energy for Al 2s photoelectrons is specified on the Calibration property page of the Spectrum Processing dialog window via the True text-field illustrated in Figure 47. The result of preparing the selection of Al 2s spectra, the peak model fitted to these selected Al 2s spectra and applying the options indicated on the Calibration property page in Figure 47 is shown in Figure 49.

After calibration has been performed, these same display tiles illustrate the action of the **Apply by Row (1st Comp)** button (Figure 49). Each set of overlaid spectra are aligned and any misalignment in spectra other than Al 2s is assumed to be chemical shifts of significance to sample chemistry.

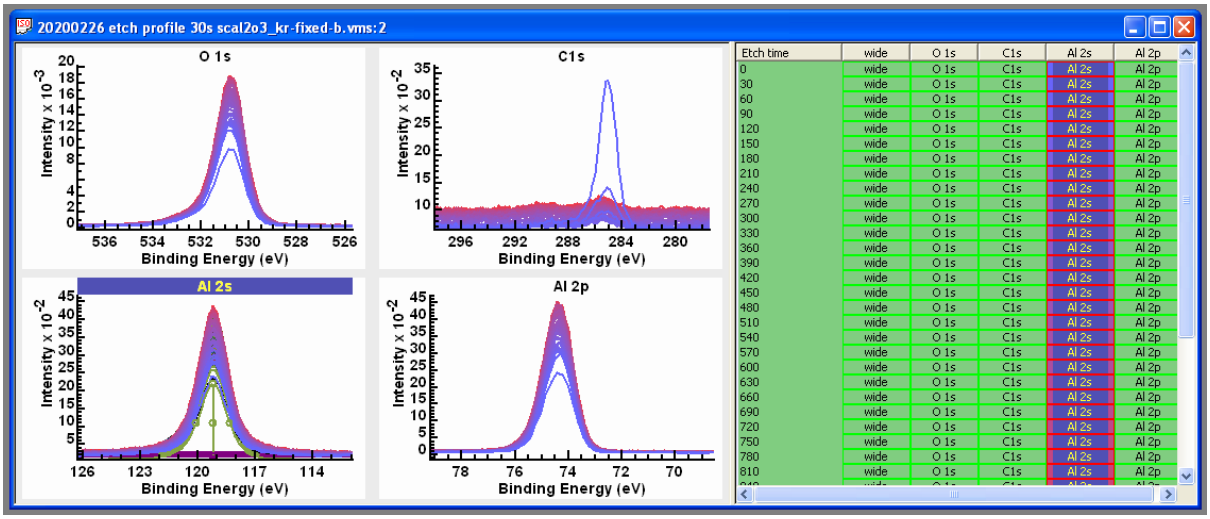

Figure 49. The energy calibrated spectra are displayed in the lefthand-pane, demonstrating the results obtained by the processing steps discussed in Figure 48 caption.

Motivation for Charge Correction

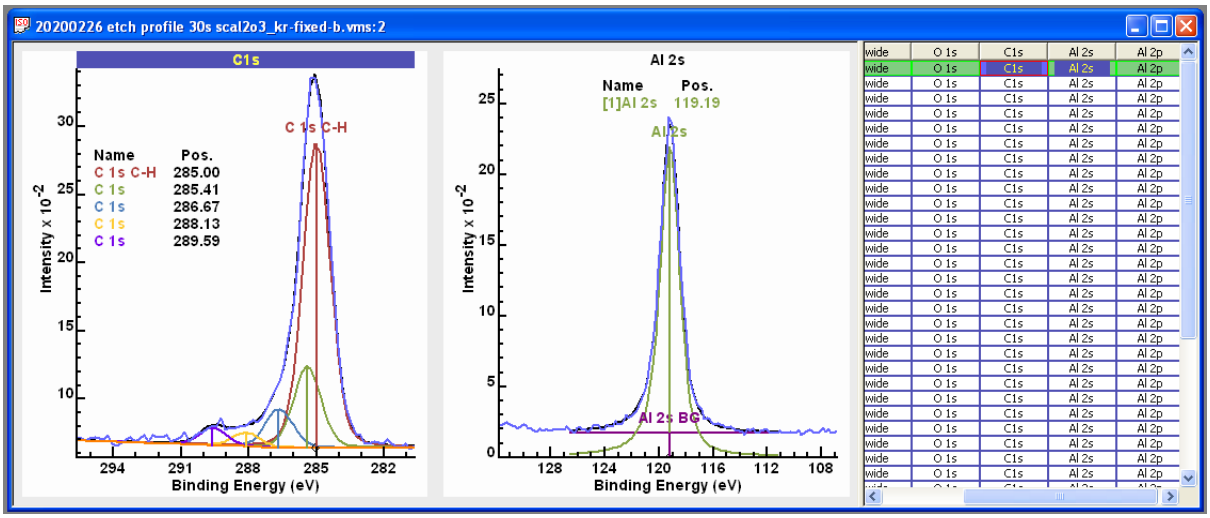

Figure 50. The calibration of the energy scale performed using the input parameters defined on the dialog windows shown in Figure 47 assumes that the initial measurement of spectra (before the surface is sputtered with an ion gun) yields C 1s spectra for which the C-H peak can be identified and appears at binding energy 285 eV. The binding energy for Al 2s used to calibrate the entire set of spectra is chosen to achieve the binding energy 285 eV for CH C 1s signal.

The normal motivation for charge correcting XPS data is a desire to identify chemical state by comparing binding energy assignments for peaks in data from a sample with unknown chemistry to binding energy from samples of known chemistry. The problem encountered in calibrating the binding energy scale for an insulating material is there is no absolute reference other than assuming a peak can be identified corresponding to photoemission of a known binding energy. For many samples the best we can do is assume a peak in C 1s spectra can be identified corresponding to C-H type carbon chemistry and assign this peak binding energy to 285 eV (Figure 50). The source for C 1s signal is assumed to be adventitious carbon. When presenting energy calibrated data, the importance of stating the calibration assumption should not be underestimated since all

assumptions about assignments of other peaks reported in a paper will be dependent on this initial assumption. Indeed, the energy calibration performed here makes use of a binding energy for Al 2s, the value for which was determined from the initial measurement before sputtering with an ion-gun making use of adventitious carbon, available at this point in the experiment, to calculate the binding energy for Al 2s that would align the C-H component within the corresponding C 1s spectrum with binding energy 285.0 eV. It is not certain that the precision achieved when fitting a peak model to C 1s spectra used to identify the component in C 1s assigned to 285 eV or the accuracy in terms of the energy assigned to the component is sufficient to support Al 2s assigned to 119.19 eV, but the common practice of calibrating to C 1s is achieved, even when carbon became unavailable following sputtering the surface with an ion gun.

A secondary motivation is to align spectra in binding energy throughout the experiment so that data can be manipulated in the sense of vector analysis. This vector analysis could be as simple as summation of spectra to improve signal to noise or analyse columns of data into principal components through an application of singular valued decomposition (SVD) followed by noise reduction based on principal component analysis (PCA). The objective in performing these types of vector analysis is to check for consistency in these measurements and by creating signal enhanced data identify subtle changes within these data.

Verification by Vector Analysis

When presented with a data set in which multiple measurements from the same sample have been performed the option is available to make use of the total acquisition time to improve signal to noise in each measurement via PCA. Before PCA can be applied to data the energy scale must be calibrated to remove variation due to charge compensation state. Once energy calibration is performed, the next step is to copy the set of VAMAS blocks to a new VAMAS file extracting processed data. The reason data needs to be copied is energy calibration is performed by shifting the energy scale rather than moving intensity between data bins. PCA or any vector operation requires the movement of intensities between data bins so that data bins correlate with binding energy. Correlating data bins with binding energy is performed by first copying the processed data then an option on the Spectrum Processing, Calculator property page is used to re-bin intensities so that data bins correspond to binding energy directly.

The following steps create a new VAMAS file containing spectra from the original data set with intensities moved between data bins so that data bins correlate with binding energy.

1. Select all VAMAS blocks in the original VAMAS file that have previously been calibrated in terms of binding energy (Figure 51).

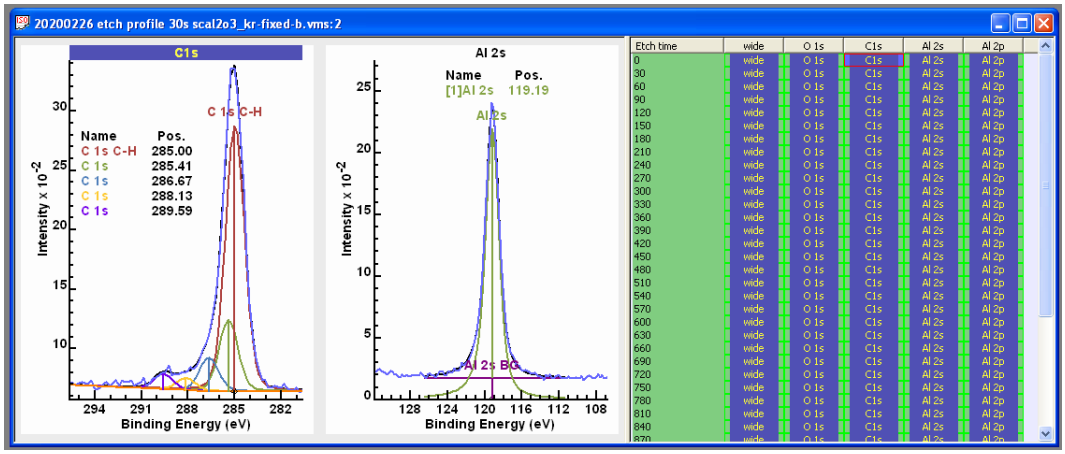

Figure 51. Experiment window showing in the righthand-pane all VAMAS blocks selected.

2. Using the top toolbar button or the New File menu option (Figure 52), create an empty experiment frame window into which processed data can be copied.

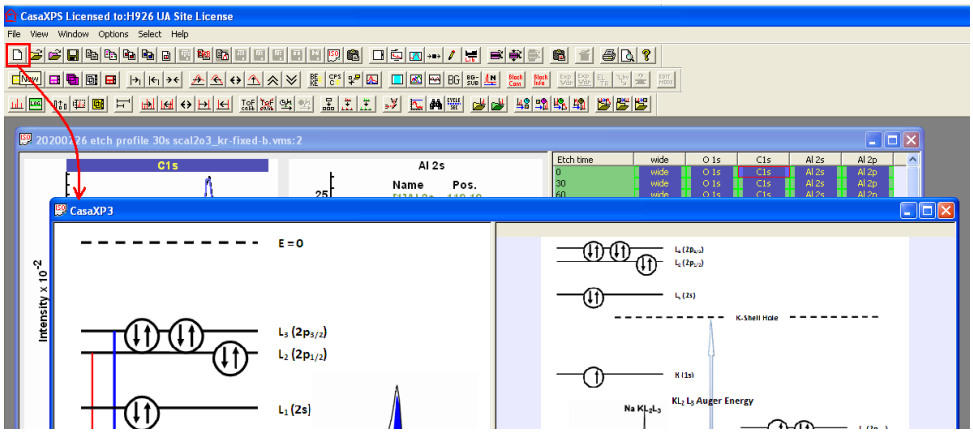

Figure 52. The toolbar button indicated by the red-box creates an empty experiment window. The File menu of CasaXPS also includes a menu-item labelled *New*, that similarly creates a new empty experiment window. Note that the Window menu includes a menu-item labelled New Window, which creates a new window that is associated with the currently selected experiment window data. That is, the Window menu via the New Window menu-item creates an additional window that allows the display and selection of VAMAS blocks from a VAMAS file already open in CasaXPS.

3. The empty frame window should be given focus before pressing the Copy VAMAS blocks toolbar button (Figure 53). Select the tick-box labelled **Process Data Only** on the Copy VAMAS blocks dialog window then press the OK button.

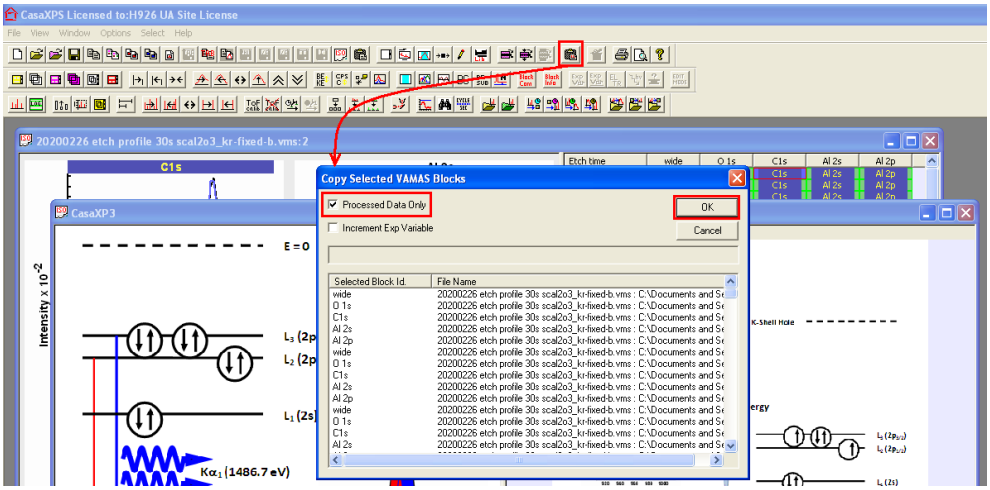

Figure 53. The Copy/Paste VAMAS blocks toolbar button indicated by the red-box copies from all experiment windows with selected VAMAS blocks, the selected VAMAS blocks into the experiment window with focus.

4. Select all the VAMAS blocks in the newly populated experiment frame before invoking the Spectrum Processing dialog window and selecting the Calculator property page (Figure 54). The set of selected VAMAS blocks are acted upon by the **Re-bin Selected VAMAS Blocks** button to create a new experiment frame containing data re-binned so that data bins align with binding energy.

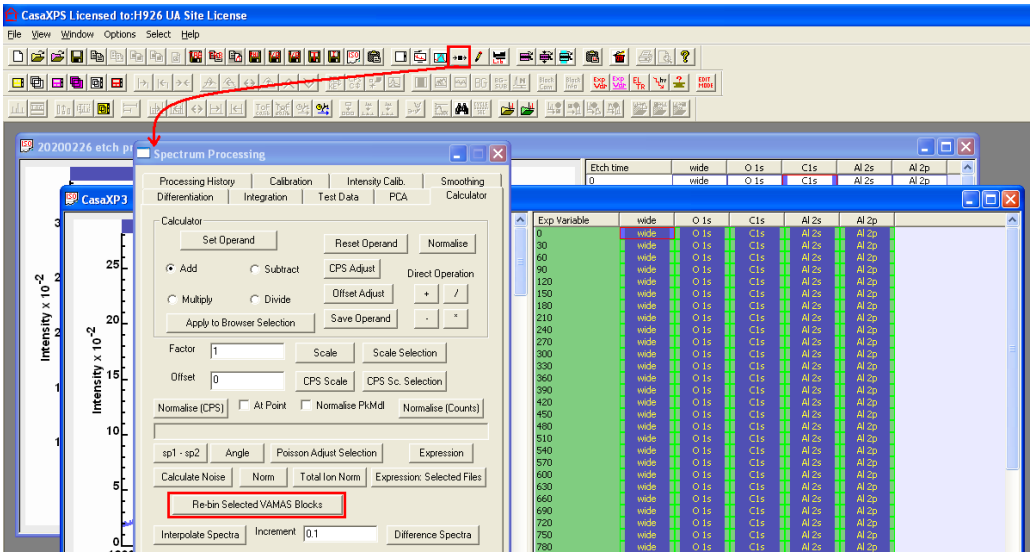

Figure 54. Spectrum Processing dialog window via the Calculator property page offers an option to re-bin spectra arranged in the righthand-pane as columns of VAMAS blocks. Interpolation is used to convert each selected VAMAS block in a column to the same start, increment and number of data bins used by the first VAMAS bock in a column.

The resulting experiment frame contains data in a format suitable for vector analysis steps including PCA calculations aimed at suppressing noise in each spectrum (Figure 55).

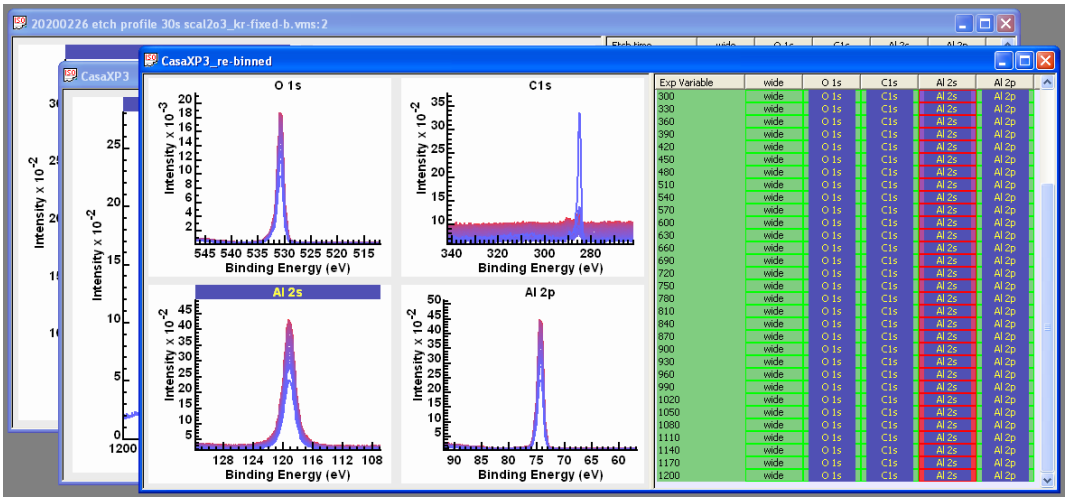

Figure 55. The result of applying to the VAMAS file shown in Figure 54 the **Re-bin Selected VAMAS Blocks** button is a new experiment window containing a new VAMAS file in which each spectrum in a column contains the same number of data bins that span the same energy interval as the first VAMAS block in each column of VAMAS blocks selected in the righthand-pane in the original VAMAS file.

The spectra of most interest are the O 1s and C 1s. Both of these photoemission lines potentially respond to chemical state and despite low signal to noise in C 1s spectra, these C 1s data are of interest and so enhancing these C 1s spectra is an objective for the following PCA calculations.

Principal Component Analysis for C 1s Spectra

While the as-received surface provides a C 1s spectrum with adventitious carbon, following cleaning cycles of sputtering with an ion beam the nature for C 1s signal changes, reducing in intensity leading to spectra with low signal-to-noise. The shapes within C 1s signal from these sputtered surfaces are potentially of interest with respect to the chemistry of the sample, so there is a need to improve signal to noise for these C 1s data to allow an analysis in terms of a model involving peaks representative of chemical state for carbon (Figure 56 and Figure 57).

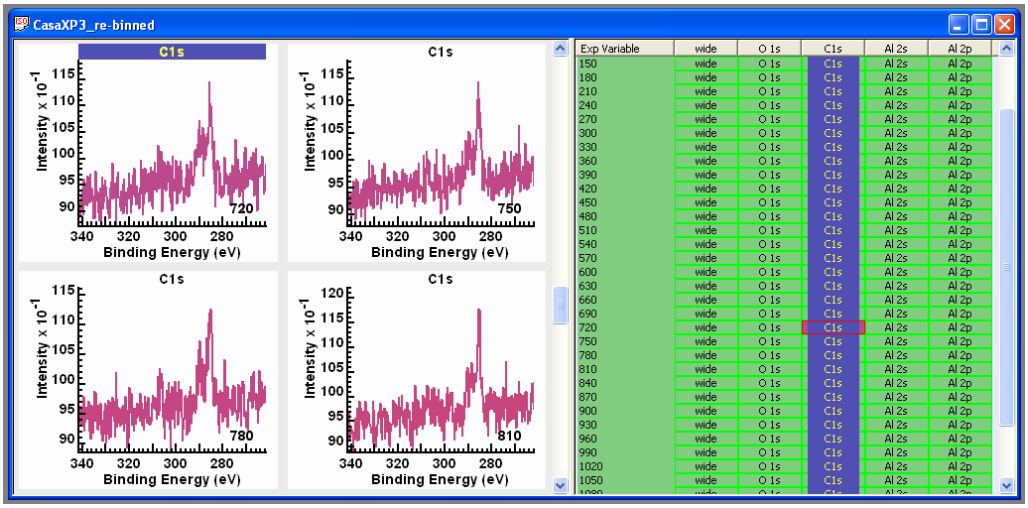

Figure 56. Examples of C 1s spectra before PCA is used to reduce the noise in individual spectra.

One way to investigate these C 1s spectra is to perform a PCA using all C 1s spectra.

The underlying concept of PCA is that a set of spectra can be partitioned into spectral shapes that are important to the analysis and a set of shapes that are unimportant and can be attributed to random noise. If we can determine a small number of shapes of significance and a large number of shapes representing noise, then if we fit each spectrum in a data using shapes with significance only, in a least squares sense, then the result is a set of spectra with reduced noise. The problem is therefore to first identify the number of shapes that can be considered of significance and then replace the spectra by linear least squares approximations to each spectrum. The success of such an approach depends on making use of the total acquisition time in the same sense that signal to noise in a spectrum formed by summing all spectra results in data with much improved signal to noise, but by virtue of the PCA calculation retaining individual spectral information for each measurement, at the cost of including a proportion of noise.

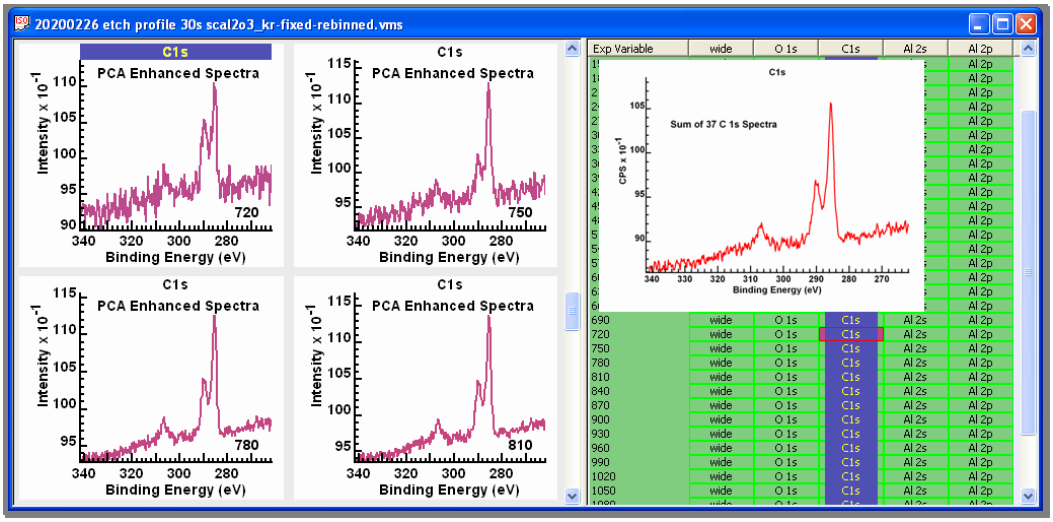

Figure 57. C 1s spectra corresponding to the spectra illustrated in Figure 56 following PCA noise reduction.

Background to SVD and PCA

Singular Valued Decomposition creates a set of orthogonal eigenvectors that can be ranked according to corresponding eigenvalue magnitude. For this reason, the results of SVD are often referred to as Principal Component Analysis. The terminology PCA encapsulates two concepts, namely, the analysis involves component shapes in an analogous way to a peak model is constructed from bell shaped components and secondly these components can be identified as principal meaning we are able to order these components so identified as some being more important than others. SVD is a mathematical procedure for computing eigenvectors and eigenvalues of real symmetric matrices. PCA is the interpretation of these mathematical results in terms of data description.

In essence, from the perspective of SVD a set of spectra are treated as vectors in a multidimensional vector space. The act of performing SVD generates a set of orthogonal vectors that form a natural coordinate system for the data set as a whole. The adjective natural applied to an n-dimensional coordinate system conveys the meaning that one can order the basis vectors by magnitude of

associated eigenvalues, and the basis vector with largest eigenvalue points in the direction of the greatest variance within the original data set.

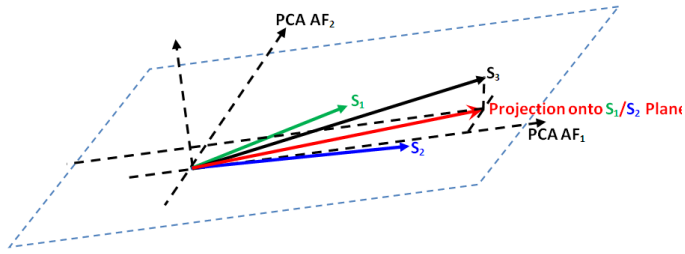

Given two linearly independent vectors (spectra) S_1 and S_2, a plane is defined by these two vectors. SVD computes from these two vectors S_1 and S_2 two new vectors **PCA AF**$_1$ and **PCA AF**$_2$ that are orthogonal and also lie in the same plane as S_1 and S_2. A third vector S_3 is approximated by the projection of S_3 on to the plane P. The projection can be defined in terms of $P = \alpha S_1 + \beta S_2$ or $P = \gamma$**PCA AF**$_1 + \eta$**PCA AF**$_2$ with the only difference between these two ways of specify P is the PCA vectors can be ordered in terms of significance.

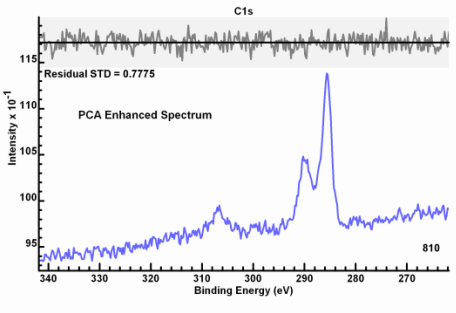

Figure 58. Vectors in a 3D space are used to illustrate the concept of projecting a 3D vector onto a 2D subspace. The projection of vectors onto a lower dimension subspace is the means by which PCA abstract factors are used to construct signal enhanced spectra.

The ordering of vectors by eigenvalues is very useful because the eigenvector with smallest eigenvalue contains the smallest variation in signal and this is noteworthy because such a characteristic would be a typical goal for fitting of data with curves. That is, a necessary condition for a peak model constructed from bell shaped curves fitted to data in an acceptable form is the difference between the sum of all curves and the spectrum should exhibit a uniform shape without structure. For a peak model the removal of intensity deemed to be of least significance is precisely the outcome of an optimisation procedure that fits components to data. This same logic applied to curve fitting using bell shaped curves can also be applied to SVD results, namely, if a data set is projected (Figure 58) onto the n-1 eigenvectors with largest eigenvalues the result is a data set with less variation than the original data set. If the vector with smallest eigenvalue contains no significant variation or put another way, simply has the appearance of noise, then SVD provides a means of reducing the influence of noise within each of the original data vectors through the act of projecting onto the subspace spanned by the eigenvectors with the largest n-1 eigenvalues. The same reduction in dimension can be repeated for each eigenvector starting with the smallest eigenvalue and continuing until it is deemed an eigenvector contains shape information of significance to the interpretation of spectra. The process of removing eigenvectors from the original data in order of least significance transforms the dimension for the original data set into a subspace of dimension defined by the number of eigenvectors of significance onto which the original data set is projected. The outcome to such a procedure is spectra with the influence of noise minimised and hence spectra width enhanced spectral shapes. A measure of success for SVD/PCA noise reduction is the residual standard deviation should be close to but below unity, and the appearance of the residual is uniform for the entire energy interval.

The first step is to inspect the abstract factors (AF) for a PCA calculation. Abstract factors are computed as part of SVD and are a set of abstract spectral forms with the property that each abstract factor is orthogonal to all abstract factors computed for a set of spectra. The most significant result of the SVD algorithm is these abstract factors are not simply mutually orthogonal but are also determined by SVD such that the first abstract factor points in the direction of the

greatest variance for the spectra involve by virtue of a least squares criterion. The iterative SVD (iSVD) algorithm used in CasaXPS computes for n initial spectra the first abstract factor by dividing the processed data into the first abstract factor and a set of processed vectors with the property that all vectors in the n-1 set of processed vectors are orthogonal to the first abstract factor but not necessarily mutually orthogonal. The procedure is then applied to the set of n-1 processed vectors to create the second abstract factor for PCA leaving n-2 processed vectors in a state suitable for computing subsequent abstract factors. The user interface for PCA in CasaXPS reflects the sequential determination of abstract factors.

PCA Options and the PCA Property Page

The Spectrum Processing dialog window, PCA property page (Figure 59) includes options that perform two steps leading to signal enhanced spectra.

The first step is to compute a number of abstract factors based on a set of VAMAS blocks. Select the column of C 1s VAMAS blocks and display these C 1s spectra overlaid in the active tile. The PCA property page, **Generate Factors** button performs an iSVD calculation using data displayed in the active display tile computing the number of abstract factors specified in the **Factors** text-field. The tick-box labelled **Calc Specified Factors** forces the calculation of the specified number of factors indicated in the **Factors** text-field. If **Calc Specified Factors** is not ticked, iSVD will terminate once abstract factors (sequentially determined) resemble Poisson distributed noise.

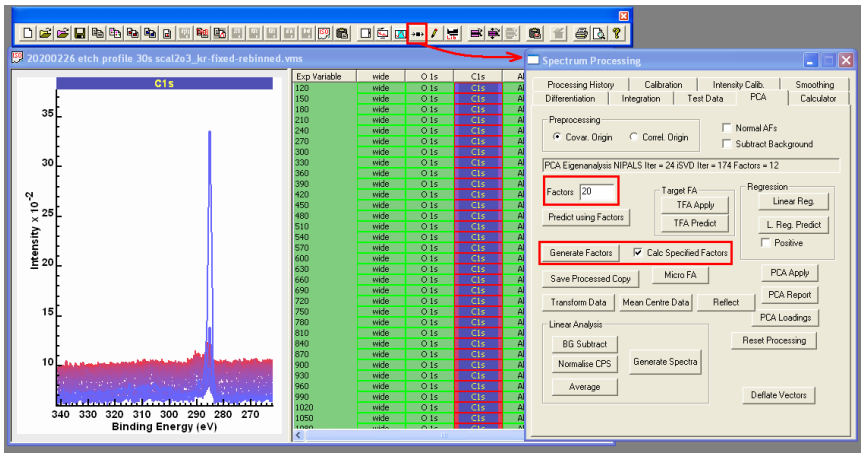

Figure 59. Spectrum Processing dialog window with the PCA property page tab selected. The options indicated are used to perform the steps necessary when constructing by PCA signal enhanced spectra.

Abstract factors and partially computed abstract factors are saved in the processed form for data in a VAMAS block. Pressing the **Reset Processing** button on the PCA property page returns each VAMAS block to the data before iSVD was applied to data displayed overlaid in the active tile.

Displaying the selected C 1s VAMAS blocks one per tile allows the inspection of abstract factors (Figure 60). For the case of C 1s spectra processed to form 20 abstract factors, the results show two very significant spectral shapes followed by potentially a third with some spectral shape accompanied by a sizable noise contribution but following the first three most significant abstract factors the remaining factors have the appearance of noise. As a consequence of these observations these raw data may be reconstructed using the three most significant abstract factors.

Figure 60. Display tiles arranged six per page. Each page of tiles is viewed by left-clicking the mouse with the cursor over the background area of the scrollbar for the lefthand-pane. The abstract factors are plotted using a change of colour in each display tile. An option on the Colours property page (Change Colour for each Tile) when enabled results in a different colour for each display tile when the selected VAMAS blocks are redisplayed.

The term reconstruction means these first three most significant abstract factors form a three-dimensional subspace of the vector space containing all C 1s spectra used in the iSVD calculation. Reconstruction is the act of projecting each spectrum onto the 3D subspace defined by these three abstract factors. The vectors formed by this projection operation contain linear combinations of only these three abstract factors and since we assume all other abstract factors formed by a full SVD applied to C 1s spectra represent noise the reconstructed also referred to as predicted spectra suppress noise.

The second step in creating noise reduced spectra makes use of the first step involving computation of abstract factors by selecting to use three abstract factors in the prediction step. Data as seen in the display tiles must be returned to the original C 1s spectra before iSVD was applied (Figure 61). The steps are therefore as follows.

1. Overlay the set of C 1s VAMAS blocks in the active tile before pressing the **Reset Processing** button on the PCA property page.

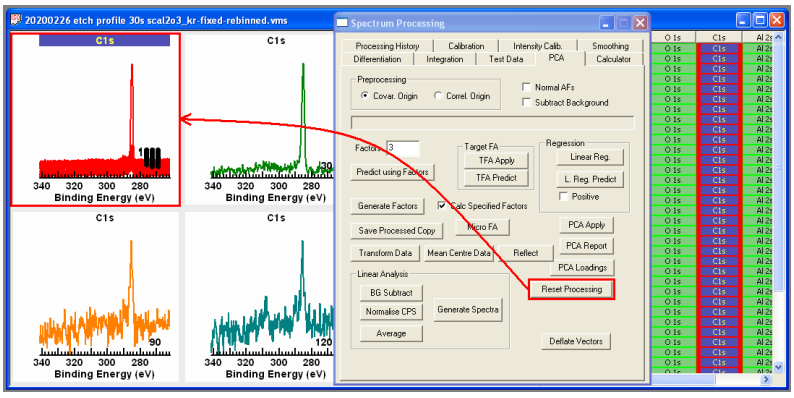

Figure 61. VAMAS blocks previously processed are returned to the original data by pressing the Reset Processing button on the PCA property page indicated by the red-box.

2. Enter the number of abstract factors intended for use in the reconstruction of C 1s spectra using abstract factors in the **Factors** text-field (Figure 62).
3. Press the **Predict using Factors** button on the PCA property page.

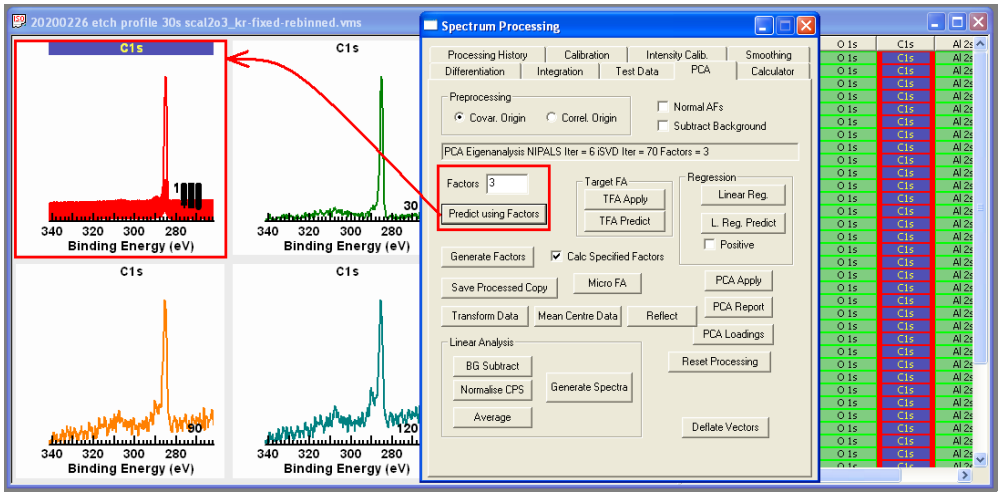

Figure 62. The Predict using Factors button and the number of abstract factors entered into the Factors text-field act on the set of VAMAS blocks with spectra overlaid in the active display tile.

Once signal is enhanced relative to noise the character of C 1s spectra can be seen to alter as a consequence of cleaning the surface with an ion beam (Figure 63). A spectrum typical of adventitious carbon is replaced progressively by spectral forms containing information relating to carbon chemistry no longer dominated by C-H bonded C 1s. Further, after sputtering C 1s peaks are superimposed on a declining background, which is an important consideration when constructing a peak model to analyse carbon chemistry for these types of samples.

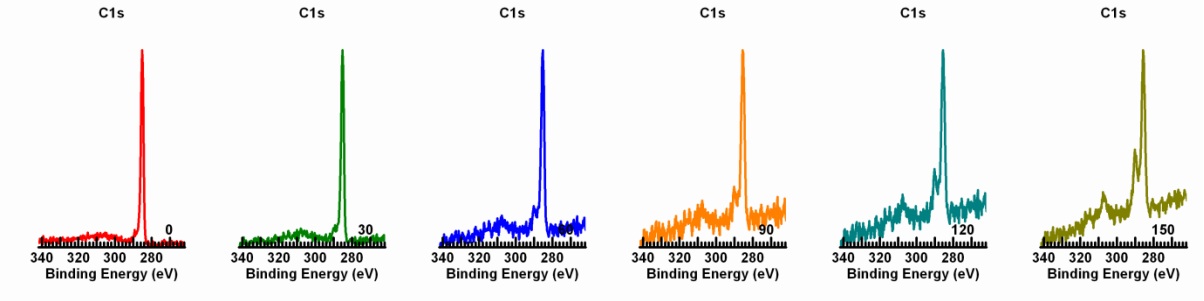

Figure 63. PCA signal enhanced C 1s spectra.

The challenge is then to establish component peaks within these C 1s spectra and correlate component peaks with carbon chemistry.

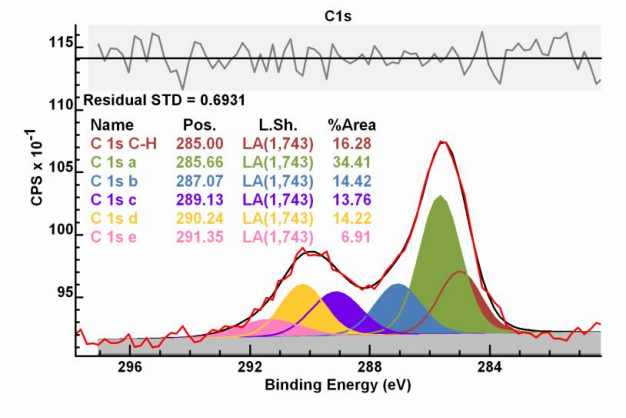

Figure 64. An example of a peak model that fits the C 1s date very well, but which is unlikely to have physical meaning.

Fitting a set of component peaks to a data envelope with good reproduction as indicated by the residual standard deviation and uniformity of residual plot (Figure 64) is no guarantee of physically meaningful component binding energies or relative intensities. At the very least, a peak model should be consistent with results from other sources (Figure 65). In the current case study, the existence of C 1s component peaks assigned to bonds with oxygen or aluminium must correlate with signal within O 1s and Al 2p spectra. However, it is not always possible to uniquely determine such correlations, for example Al 2p in this case study lacks any features that would allow meaningful separation of chemical state by means of Al 2p. In the absence of such supporting evidence conclusions drawn from fitting C 1s in isolation should be treated as circumstantial evidence rather than evidence to support a hypothesis.

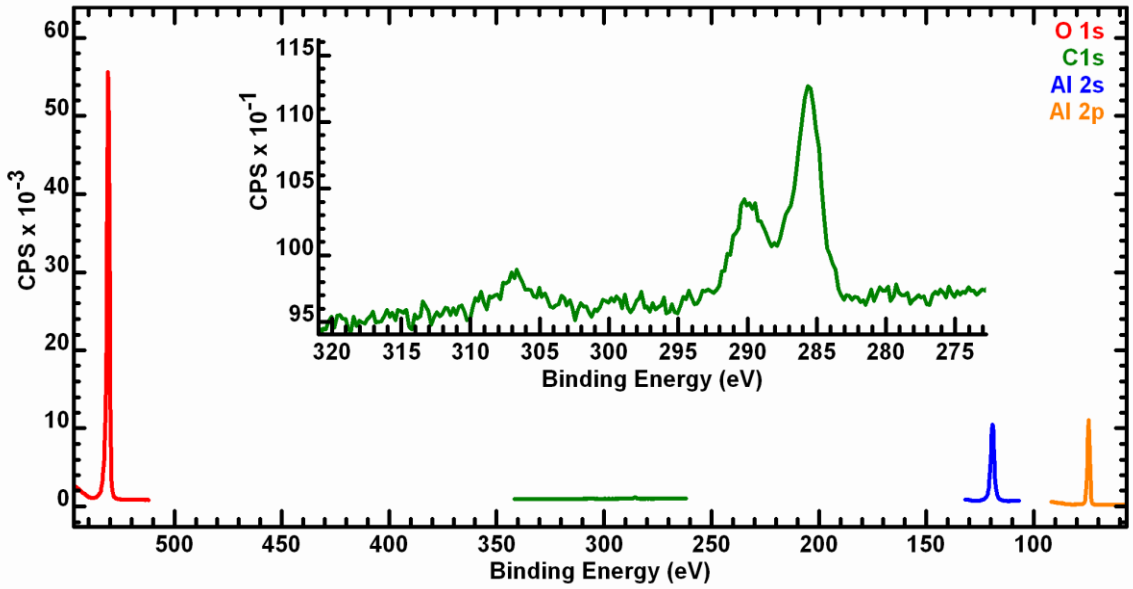

Figure 65. Data relevant to the analysis of carbon chemistry. Correlating information from different photoelectron sources is an important part of doing science by XPS.

Peak Models and Curve Fitting

Energy Resolution and Line Shapes

Energy resolution for XPS is determined by a number of instrumental design factors. For instruments based on hemispherical energy-analysers, the size of the HSA defined by the mean radius for two concentric hemispherical electrodes is one factor influencing energy resolution. A second factor is the Voltages applied to these two hemispherical electrodes. These hemispherical electrodes create a spherically symmetrical electrostatic field through which electrons travel and varying the potential difference alters the energy resolution of an instrument.

For electrons entering the HSA perpendicular to these electrostatic field lines, the force acting on an electron due to a charged particle moving in the spherically symmetrical field maintains the trajectory of an electron along the mean radius for the HSA provided the energy for the electron is a precise value. This precise energy is determined by the potential difference between the hemispherical electrodes. Positioning a detector at the opposite end of a trajectory for an electron following the mean radius allows the counting of electrons with a specific energy. Given a specific pair of Voltages applied to the HSA electrodes the energy for electrons following the mean radius is called the pass energy for the HSA. XPS instruments typically offer a set of pass energies.

The width of apertures located at the entrance and exit to the HSA alter energy resolution.

During the measurement of a spectrum, electrons are emitted from a sample with energies spanning a wide range of energies. At any one time only electrons with energies close to the pass energy of the HSA will be detected. If it is assumed all electrons from the sample enter the electrostatic field of the HSA perpendicular to the field lines and act as a point source, electrons with energies higher than the pass energy follow trajectories resulting in an exit from the electrostatic field with greater radial distance from the centre of the HSA. Similarly, electrons with energies lower than the pass energy, exit the electrostatic field with radial distances less than the mean radius. An aperture of finite width in the radial direction placed at the exit in front of a detector will allow a narrow range of energies for electrons to be counted by the detector. The width of the exit aperture therefore is a factor in energy resolution.

Energy resolution is also determined by the width of the entrance aperture to the HSA, but for a different reason to the width of the exit aperture. An HSA moves electrons from the entrance to the exit, as described above, dispersing electrons with different energies thus acts as an energy filter. However, if all electrons arriving at the entrance have the same energy, and if the entrance is an aperture of a given width in the radial direction, then the trajectories of electrons passing through the entrance aperture perpendicular to the electrostatic field lines follow paths forming an image of the entrance aperture at the exit aperture with a magnification of minus one. If the entrance aperture width is equal to the exit aperture width, the energy resolution limitation is defined in terms of the common width. If the entrance aperture is wider than the exit aperture then spatial information and energy information is mixed resulting in energy resolution limited by the entrance aperture width. When the detection system is an array of detectors arranged in the radial direction at the exit of electrons from the HSA then the width for each detector defines the effective exit width aperture size. Multiple detectors facilitate the scenario of an entrance aperture wider than the

exit aperture per detector channel. Under these conditions the entrance aperture width is an important parameter that contributes to energy resolution of an operating mode.

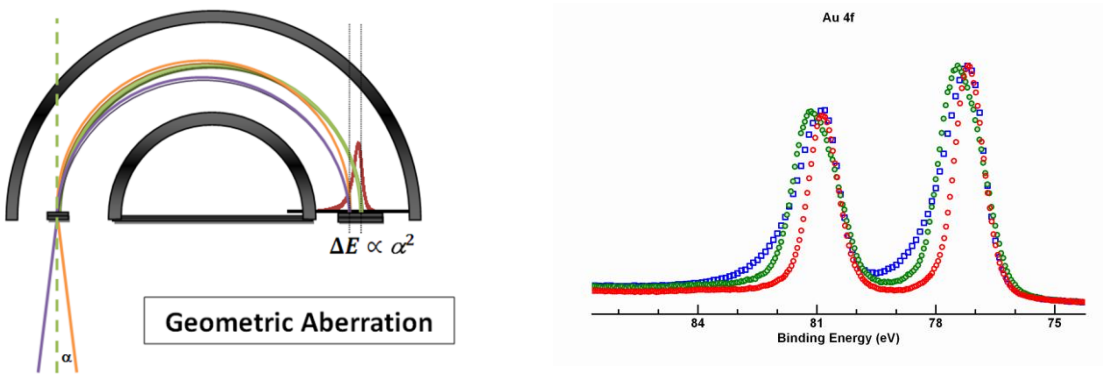

Figure 66. Illustration showing the consequences of geometric aberration for line shapes measured by XPS.

Up to this point electrons entering the HSA are stipulated to follow ideal trajectories, namely, trajectories perpendicular to the electrostatic field lines at the point of entry to the HSA. If electrons enter the HSA with an angular spread (Figure 66) at the point of entry to the electrostatic field, a well-formed image of the entrance aperture is compromised and electrons systematically move towards the centre for the HSA as a function of angle with respect to the normal to the electrostatic field. The consequences for angular spread in the radial direction for the HSA is deformation to peak shapes notable for introducing asymmetry into photoelectron peaks that otherwise would be symmetrical. This too influences energy resolution for energy spectra. The transfer lens system is responsible for moving electrons from the sample to the entrance aperture of the HSA and therefore these transfer lenses and the tuning of these transfer lenses is influential in energy resolution.

X-ray guns generate photons of a specific energy, but in reality, photons are emitted with a distribution of energies centred about the specific energy typically described as the source excitation energy. As a result, the excitation source is yet another factor influencing energy resolution.

The most commonly used X-ray source makes use of Al Kα photons resulting from relaxation of energy for electrons in an excited state of aluminium ions. Generation of X-rays is performed by exciting aluminium atoms in an anode paired to an electron emitting cathode which together accelerates electrons towards aluminium atoms with energy sufficient to create holes in the K shell forming aluminium ions. A resonance peak in the X-ray spectrum is available for exciting photoemission, but without the use of X-ray diffraction by a quartz crystal, the width for Al Kα radiation places a limitation of about 0.85 eV for the FWHM of photoelectron peaks. Introducing a monochromator reduces the FWHM for X-rays to about 0.26 eV. It is not possible to observe photoelectron peaks with FWHM less than these limits imposed by X-ray energy distributions.

When photoelectron peaks are measured, both the instrument and the photoemission process alter the shapes observed. A broad photoelectron line can dominate the peak shape recorded which means broad photoelectron peaks tend to offer insight in to the true line shape created by photoemission. As a consequence of desiring chemical state information reliant on binding energy shifts, narrow photoelectron lines are the features of choice for XPS, but narrow peaks suffer more

than broad peaks from instrumental factors. Establishing the optimum instrumental modes aimed at narrow photoelectron lines is an important part of designing a measurement protocol.

Fitting of data with synthetic curves is enhanced by the use of curves that are representative of the true photoelectron peak shape as recorded by an instrument. It is therefore important to understand the types of shapes a particular photoelectron peak might take as a consequence of choices made at the time of data acquisition. The two most influential choices made for collecting XPS data are pass energy and transfer lens mode. One might think there should be one mode for general use, but this is not the case for the simple reason photoemission of electrons varies in intensity and shape depending on material. There are trade-offs between acquisition time, signal to noise and instrumental deformation to line shapes. Flexibility for acquisition conditions is also required because some materials degrade over the period of analysis so maximising sensitivity at the expense of spectral quality is necessary at times.

With the understanding that XPS of samples of scientific interest is rarely simple, the discussion will now focus on simple materials with a narrow underlying peak width.

The first example is photoemission of electrons from silver resulting in the creation of a hole assigned to a d-orbital in the M shell. In XPS notation this photoelectron process is assigned the label Ag 3d. Spin-orbit interactions for d-orbitals with a hole or missing electron means there are two distinct energy levels for Ag ions, therefore a doublet peak is formed by Ag 3d photoemission. Each peak in the doublet pair is assigned different j quantum numbers to distinguish these two electron configurations with different energies, namely, Ag $3d_{3/2}$ and Ag $3d_{5/2}$.

The objective in measuring Ag 3d data is to characterise an instrument with respect to a material that is both readily available and can be cleaned using an ion gun to sputter the surface before measurement by XPS. Instrumental specification for performance is often described in terms of Ag $3d_{5/2}$ peak characteristics. Therefore, measuring the Ag 3d doublet is a good starting point from which to understand the potential energy resolution available for analysis of other materials.

It is difficult to separate the possible factors influencing energy resolution, so measuring Ag 3d using a range of operating modes is a method for verifying the performance of an instrument and also observing the changes in peak shape as a consequence of operating mode. The example presented here is a set of measurements from a Thermo K-Alpha XPS instrument (Figure 67). Two variables are assessed within these measurements. Each row of Ag 3d spectra is measured using the same pass energy. Each column of spectra is measured using different pass energies using the same X-ray spot size.

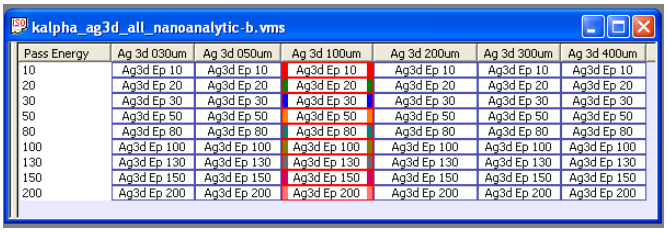

Pass Energy	Ag 3d 030um	Ag 3d 050um	Ag 3d 100um	Ag 3d 200um	Ag 3d 300um	Ag 3d 400um
10	Ag3d Ep 10	Ag3d Ep 10	Ag3d Ep 10	Ag3d Ep 10	Ag3d Ep 10	Ag3d Ep 10
20	Ag3d Ep 20	Ag3d Ep 20	Ag3d Ep 20	Ag3d Ep 20	Ag3d Ep 20	Ag3d Ep 20
30	Ag3d Ep 30	Ag3d Ep 30	Ag3d Ep 30	Ag3d Ep 30	Ag3d Ep 30	Ag3d Ep 30
50	Ag3d Ep 50	Ag3d Ep 50	Ag3d Ep 50	Ag3d Ep 50	Ag3d Ep 50	Ag3d Ep 50
80	Ag3d Ep 80	Ag3d Ep 80	Ag3d Ep 80	Ag3d Ep 80	Ag3d Ep 80	Ag3d Ep 80
100	Ag3d Ep 100	Ag3d Ep 100	Ag3d Ep 100	Ag3d Ep 100	Ag3d Ep 100	Ag3d Ep 100
130	Ag3d Ep 130	Ag3d Ep 130	Ag3d Ep 130	Ag3d Ep 130	Ag3d Ep 130	Ag3d Ep 130
150	Ag3d Ep 150	Ag3d Ep 150	Ag3d Ep 150	Ag3d Ep 150	Ag3d Ep 150	Ag3d Ep 150
200	Ag3d Ep 200	Ag3d Ep 200	Ag3d Ep 200	Ag3d Ep 200	Ag3d Ep 200	Ag3d Ep 200

Figure 67. VAMAS file viewed in the righthand-pane of CasaXPS, where each column of VAMAS blocks includes measurements of Ag 3d narrow scan spectra using a range of pass energies. The

rows of VAMAS blocks corresponding to the same pass energy are formed by including in the element/transition VAMAS block field the X-ray spot-size used to acquire the Ag 3d spectra.

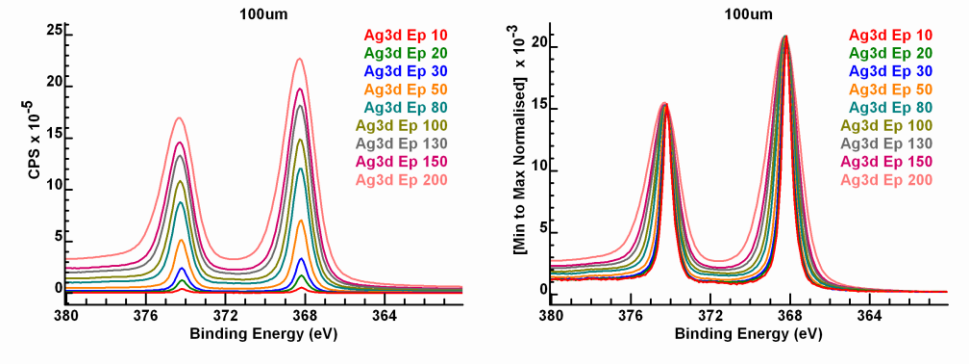

Figure 68. Displayed overlaid are Ag 3d spectra corresponding to the 100um X-ray spot-size and the set of pass energies shown in Figure 67. The lefthand spectra are plotted using with count-rates consequential of pass energy. The righthand spectra are identical to the lefthand spectra plotted using scaling of spectra to the maximum and minimum intensity of spectra measured at each pass energy.

These Ag 3d spectra illustrated in Figure 68 include a number of points worthy-of-mention. Firstly, progression of spectra for a given X-ray spot size varying pass energy demonstrates how the line shape for a given photoemission process is determined by instrumental factors to a greater or lesser extent depending on the energy dispersive mode of the HSA. The key point to notice is that any distortion in recorded peak shape is amplified by increasing pass energy. The second point of interest is the FWHM for Ag $3d_{5/2}$ is not significantly altered by changing the X-ray spot size which ranges between 30µm and 400µm (Figure 69). The implication for this observation is the entrance aperture to the HSA is filled with electrons independently of the analysis area defined by the X-ray gun. A third observation is count-rates change with X-ray spot size. Such a statement is not unexpected since collecting electrons from a larger area should increase the potential for collecting photoemission. However, a third variable is at play within these data, namely, the X-ray power changes with X-ray spot size and signal count rate in these data correlates more with X-ray power than analysis area. These observations demonstrate the difficulty in determining line shapes for photoelectron peaks without full disclosure of instrument design.

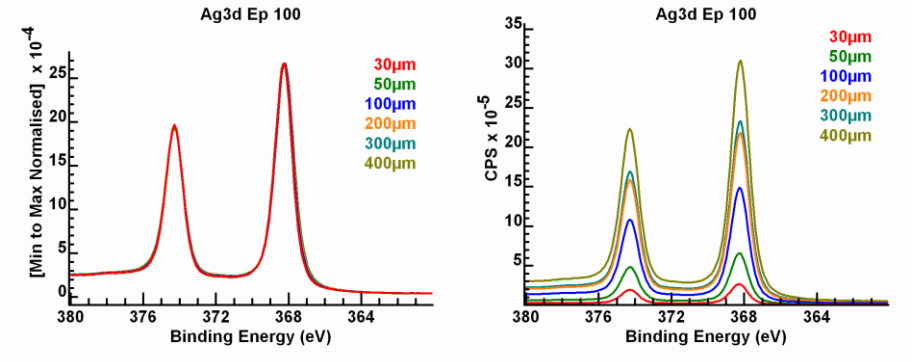

Figure 69. Displayed overlaid are Ag 3d spectra corresponding to pass energy 100 eV and the set of X-ray spot-sizes shown in Figure 67.

As a further example of instrumental influences on line shapes a set of Pt 4f spectra acquired for sputter cleaned platinum foil using a Thermo K-Alpha demonstrate how peaks exhibiting asymmetry respond to pass energy (Figure 70).

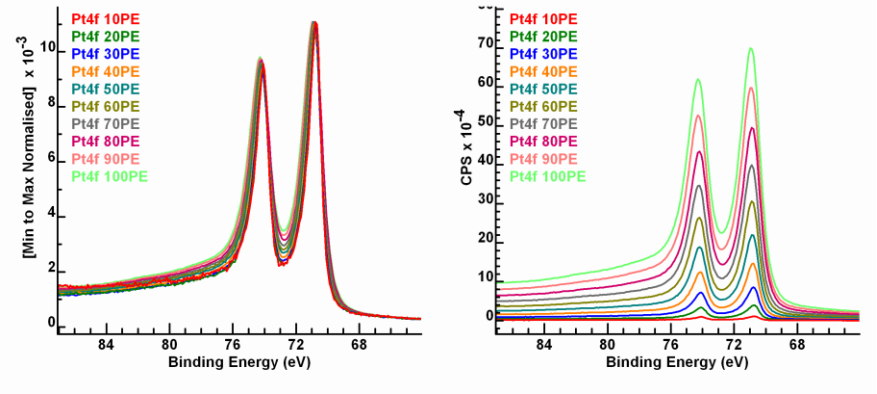

Figure 70. Platinum 4f spectra measured from a clean foil using a range of pass energies. The loss of energy resolution when measuring Pt 4f spectra with higher pass energies creates peak shapes for Pt 4f that appear more asymmetric than is apparent for spectra measured using lower pass energies.

Pass energy is one tool for suppressing the influence of the instrument on line shapes. Assuming a smaller width for the exit aperture than the entrance aperture, an alternative way of performing the same task of limiting the influence of the measurement process on line shapes is by reducing the size of the entrance aperture to the HSA. Some instruments are configured with a range of entrance aperture widths that can be selected as one of the parameters defining the experimental mode used to acquire spectra. An alternative to physically changing the size for the entrance aperture is to use the properties of the transfer lens system. Apertures within the lens column select an area of the sample for analysis. An image of this aperture used to select the analysis area at the sample is projected by lenses into the entrance slot aperture to the HSA. The size and shape of the selected area aperture image within the entrance to the HSA can result in changes to energy resolution. If the image of the selected area aperture projected into the entrance aperture is of smaller dimensions than the entrance aperture width, the result is a narrow beam of electrons entering the HSA compared to the physical entrance aperture width and so energy resolution is enhanced by use of selected area apertures.

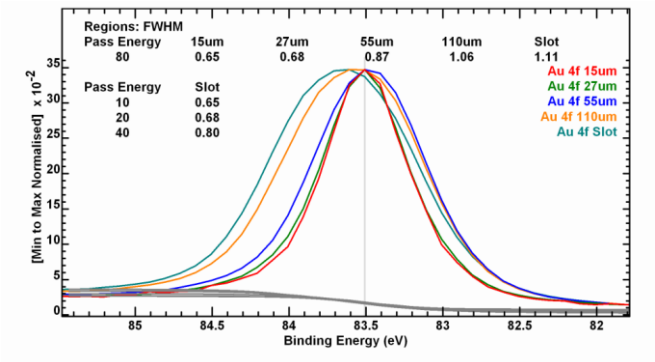

Figure 71. Au $4f_{7/2}$ photoelectron peak measured using pass energy 80 eV for a range of dimensions for the selected-area aperture. Note how the FWHM measured from spectra increases as the aperture size increases.

Au 4f spectra measured using the same pass energy and FoV2 lens mode change in shape depending on the size selected for the selected area aperture on a Kratos Axis Nova (Figure 71). Pass energy 80 making use of a 15µm selected area aperture results in a FWHM of 0.65 eV for Au $4f_{7/2}$ peak, which is identical to the same peak when measured using pass energy 10 combined with the full slot to define electrons entering the HSA. Pass energy 80 using the full slot entrance aperture results in a FWHM for Au $4f_{7/2}$ of 1.11 eV. The cost of using smaller selected area apertures is lower count rates. A benefit of using narrower widths for electrons entering the HSA is obtaining line shapes closer to the underlying line shape due to photoemission.

The importance of establishing the correct line shapes for data resides in both chemical state determination and quantification by XPS. The example of single crystal Al_2O_3 illustrates (Figure 72) how line shapes appropriate for both Al 2s and Al 2p facilitate the use of Scofield cross-sections to yield the expected relationship between these three photoemission peaks. The use of a strongly Lorentzian line shape for Al 2s is essential for both fitting a single component to Al 2s data and obtaining the correct peak area for comparison with the corresponding Al 2p doublet peaks.

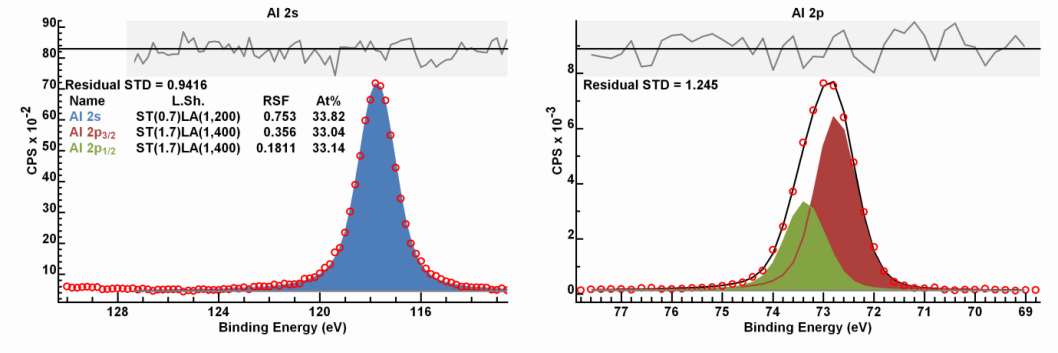

Figure 72. Aluminium photoelectron peaks measured from a single crystal Al_2O_3 sample. Note that the line shape for the Al 2s is more Lorentzian than the line shape used for Al 2p. A quantitative comparison between the three component peaks used in the quantification table is made based on assigning the individual Scofield cross-sections for the Al $2p_{1/2}$ and Al $2p_{3/2}$ to these components that model doublet intensity.

Synthetic Line Shapes

Synthetic line shapes are approximations to photoelectron peak shapes based on mathematical formulae. The basis for most synthetic line shapes is a Cauchy/Lorentzian function which is modified by various adjustments to allow for asymmetry before convolution with a Gaussian to simulate instrumental broadening.

Voigt Based Line shapes

$$Lorentzian: l(x) = \frac{1}{1+4x^2}$$

$$Gaussian: g(x:w) = e^{-4ln2\left(\frac{x}{w}\right)^2}$$

$$Generalised\ Lorentzian: l_g(x:\alpha,\beta) = \begin{cases} [(l(x)]^{\alpha} & x \le 0 \\ [l(x)]^{\beta} & x > 0 \end{cases}$$

$$Lineshape\colon LA(x\colon \alpha,\beta,w) = N\int_{-\infty}^{\infty} l_g(\tau\colon \alpha,\beta)g(x-\tau\colon w)d\tau$$

$$Abbreviation\ for\ LA\ lineshape\colon LA(x\colon \alpha,w) = LA(x\colon \alpha,\alpha,w)$$

$$Asymmetric\ Lorentzian:\ T(x\colon \alpha,\mu) = \left[\frac{1}{1+4x^2}\right]^{\alpha} \times \left[\frac{\pi}{2} - \tan^{-1}(2x) + \frac{\pi}{\mu}\right]\cdots \quad \mu > 0\ \&\ \alpha > 0$$

$$Lineshape\colon TLA(x\colon \alpha,\mu,w) = N\int_{-\infty}^{\infty} T(\tau\colon \alpha,\mu)g(x-\tau\colon w)d\tau$$

Generalised TLA Asymmetric Line shape:

Rather than using a Lorentzian any line shape can be used to generalise the TLA for all line shapes $F(x)$ in CasaXPS. The specification for the ST modification is described below in terms of the LA line shape but the same applies to all line shapes used to define component peaks in a model.

$$A = \int_{-\infty}^{\infty} F(\varphi)d\varphi$$

$$S(\mu)F(x) = N \times F(x) \times \left[\int_{x}^{\infty} F(\varphi)d\varphi + \frac{A}{\mu}\right]\cdots \quad \mu > 0$$

$$ST(\mu,\gamma)F(x) = N\int_{-\infty}^{\infty} S(\mu)F(\tau)g(x-\tau\colon \gamma)d\tau$$

Doniach Sunjic

Doniach Sunjic profile P with asymmetry parameter α is defined by

$$P(x,\alpha) = \frac{1}{[1+4x^2]^{\frac{1-\alpha}{2}}} \times cos\left(\frac{\pi\alpha}{2} + (1-\alpha)tan^{-1}(2x)\right)$$

A line shape is derived from the Doniach Sunjic profile by convolution with a Gaussian G of width characterised by the parameter n.

$$DS(x,\alpha,n) = P(x,\alpha) * G(n)$$

A Shirley background response for a Doniach Sunjic profile is defined as follows.

$$S[P(x,\alpha)] = \int_{x}^{\infty} P(x,\alpha)d\varphi$$

The definition for a Doniach Sunjic Shirley profile is as follows.

$$Q(x,\alpha,n,l) = \begin{cases} 0, & x < -l \\ [P(x,\alpha) - k \times S[P(x,\alpha)]], & x \geq -l \end{cases}$$

$$DS(x,\alpha,n,l) = Q(x,\alpha,n,l) * G(n)$$

Where k is determined such that

$$S[P(-l,\alpha)] = P(-l,\alpha)$$

Pseudo Voigt Line shapes

Product form of the pseudo-Voigt line shape is formed from a product of a Lorentzian and Gaussian functions where the FWHM for each function varies with the parameter m.

$$GL(x,m) = \frac{1}{(1+4\frac{m}{100}x^2)} \times exp\,(-\left(1-\frac{m}{100}\right)(4ln2)x^2)$$

For $0 < m < 100$

$$GL(x,m) = \frac{1}{1+4\left(\frac{x}{f_L}\right)^2} \times exp\left(-(4ln2)\left(\frac{x}{f_G}\right)^2\right)$$

$${f_L}^2 = \frac{1}{\frac{m}{100}} \text{ and } {f_G}^2 = \frac{1}{1-\frac{m}{100}}$$

The sum form for a pseudo-Voigt function combines a Lorentzian and a Gaussian of unit FWHM by varying the relative height for these two functions before summation.

$$SGL(x,m) = \frac{m}{100}\frac{1}{(1+4x^2)} + \left(1-\frac{m}{100}\right)exp\,(-(4ln2)x^2)$$

$$SGL(x,m) = H_L\frac{1}{(1+4x^2)} + H_G exp\,(-(4ln2)x^2)$$

$$H_L = \frac{m}{100} \qquad H_G = 1-\frac{m}{100}$$

Both sum and product forms are computationally expedient tools for creating line shapes, but do not simulate the response of an analyser as well as the Voigt formalism.

Generalised Pseudo Voigt Line Shapes

$$SGL(x,m,n) = SGL(x,m) * G(n)$$

$$GL(x,m,n) = GL(x,m) * G(n)$$

Exponential Tail Modification Line Shapes

$$E(j,k) = \begin{cases} j \times exp\,(kx), & x < 0 \\ 0, & x \geq 0 \end{cases}$$

$$SGL(x,m,n)PHI(j,k) = \big(SGL(x,m) + \big(1-SGL(x,m)\big)E(j,13.8/k)\big) * G(n)$$

$$SGL(x,m,n)T(k) = \big(SGL(x,m) + \big(1-SGL(x,m)\big)E(1,k)\big) * G(n)$$

$$GL(x,m,n)PHI(j,k) = \big(GL(x,m) + \big(1-GL(x,m)\big)E(j,13.8/k)\big) * G(n)$$

$$GL(x,m,n)T(k) = \big(GL(x,m) + \big(1-GL(x,m)\big)E(1,k)\big) * G(n)$$

Shirley Background Profile

For any synthetic line shape $F(x)$ a Shirley profile line shape is computed as follows.

$$SB(0)F(x) = \int_{x}^{\infty} F(\varphi)d\varphi$$

Trapezium Profile

$$R(x,\alpha,\beta) = \begin{cases} \alpha + (\beta - \alpha)(x + 0.5), & |x| \leq 0.5 \\ 0, & |x| > 0.5 \end{cases}$$

$$TP(x,\alpha,\beta,n) = R(x,\alpha,\beta) * L(n)$$

Background Signal

The influence of all electrons in solid state on photoemission spectra goes beyond photoemission peaks. In particular outer electrons and bonds formed with other elements have an influence on core-level spectra creating structures and shapes within XPS background intensity at or close to photoemission lines. There are situations where photoemission peaks appear to be classically formed from two components added to simple background signal, but even for these relatively simple cases closer inspection reveals structure important to understanding of chemical state and also elemental quantification by XPS.

Background Specification and the Regions Property Page

A particular background definition is specified using the Quantification Parameters dialog window, Regions property page. A list of background types is available for selection via a dialog window invoked by selecting a BG Type field followed by left-clicking the label field for the BG Type row on the Regions property page (Figure 73).

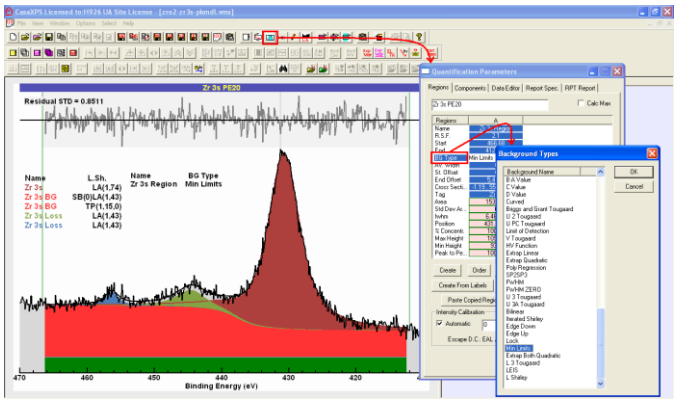

Figure 73. The toolbar button indicated by the red-box invokes the Quantification Parameters dialog window. The Regions property page displays each quantification region defined on the active VAMAS block (first selected VAMAS block before being displayed in the active display tile). A list of available background types is invoked by selecting the BG type field for a region, then placing the cursor over the label BG Type indicated by the red-box before left-clicking the mouse.

Other fields entered on the Regions property page of significance to background specification are Av Width, St. Offset, End Offset and Cross-Section. The Cross-Section fields are part of defining a Tougaard background, but these four parameters are also used to specify other backgrounds within CasaXPS.

The Av Width region parameter allows the intensity at which a background approaches spectral data to be determined by averaging data bins at either limit to a region. The purpose of the Av Width parameter is to reduce the influence of noise on how a background curve connects with spectral data bins.

For many backgrounds, the Start Offset and End Offset parameters are a percentage offset to the intensity computed for the background at the start and end energies for a region. These Start Offset and End Offset parameters can be entered on the Regions property page or when the Components property page is top-most, pointing the cursor at either the start or end of a region and dragging with the left-mouse button held down will allow the Start Offset and End Offset parameters to be adjusted under mouse control.

Shirley Background

While it is common practice to remove inelastic scattered background using the approach described as a Shirley background, the background shape represents a step in signal centred on peak maxima and does not include the option to offset the onset of inelastic scattering. There is therefore some doubt as to whether a Shirley background is appropriate for materials such as TiO_2. One merit of Shirley backgrounds is that for isolated peaks the algorithm computes a background that is systematic. A disadvantage for the Shirley background occurs when complex peak structures are involved over extended energy intervals with rising count rates, an example of which is Ce 3d, at which point the systematic nature of a Shirley background breaks down.

Assuming the Shirley background is already known for a specific spectrum and given by $S(E)$, then each point within an energy interval follows the relationship in terms of area above background as shown in Figure 74. Essentially for any energy E within the interval $[E_1, E_2]$ the Shirley background is computed from the photoelectron peak area within the interval partitioned into the area to the left and right of a given energy. The obvious problem for computing a background is that, for a photoelectron peak, initially the area for the photoelectron peak is unknown. For this reason, a Shirley background is computed by means of an iterative scheme where the initial guess for the background might be a constant background. The iterative scheme is as follows.

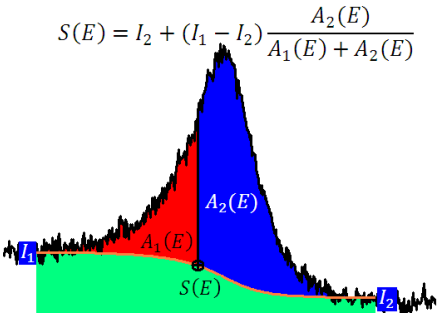

Figure 74. The Shirley background S(E) is calculated from the areas $A_1(E)$ and $A_2(E)$. However, before S(E) is known, $A_1(E)$ and $A_2(E)$ are unknown.

Given a spectrum $J(E)$ and an interval $[E_1, E_2]$. Define background signal such that: $B_{Sh}(E_1) = I_1$, $B_{Sh}(E_2) = I_2$ then the Shirley background is calculated by iteration using the formula

$$B_{Sh_{n+1}}(E) = I_2 + \frac{(I_1 - I_2)}{\int_{E_1}^{E_2} J(x) - B_{Sh_n}(x)\,dx} \int_E^{E_2} J(x) - B_{Sh_n}(x)\,dx$$

Note that the zero-loss photoelectron peak shape is given by $J(x) - B_{Sh_\infty}(x)$. Thus, given a component peak shape, it is possible to directly compute the curve corresponding to a Shirley background. If signal above inelastic scatter background is Lorentzian then without iteration the background equivalent to a Shirley background is given by:

$$B_L(E) = I_2 + \frac{(I_1 - I_2)}{\int_{-\infty}^{\infty} \frac{1}{1+x^2}\,dx} \int_E^{\infty} \frac{1}{1+x^2}\,dx = I_2 + \frac{(I_1 - I_2)}{\pi}\left(\frac{\pi}{2} - \tan^{-1} E\right)$$

U 4 Tougaard Background

An alternative approach to the Shirley background is computing background signal based on the Tougaard method.

The background $T(E)$ is computed from the measured spectrum $J(E)$, representing the photoelectron peak plus signal due to inelastic scattering of these photoelectrons by electrons within the sample, using the integral:

$$T(E) = \int_E^{\infty} F(E' - E) J(E') dE'$$

The integral is formed with additional information in the form of the Tougaard Universal Cross-Section that provides a means of modifying background signal in response to material properties of a sample. These material properties are input via a cross-section defined as follows.

$$F(x) = U(x{:}\,B, C, D, T_0) = \begin{cases} \dfrac{Bx}{(C - x^2)^2 + Dx^2} & x > T_0 \\ 0 & x \leq T_0 \end{cases}$$

One advantage of the Tougaard approach is the use of T_0 to delay the onset of background signal. The more powerful aspect of the Tougaard approach is the cross-section, when available, provides informed guidance for shapes within background signal. Figure 75 is an example of poly (styrene) (PS) where the cross-section parameters were determined by Tougaard for general polymer materials. The offset T_0 is adjusted to allow for a flat response beneath the primary photoemission peaks.

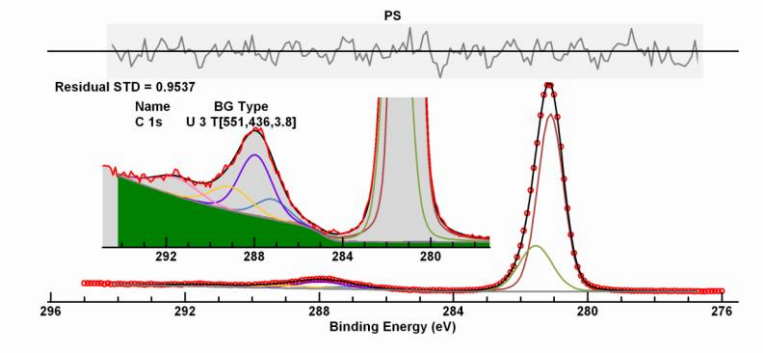

Figure 75. An application of a Tougaard background to poly(styrene).

Linear Background Types

There are a number of backgrounds based on straight lines.

The simplest of these backgrounds are horizontal straight lines where, as normal, the start and end are determined by the energy limits to the region and located with respect to the data using the intensity of data at these region limits.

There are two scenarios where a horizontal background is useful. The first is for materials with a significant band gap compared to photoelectron peak FWHM. That is, no change in background occurs beneath the peak envelope. The other scenario is where a curve is added to a peak model as a component representing background signal. The first example of Zr 3s (Figure 76) makes use of two component curves used to model background signal. One of these components makes use of the SB prefix to convert a bell-shaped curve to a Shirley background shape. The other is a trapezium line shape used to account for a sloping background modelling background signal from photoelectrons with kinetic energy greater than the Zr 3s peak. The background upon which these background-components sit is a Min Limits background type. A horizontal line is defined by the intensity computed for the start or end of the region that is the minimum of these two intensities. Depending on which end of the region defines the minimum the Start Offset or the End Offset parameters are used to shift the horizontal line away from the data.

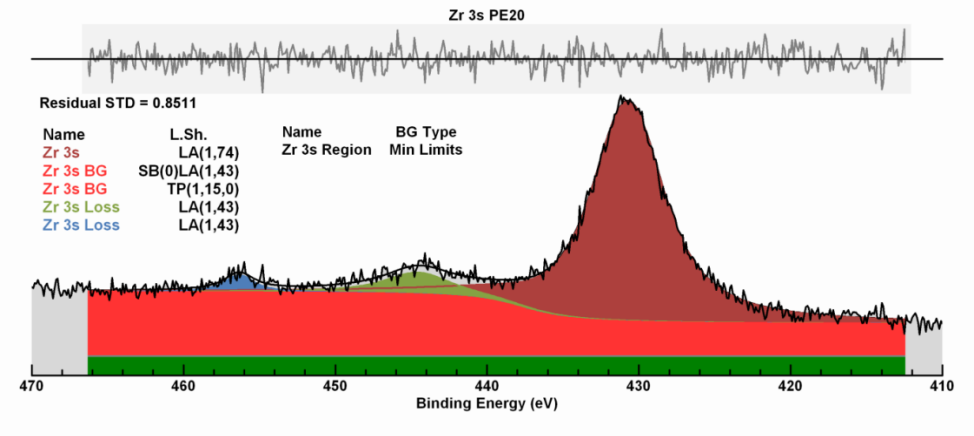

Figure 76. Zr 3s photoelectron peak modelled using a Voigt line shape (LA(1,74)) which is predominantly Lorentzian in shape. The response in the background due to the Zr 3s peak is offset in energy, and in this example is modelled using a component in the peak model SB(0)LA(1,43) representing a Shirley background that is determined by optimisation.

The peak model in Figure 76 makes use of LA(1,74) to create a Voigt synthetic line shape used to fit the primary Zr 3s photoelectron peak. A LA(1,43) Voigt line shape is used to model two loss structures for these data. The role of the two components in the peak model with line shapes SB(0)LA(1,43) and TP(1,15,0) is to allow optimisation to fit background shapes at the same time as the photoelectron peaks. The component with the line shape TP(1,15,0) allows for a linear approximation with a gradient to represent a trend in background as a consequence of Zr 3p photoelectrons and other photoelectrons with initially more kinetic energy than Zr 3s signal. Added to the TP(1,15,0) component is a Shirley shape calculated using the SB prefix applied to the same line shape as the Zr 3s component. The motivation for using a component to compute a Shirley

background is the Shirley component can be offset in energy from the photoelectron component which allows for a delay in energy-loss events for a material with a band gap (Figure 77).

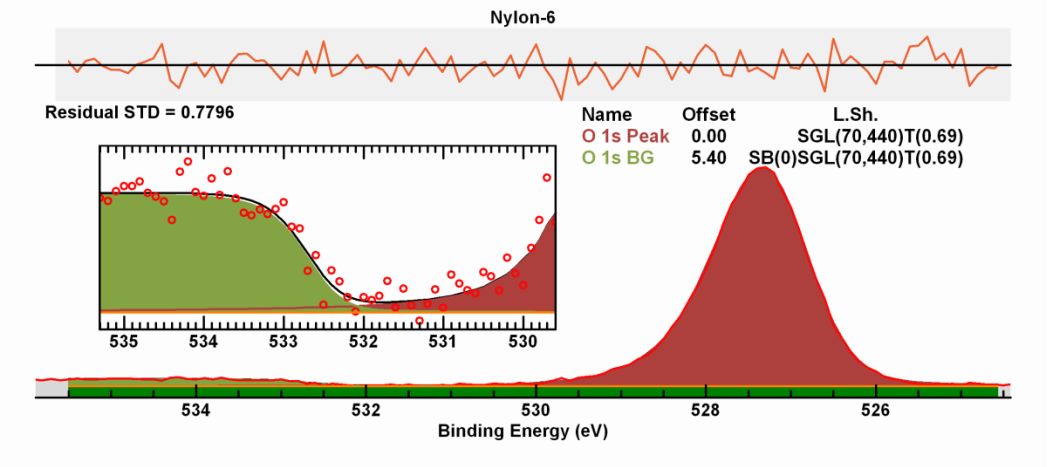

Figure 77. Nylon is a material with sufficiently wide band gap and narrow photoelectron peaks to illustrate where the step in background intensity due to the photoelectron peak occurs as a consequence of the band gap.

While a direct calculation of a Shirley background allows a comparable fit to Zr 3s (Figure 78), a background calculated from data necessarily follows the peak shape and therefore the rise in background occurs centred on the peak maximum. It is difficult to justify the location for a step in background computed by the Shirley algorithm for a material such as ZrO_2 for which a band gap of between 5 and 7 eV is expected.

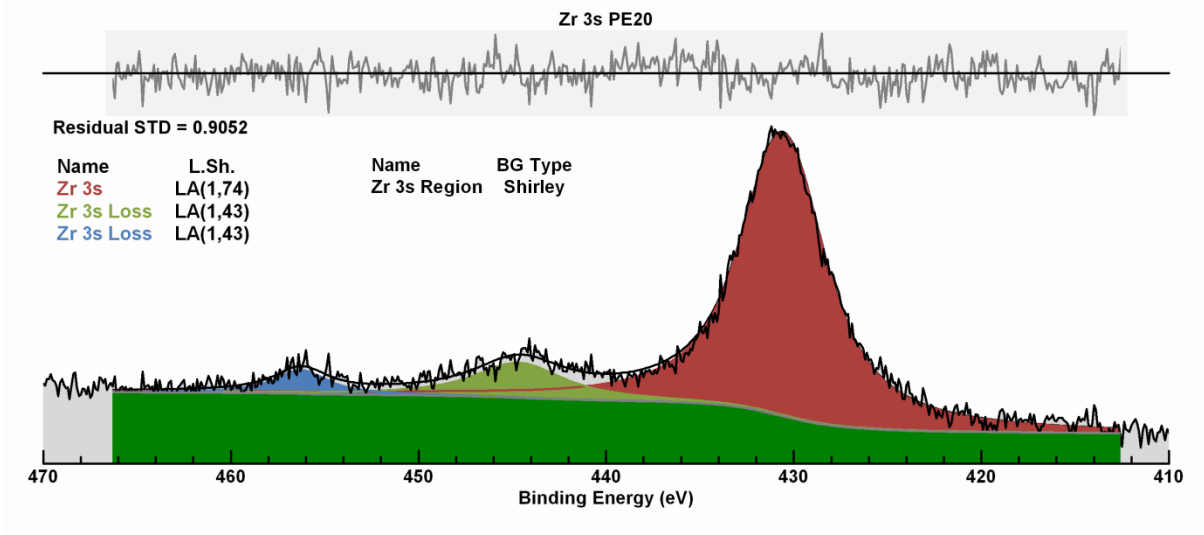

Figure 78. The spectrum in Figure 76 where the peak model is designed relative to a Shirley background calculated directly from data. Note that the step in the Shirley background is centred on the Zr 3s peak rather than offset in energy (Figure 76).

Goodness of Fit for a Peak Model

A peak model is constructed from one or more synthetic component curves. The sum of all synthetic components for a peak model yields a synthetic envelope intended as an approximation to spectral

data. During optimisation component parameters are adjusted until the synthetic envelope matches closely with spectral data. The final synthetic envelope determined by optimisation algorithms is selected as the best approximation to spectral data based on a figure of merit. The figure of merit is calculated from differences between spectral intensity and synthetic envelope at each data bin in a spectrum. The outcome for a sequence of optimisations steps may differ depending on the figure of merit used during optimisation, but regardless of outcome a unifying statistic for all figure-of-merits is the computation of the residual standard deviation supported by visual inspection via a residual plot.

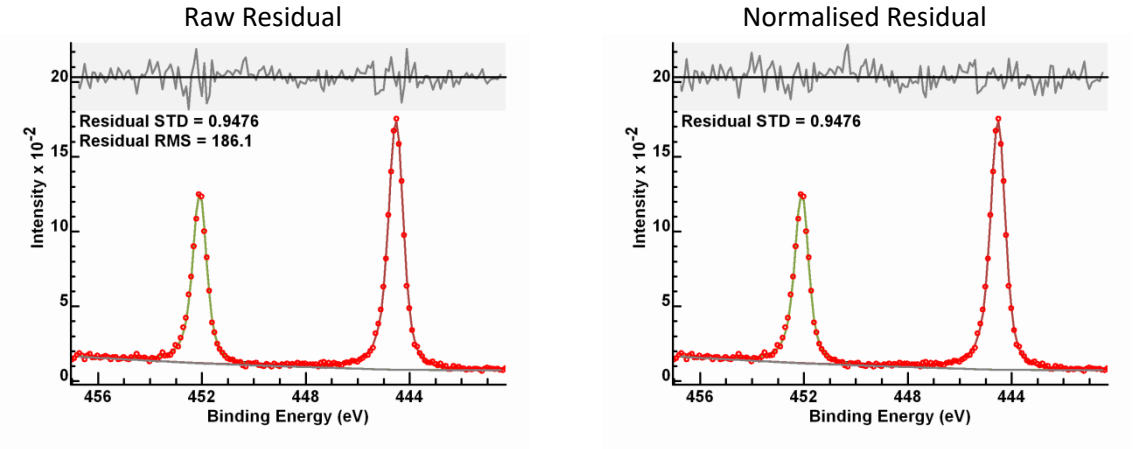

Figure 79. The residual for a peak model fitted to a spectrum is displayed either with or without normalisation to the standard deviation expected for pulse counted data. For pulse counted data, the noise scales as the square root of the counts per data bin. Therefore, the raw residual plot appears to vary more in the vicinity of the peak maximum than compared to the normalised residual.

The residual is the difference between a synthetic envelope and signal for each data bin. The residual may be plotted in a raw state without any scaling or alternatively is plotted in a, so called, normalised form where the expected standard deviation for intensity in each data bin is used to scale raw residual differences (Figure 79). The objective in plotting a normalised residual is to remove, from the residual, variations that result from amplification due to noise characteristics in data. If performed correctly, a normalised residual when plotted has the appearance of uniformly distributed variations about zero. Without normalisation, pulse counted data typical of XPS would result in a residual with variations that increase in amplitude in the proximity of intense signal, such as for peak maxima, compared to low intensity intervals, such as background signal near to a peak. These variations in the residual are well defined for data recorded using a pulse counting detector, provided data are not modified by smoothing or other processing prior to fitting with a synthetic envelope.

For pulse counted data the residual standard deviation is close to unity (Figure 80). The caveat to relying on a single statistic to measure goodness-of-fit is not all XPS data are presented as spectra without processing. Data collected from a single data detector are more likely to be raw counts, but data recorded using multiple detectors to acquire signal in parallel when presented as a single spectrum represents processed data rather than raw counts per bin. For this reason, most modern instruments generate spectra with noise suppressed and the target for optimisation is a residual standard deviation less than unity.

It is also possible data are scaled as part of acquisition processing steps resulting in standard deviation significantly greater than unity. It is therefore advisable to determine the target residual standard deviation for a particular instrument and for a particular mode used to collect data. A simple test can be performed for spectra that include an energy interval representative of background signal. Placing a region on an energy interval typical of background signal using the background type Regression computes a straight-line approximation to data fitted in a least squares sense (Figure 81). Observing the residual standard deviation for the region provides the target value when synthetic components are fitted to data.

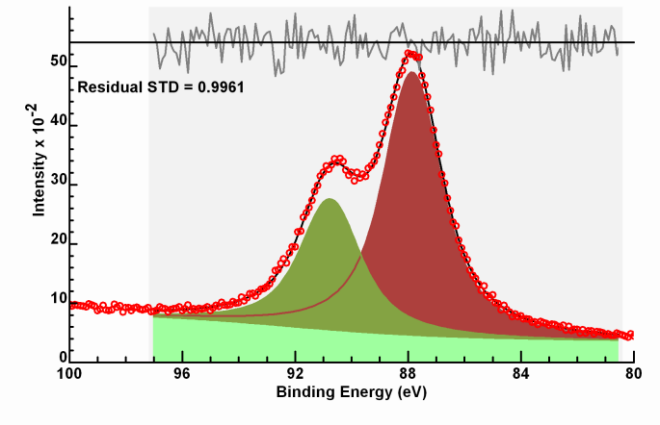

Figure 80. A peak model fitted to pulse counted data returning the expected residual standard deviation and a normalised residual-plot which confirms that the fit to data is consistent over the entire interval used to optimise the parameters available to the peak model during fitting.

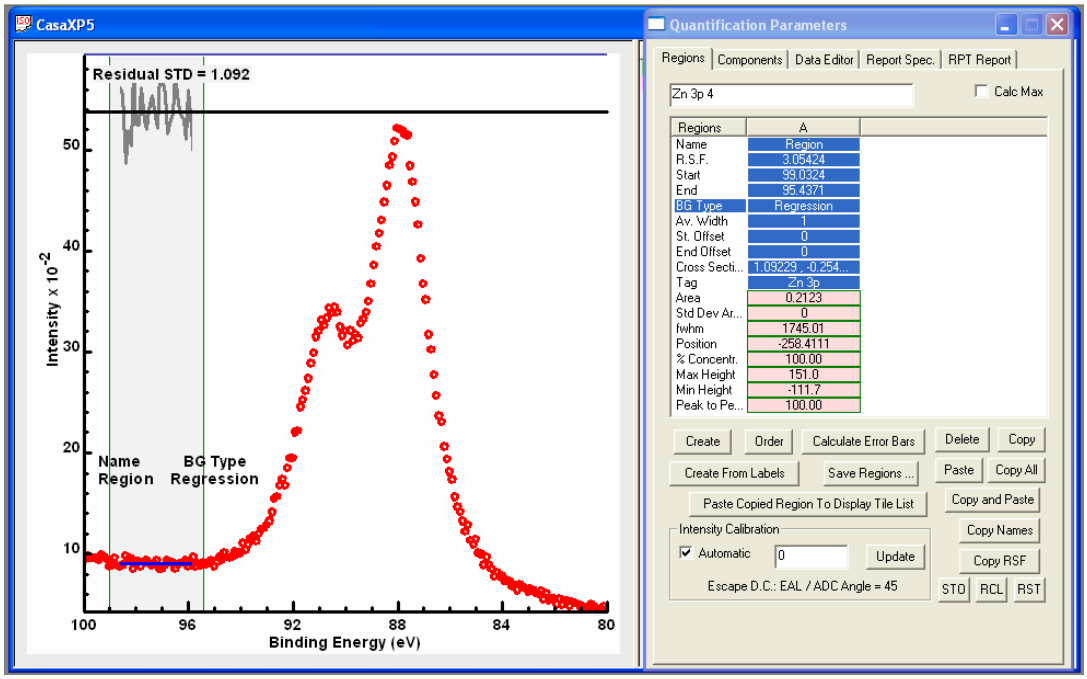

Figure 81. The Regression background type is used to estimate the expected residual standard deviation for these specific data. A linear approximation fitted to background signal results in a residual statistic that suggests the target statistic for fitting of the peak model in Figure 80 to these data.

Examples of Peak Models using Synthetic Line Shapes

Germanium Oxide Film on Germanium

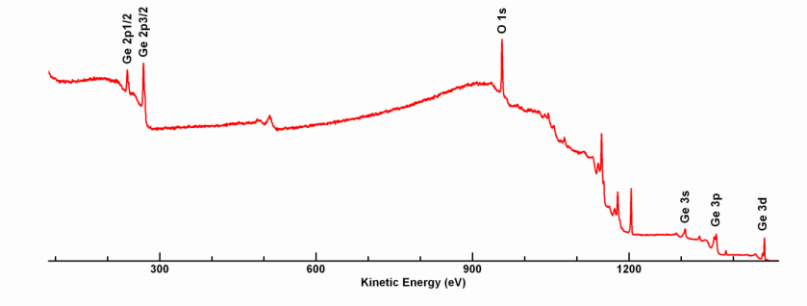

Figure 82. Survey spectrum in which photoelectron peaks are labelled for germanium and oxygen. The use of kinetic energy for the abscissa is to illustrate the wide range in energy between Ge 2p and Ge 3d. The rate of inelastic scattering of photoelectrons is influenced by the kinetic energy of electrons.

Germanium oxide films on germanium provide a vivid illustration of the effects of inelastic scattering on escape depth for photoelectrons and how escape depth changes as a function of energy. Two photoemission peaks due to Al Kα X-rays appear in the energy spectrum at opposite ends of the energy range (Figure 82). Chemical shifts between elemental and oxide peaks allows separation of signal for Ge 3d and Ge 2p doublets, however for films of germanium oxide with thickness sufficiently thin, the relative intensity for elemental and oxide peaks when measured using Ge 2p and Ge 3d data varies as a function of film thickness due to sampling depth differences for electrons with kinetic energy corresponding to these two binding energies for core level photoemission (Figure 83). Ge 2p is more surface sensitive due to the low kinetic energy for these photoelectrons. An oxide film at the surface means photoelectrons from the oxide are only scattered by oxide atoms. Elemental signal is scattered by the oxide overlayer and the bulk elemental germanium, thus elemental signal is attenuated differently from the oxide. The relative proportions of signal from oxide and elemental germanium measured (Figure 84 and Figure 85) using Ge 2p is greater than the same ratio measured using Ge 3d signal (Figure 86). The greater sampling depth available to Ge 3d allows a greater proportion of elemental signal without energy loss.

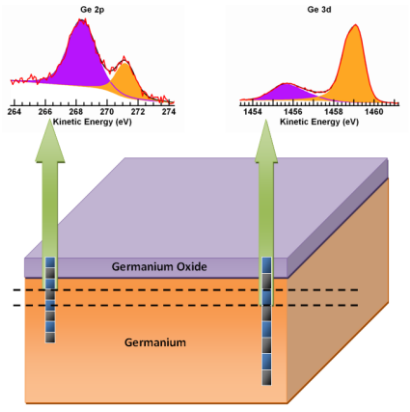

Figure 83. Ge 2p and Ge 3d spectra measured from a sample of germanium with a thin film of germanium oxide. The ratio of oxide to elemental germanium alters in intensity due to the influence of kinetic energy on escape depth for Ge 2p and Ge 3d spectra.

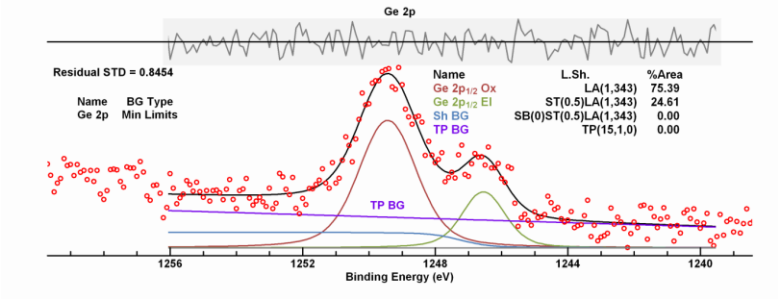

Figure 84. Peak model for Ge $2p_{1/2}$ photoelectrons designed to estimate the relative proportion for oxide signal to elemental signal. The rising background and the Shirley-like response in the background to inelastic scattering of elemental Ge $2p_{1/2}$ are modelled using components to the peak model that are fitted together with components representing zero-loss photoelectron peaks.

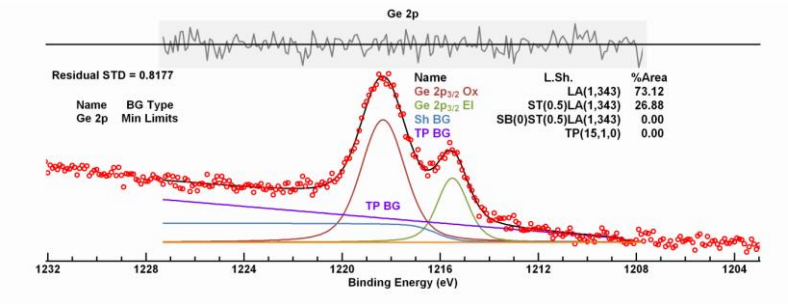

Figure 85. Peak model for Ge $2p_{3/2}$ photoelectrons designed to estimate the relative proportion for oxide signal to elemental signal. The rising background and the Shirley-like response in the background to inelastic scattering of elemental Ge $2p_{3/2}$ are modelled using components to the peak model that are fitted together with components representing zero-loss photoelectron peaks.

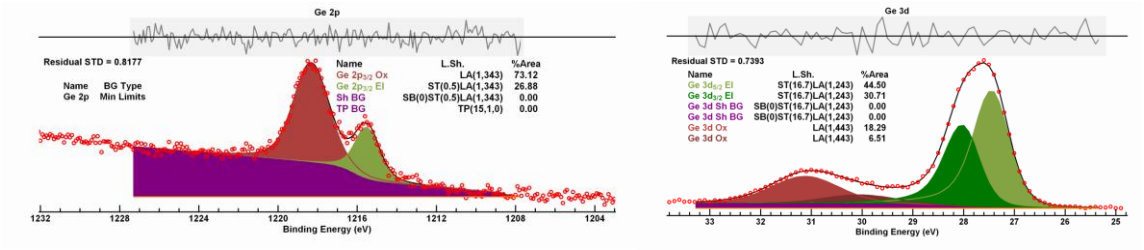

Figure 86. Ge $2p_{3/2}$ and Ge 3d photoelectron peaks with peak models fitted to data to estimate the proportions of elemental and oxide signal recorded by XPS for two photoelectron peaks differing in kinetic energy as shown in Figure 82. The reversal in ratio for elemental and oxide composition of the same sample is due to the energy dependence of escape depth illustrated in Figure 83.

Polymer Peak Model

Polymer data is arguably the most fruitful ground for XPS and chemical state analysis by fitting sets of components to data envelopes. A feature of polymer spectra is photoemission from limited numbers of elements with simple photoemission peak shapes provides evidence of chemical state, and correlating signal in different chemical state between elements is often possible. These correlations between carbon, oxygen and nitrogen in a material such as PVP (Figure 87) are an important part of justifying a peak model.

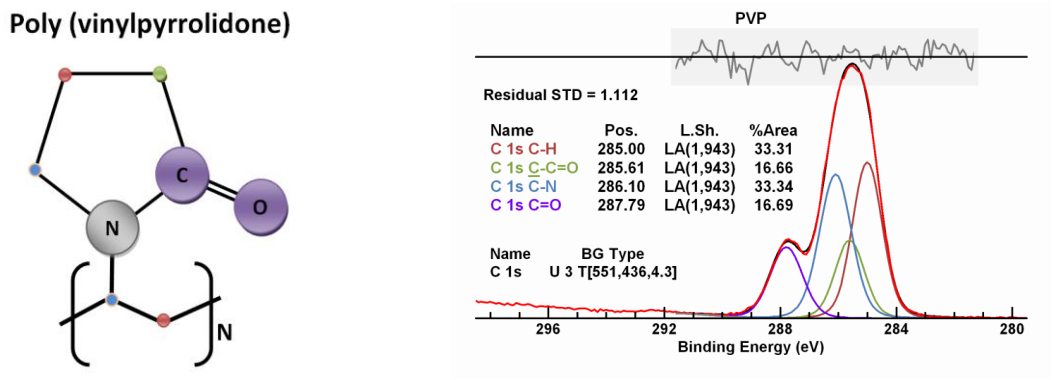

Figure 87. Expected chemistry of PVP and the XPS of PVP. A peak model for C 1s composed of four bell-shaped curves with appropriate constraints mirrors the chemistry expected for PVP through correlating the number of carbon atoms in these four chemical states to the relative intensities of components offset in energy by variation in bond-state for carbon atoms.

The example now used to illustrate a typical peak model for a polymer material is carefully chosen to illustrate how C 1s spectra can be fitted with many components. However, the use of many components while yielding good data reproduction does not result in good science unless there is a means to justify the use of each component and components are constrained to ensure optimisation creates meaningful outcomes. A spectrum measured as part of a sputter depth profile from a material constructed from layers of poly (styrene) (PS) and Poly (vinylpyrrolidone) (PVP) offers a surface composed of PS, PVP and potentially sputter-damaged fragments or X-ray damage bye products. A C 1s spectrum measured from the surface represents a data envelope for which (if we assume no sputter or X-ray damage) ten synthetic components can be justified based on these two polymers PS and PVP (Figure 88).

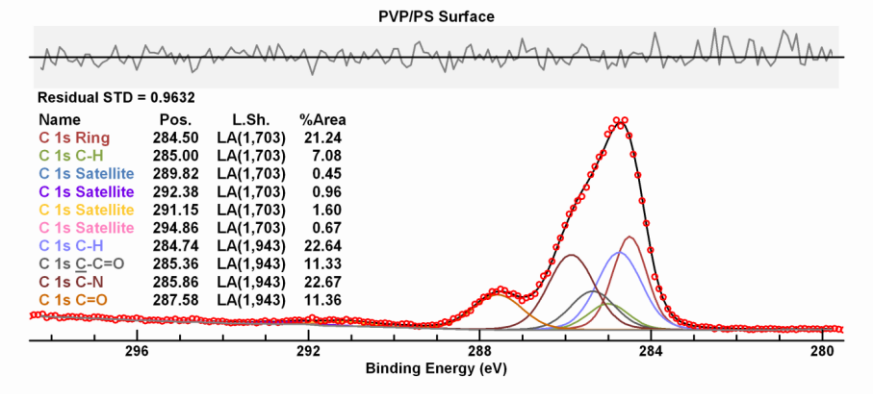

Figure 88. Peak model for the surface chemistry of the sample composed of PVP and PS.

Without constraints between parameters used to fit ten component peaks to spectra of the form in Figure 88, nonlinear optimisation should not be trusted to return physically meaningful results. Therefore, the peak model for spectra from the PS/PVP surface is constructed by first fitting spectra representative of PS and PVP with components making use of Beamson and Briggs XPS of Polymers Database to support these two peak models. The sputtered surface yields C 1s data for which the two spectra measured from PS and PVP surfaces within the depth profile can be used as estimates for spectra representative of PS and PVP. These spectra selected from the data set comprising a

depth-profile are used as basis spectra in a linear least square (LLS) fit to spectra from each cycle of the depth-profile in which the sample surface is a blend of PS and PVP. For each cycle of the depth-profile, all ten components are scaled by the LLS fit and copied to the PS/PVP spectrum (Figure 89) resulting in a peak model containing ten synthetic components justified by these data analysis steps.

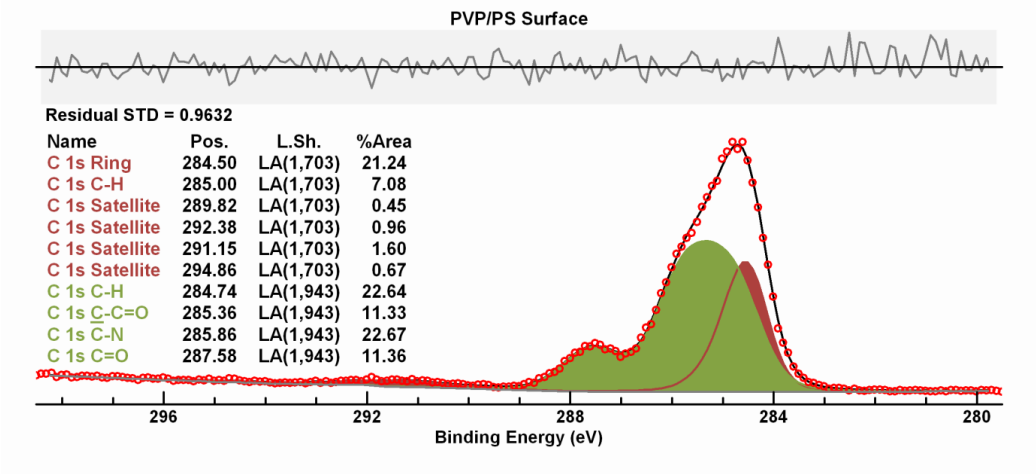

Figure 89. A peak model nominally formed using ten components, but which is constructed from components constrained by their relationships to PVP and PS basis spectra. These PVP and PS basis spectra are fitted with four and six components, respectively, then the basis spectra are fitted to the spectrum in the LLS sense. Therefore, the peak model containing ten components is effectively a peak model containing two ensembles of components that are constrained to the chemistry of PVP and PS.

It is worth noting PS (Figure 90) and PVP in principle both include C-H C 1s signal. One might expect a single C-H component with identical binding energy for these two equivalent peaks within the model for the PS/PVP sputtered surface. However, the peak model contains component peaks consistent with PS and PVP, but there is evidence within the sputter depth profile that charge compensation used during acquisition does not achieve uniform results throughout the profile and when sputtering yields a mixed PS/PVP surface these two polymers may not respond identically to the charge compensation. The charge correction offset applied to these data is based on aligning the C-H component in PS to binding energy 285 eV. The binding energy values computed for these components assigned to known chemical state in PS and PVP suggest there may be other factors at play within the sample at the point in the depth profile C 1s signal is measured.

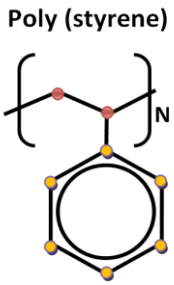

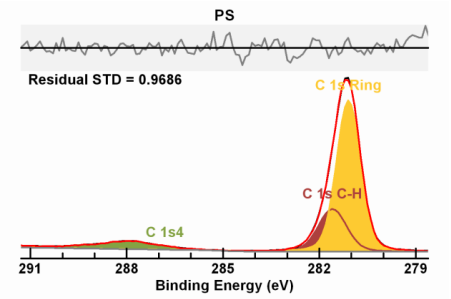

Figure 90. Peak model designed to mimic the chemistry of poly (styrene).

The sputter depth profile was performed to investigate different strategies for making use of an argon cluster ion gun when profiling polymer samples. While successful in this goal, these data are not ideal for chemical state determination by fitting synthetic components to C 1s spectra. These C 1s spectra were measured using pass energy 40 eV on a Kratos Axis Supra. The energy resolution is enhanced by the use of the 110µm selected area aperture, but may still be insufficient to rely fully on binding energy to make definitive assertions regarding chemical state. Nevertheless, the peak model is certainly suitable for profiling the multilayer sample in terms of depth resolution (Figure 91).

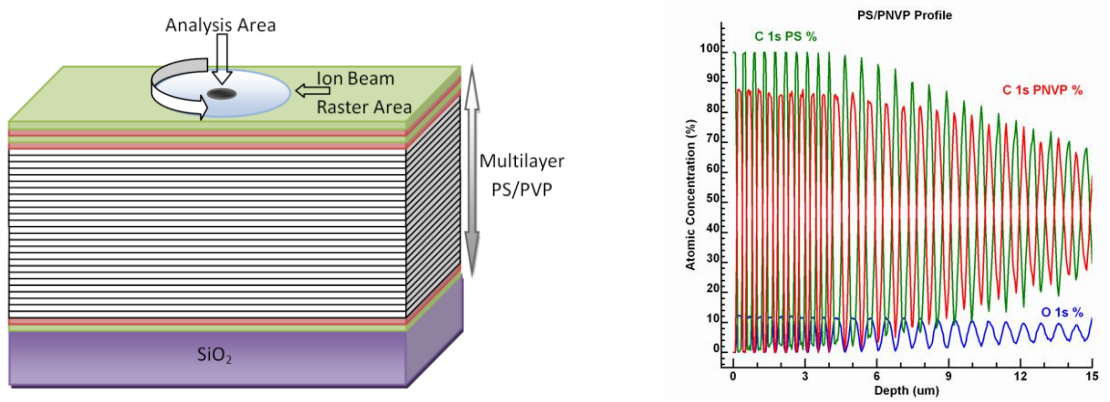

Figure 91. Idealised model for the multilayer PS/PVP sample and the corresponding depth profile obtained by the method used to construct the peak model in Figure 89.

A consistency test for the analysis of C 1s is the behaviour of O 1s throughout the profile compared to PVP signal measured by C 1s. Since PS does not contain oxygen, O 1s intensity and PVP C 1s intensity should demonstrate identical depth resolution throughout the sputter depth profile (Figure 91).

XPS of Ionic Liquids

When modelling photoelectrons with narrow peaks, instrumental energy resolution plays an important role in modelling data with synthetic components. There are however many materials for which sample chemistry dictates the width of photoemission peaks and also line shapes are not limited by instrumental artefacts, but rather properties of the sample. Ionic Liquids (IL) are an example of where instrumental energy resolution is not the limiting factor and component FWHM are typically broad compared to the energy resolution of an instrument. Data presented in Figures 92-98 were measured using pass energy 20 eV in Hybrid lens mode making use of the full slot width on a Kratos Axis Ultra. The FWHM of Ag $3d_{5/2}$ for an Axis Ultra operating in this mode is expected to be close to 0.58 eV. The range of FWHM for components within these peak models for two different ILs (Figure 92 and Figure 95) are broad by comparison suggesting sample properties are determining the width and, most likely, the shape for these photoemission peaks.

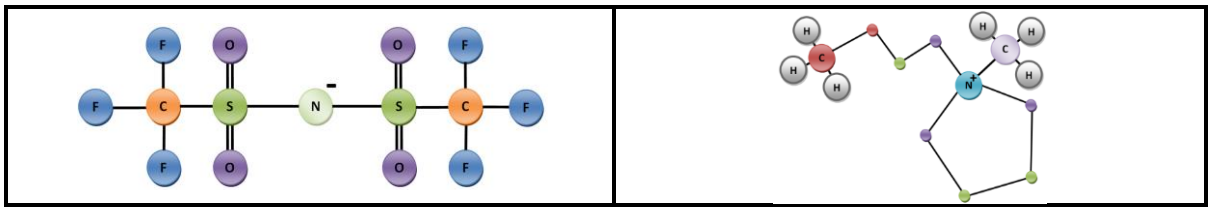

Figure 92. $[TF_2N][C_4C_1Pyrr]$.

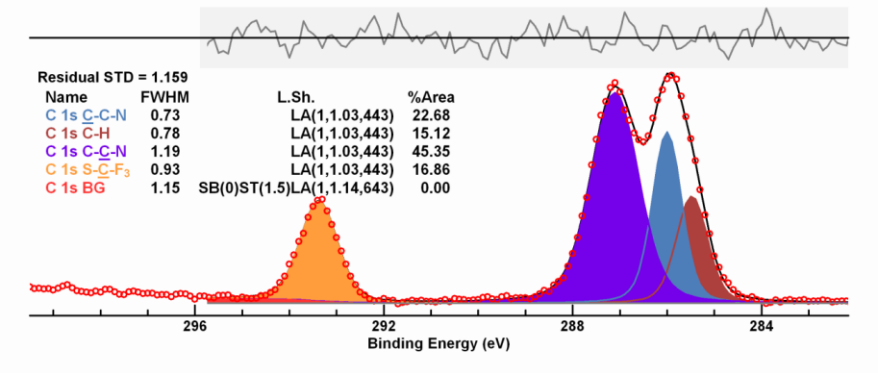

Figure 93. Peak model for C 1s photoelectrons emitted from $[TF_2N][C_4C_1Pyrr]$.

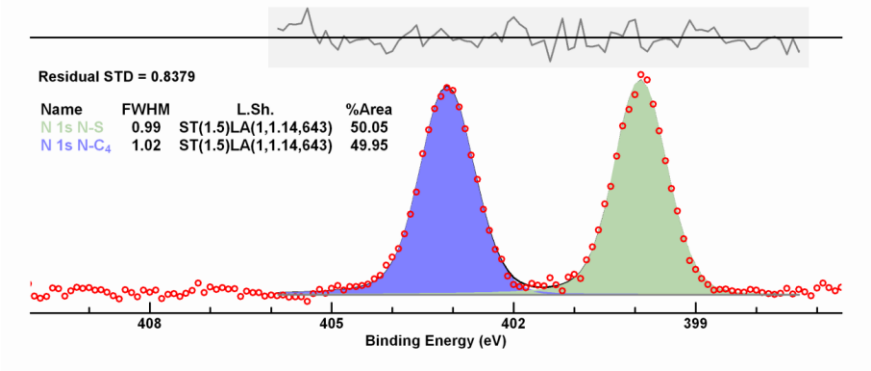

Figure 94. Peak model for N 1s photoelectrons emitted from $[TF_2N][C_4C_1Pyrr]$.

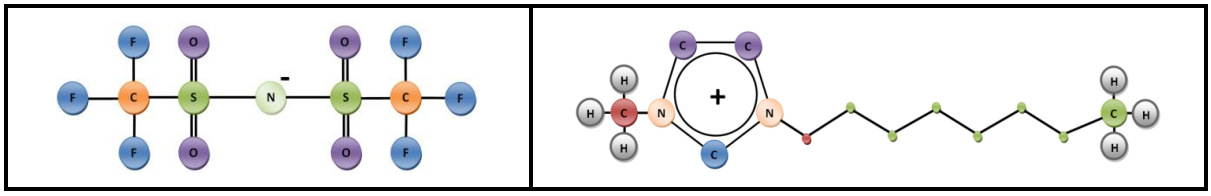

Figure 95. $[TF_2N][C_8C_1m]$.

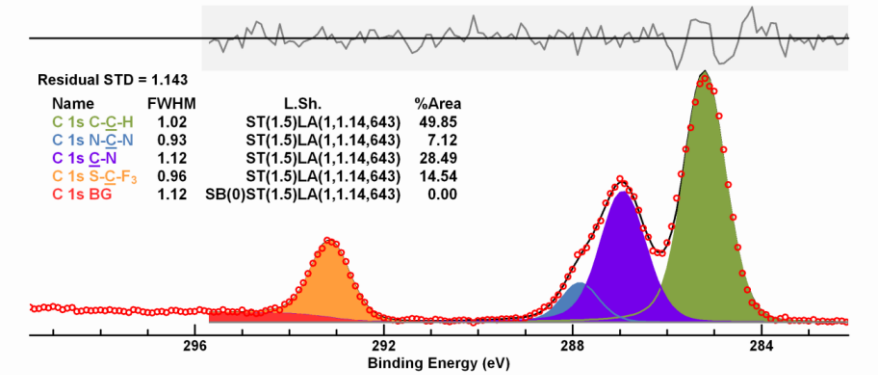

Figure 96. Peak model for C 1s photoelectrons emitted from $[TF_2N][C_8C_1m]$.

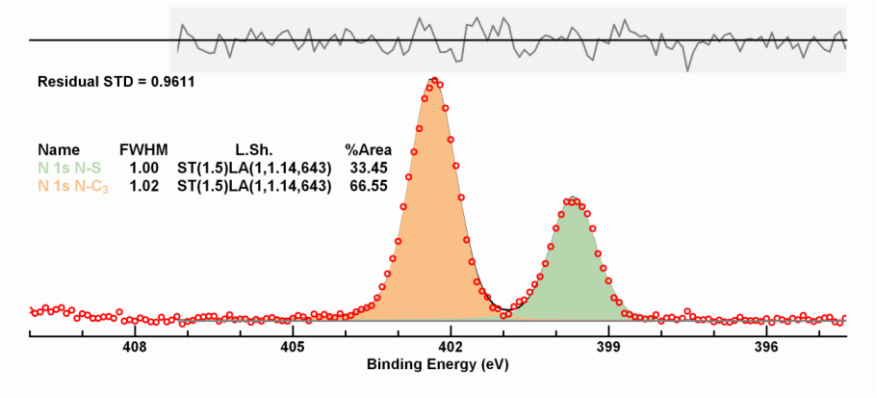

Figure 97. Peak model for N 1s photoelectrons emitted from $[TF_2N][C_8C_1m]$.

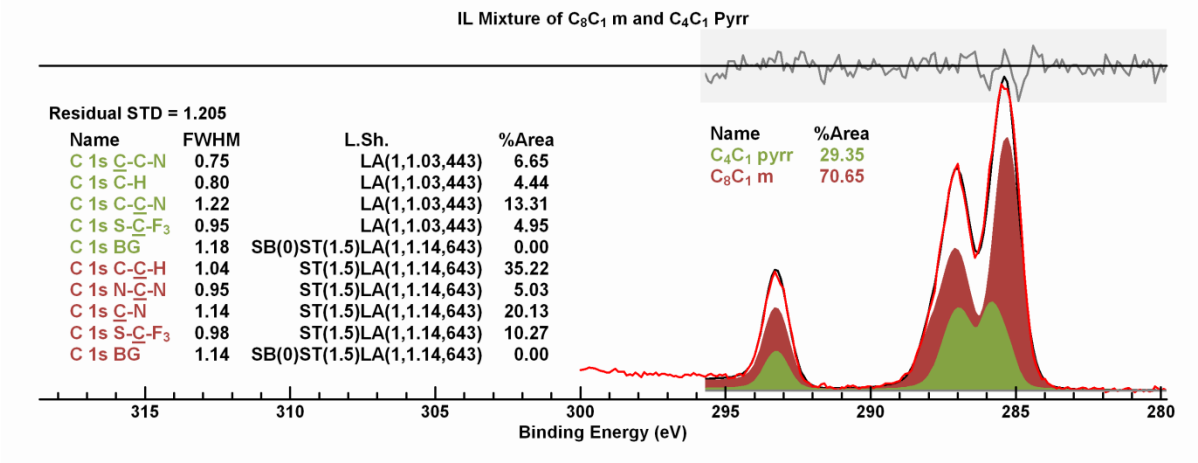

Figure 98. Peak model for C 1s photoelectrons emitted from a mixture of $[TF_2N][C_4C_1Pyrr]$ and $[TF_2N][C_8C_1m]$.

Silver on Silicon Wafer

Deposition of silver on a silicon wafer provides an example of where XPS offers information about a sample in terms of material distribution (Figure 99). Combining information from survey measurements with high energy resolution data fitted with synthetic components suggests the deposition of silver formed island-type covering of a silicon wafer rather than a uniform thin film. The three clues to the relationship between silver and the silicon wafer are:

1. The background intensity relative to silver peaks in survey measurements is approximately constant as the amount of silver relative to silicon increases (Figure 100).
2. The ratio of Ag $3p_{1/2}$ and Ag 4p is independent of amount of silver relative to silicon (Figure 101).
3. Peak models prepare from silver and a silicon wafer, including background components fit pass energy 20 spectra with equal precision over the range of samples with varying silver to silicon composition (Figures 102 – 105).

These statements are consistent with an interpretation that silver is added to the silicon wafer so that islands of silver are formed of depth greater than the sampling depth for electrons emitted from silver by Al Kα X-rays.

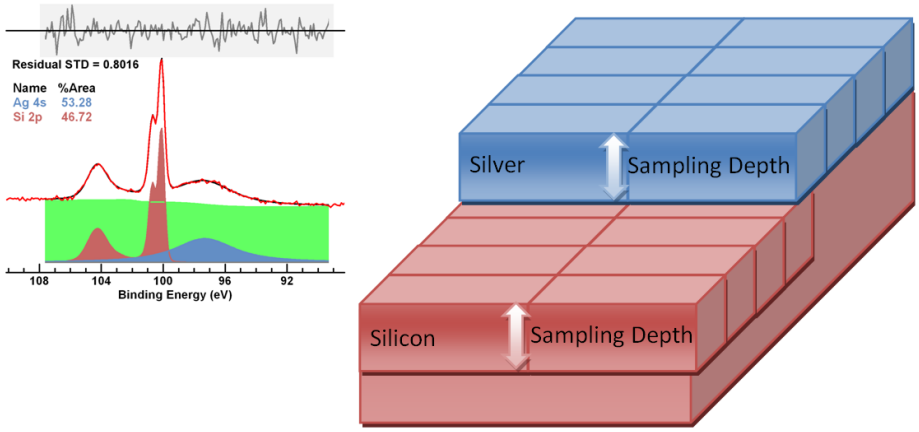

Figure 99. A feasible peak model for a sample containing silver and silicon suggests the sample is formed by a substrate of silicon and islands of silver of thickness greater than the sampling depth of XPS for photoelectrons corresponding to Ag 4s and Si 2p kinetic energies.

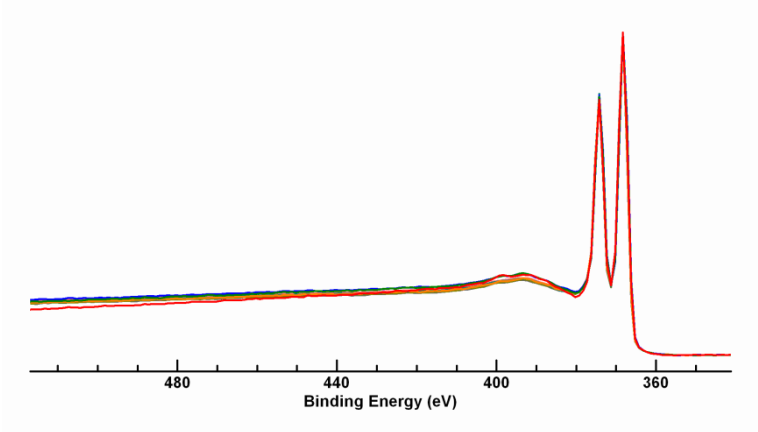

Figure 100. Uniform response in the background to lower kinetic energy for Ag 3d photoelectrons suggests the silver is of sufficient thickness to be considered by XPS as a bulk material.

XPS is a surface sensitive technique since 95% of signal originates from within the first three effective attenuation lengths (EAL). For Al Kα X-rays three EALs for electrons with kinetic energy 1486.6 eV in silver is about 6.3 nm. The processes that limit XPS photoemission without energy loss to the outer layers determines the shapes observed in background signal. These shapes in background signal change for a thin film compared to a bulk material. A consistent relationship observed via Ag 3d photoemission for samples with differing amounts of silver compared to silicon represents circumstantial evidence these films act as bulk materials independently of the relative proportions of silver and silicon. The implication is silver is greater in depth than three EALs. If silver is sufficiently thick, no silicon signal of significance emerges from locations where silver is present.

Another consequence of escape depth limitations for photoemission is as follows. The ratio of photoemission peaks with significantly different kinetic energy from the same element in overlayer materials with identically uniform film thickness should be constant. The ratio of two photoemission peaks such as Ag $3p_{1/2}$ and Ag 4p should be identical for films of equal thickness,

and thin films of less than one effective attenuation length (EAL) the ratio should be noticeably different from a film of greater than the sampling depth equivalent to three times the EAL. The set of samples in this experiment yield identical ratios for these two silver photoemission peaks independently of the amount of silver per sample.

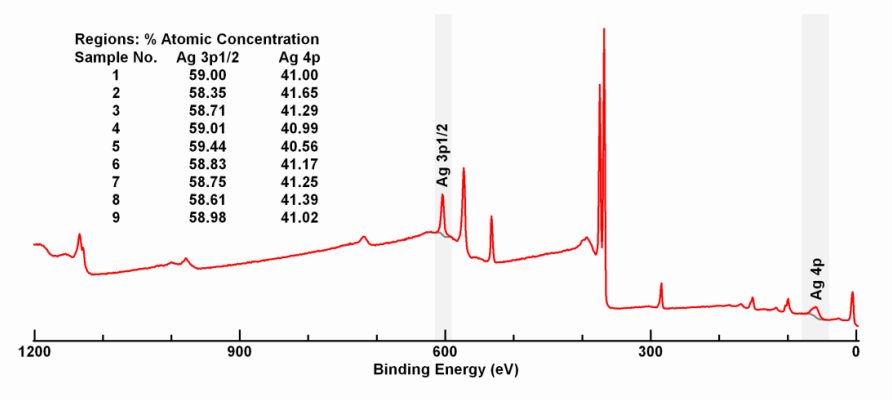

Figure 101. Nine samples prepared with differing amounts of silver on silicon when the percentage atomic concentration calculation is performed using two photoelectron peaks from silver yield similar proportions independently of the amount of silver. The implication from these results is that the thickness of silver on silicon is the same for all samples.

The basis for a peak model is often the use of synthetic components designed and fitted to data of similar origin to the spectra of interest. Access to XPS databases provides the means of understanding potential shapes for a bulk silver sample, and constructing a peak model for these standard data offers insight in addition to insights gained from sample data. Ag 4s and Ag 4p data are from the La Trobe XPS database. The insight from these spectra is that fitting a single component to Ag 4s, while seemingly plausible, is demonstrated by use of these database spectra to be an over simplification. Background signal from Ag 4p plays a role when fitting Ag 4s spectra.

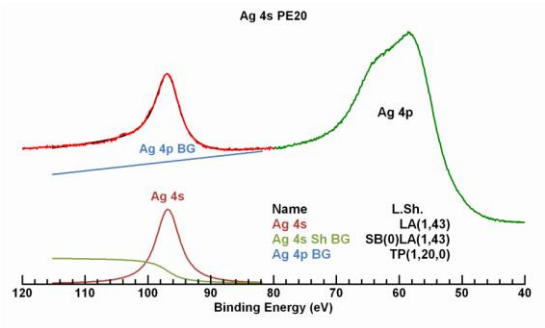

Figure 102. Peak model prepared for Ag 4s using spectra from sputter cleaned silver foil.

Similarly, measuring the silicon wafer before deposition of silver is of equal value to Ag 4s/Ag4p database spectra when attempting to understand samples with both silver and silicon signal within spectra.

The third piece of circumstantial evidence pointing to possible silver islands on silicon is via a model constrained to follow these two relationships for photoemission and background from

bulk silver, combined with the initial silicon wafer peak model. Models defined in terms of these known materials when applied to samples with unknown composition over the Si 2p/Ag 4s energy interval produce a precision that is expected for pulse counted data (Figure 104 and Figure 105). The quality of the fit and the construction of the model suggest silicon and silver signal from the unknown samples derive from different locations within the analysis area. If silicon is buried beneath an overlayer of silver of varying silver thickness, then one might expect silicon to contribute to the background with different shapes from silicon located at the surface. These peak models and the quality of fit to each spectrum would suggest little change to silicon background-intensity therefore these samples when measured by XPS behaves similarly to bulk silicon.

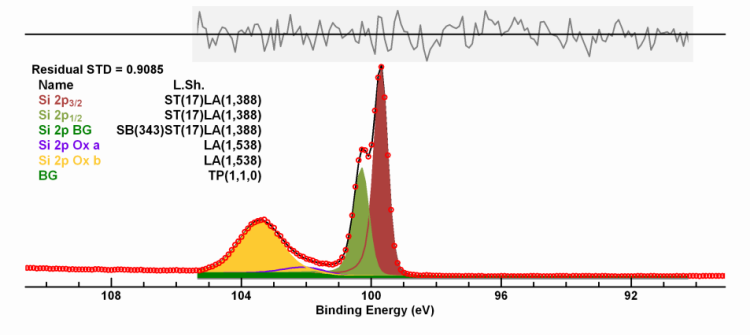

Figure 103. Peak model constructed for Si 2p spectrum measured from a silicon wafer.

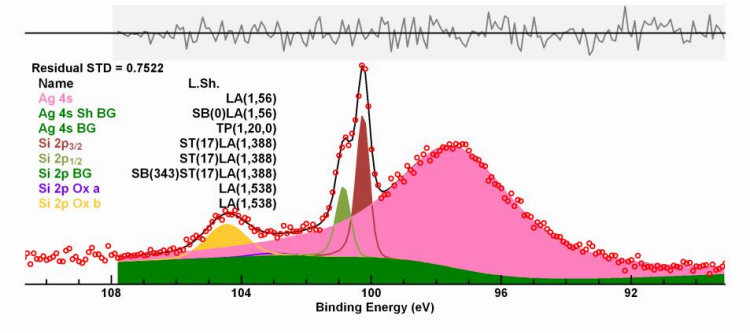

Figure 104. Peak model constructed for Ag 3s/Si 2p spectrum measured from a silicon wafer with silver deposited with greater concentration than Figure 105.

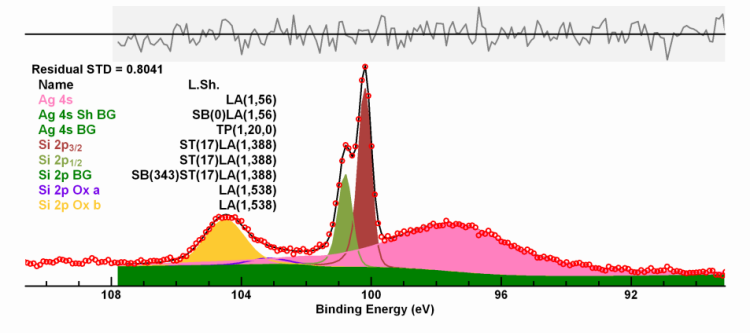

Figure 105. Peak model constructed for Ag 3s/Si 2p spectrum measured from a silicon wafer with silver deposited with lesser concentration than Figure 104.

A peak model in isolation would not be sufficient to assert an island structure for silver with islands of depth greater than the sampling depth for silver. The peak models presented here are offered as the preferred solution out of a set of peak models capable of acceptable data reproduction. Uniqueness of solution is often a problem when fitting data by means of synthetic components, but none of the alternative models were consistent with results obtained from survey spectra. When preparing a peak model, the use of survey data to support the number and type of components should be considered as essential.

Other interpretations of these XPS data are certainly possible. Indeed, these three observations are not necessarily conclusive, but rather suggest directions for further measurements from these types of samples.

Gold 4d Doublet: Choosing between Count Rate or Data Quality

Curve fitting XPS data is the task of selecting shapes that when summed best fit a data envelope. A key factor for successful curve fitting is the use of the most appropriate curve shapes for data of interest. An alternative perspective is to consider how to acquire data that assists in identifying the most appropriate curve shapes. Ideally data should be recorded with highest signal-to-noise and highest quality. Highest signal-to-noise means measuring for a length of time appropriate for the intrinsic count-rate for a particular photoemission line and operating an instrument in a mode optimised for counts recorded. Quality of data means shapes recorded for any given operating mode are representative of the shapes generated by the photoemission process. Unfortunately, collecting the maximum counts for a given photoemission process involves compromises in terms of signal quality. Essentially, gathering more electrons emitted from a sample requires larger apertures, less refined use of lenses and the use of detectors placed in sub-optimal locations with respect to the ideal detector position for an HSA. Hence, choices must be made prior to acquisition-of-data that affect the outcome when chemical state is sought via curve fitting.

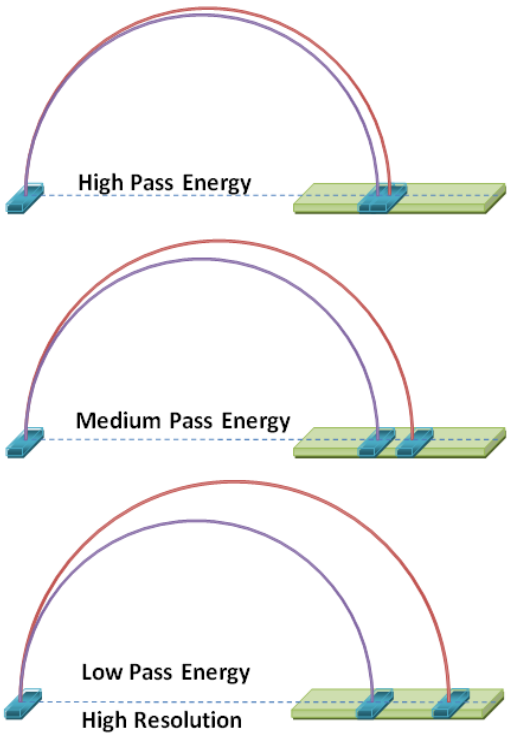

Figure 106. Given a source of electrons with only two discrete energies E_1 and E_2 focused to form paraxial trajectories entering the HSA, assuming the retarding lens system matches energy E_1 to the HSA pass energy then an image of the entrance slot is projected onto the detector plane in two locations. These images in the detector plane vary in spatial offset in the energy dispersive direction depending on the pass energy for the HSA. Detectors arranged in the energy dispersive plane record signal from these two images with meaning in terms of energy dependent on pass energy. The energy interval equivalent to the image of the entrance slot scales in proportion to pass energy. When electrons enter the HSA with less than ideal trajectories the image of the entrance slot is less well defined and as a consequence uncertainty is introduced into the allocation of signal to energy. As a result, energy resolution and line shape depends on pass energy, entrance slot aperture width and effective width for each detector located at the exit to the HSA.

Instrumental design determines the underlying shape that is recorded for a given photoemission line. The two parameters that can be changed between measurements are the width of the entrance aperture and, more commonly, the pass energy for the HSA (Figure 106). When changing the pass energy, the effect is to amplify or suppress the distortions to line shapes introduced by instrumental design. The higher the pass energy the less dispersed in energy are electrons entering the HSA and the more instrumental artefacts enter the shapes recorded for photoemission lines. The lower the pass energy the greater the dispersion in energy allowing each detector to record electron energy with better precision and therefore superior quality in line shape is achieved (Figure 107).

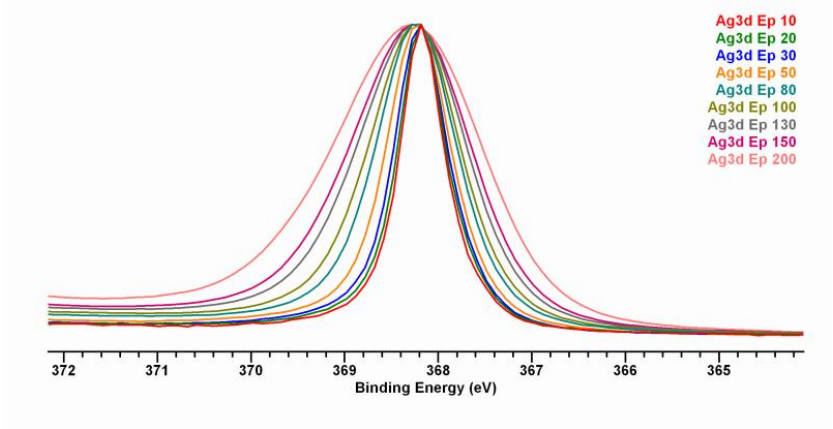

Figure 107. Plot of normalised Ag $3d_{5/2}$ spectra measured using a range of pass energies (Ep). Increasing the pass energy increases the count rate, but owing to the loss of energy resolution, deforms the shape of the peak. What appears when measured using pass energy 10 eV mostly Lorentzian, progressively becomes less open to the use in a peak model of a Lorentzian line shape.

When selecting the pass energy for acquiring spectra it is therefore useful to understand the consequences of this choice for data quality and, for a given data quality, the efficacy of a peak model in determining chemical state.

The importance of data quality is related to the ability to define synthetic line shapes capable of modelling specific photoemission processes. The use of synthetic line shapes close in shape to the true shape for a photoemission line is a significant help when fitting these shapes to data by mathematics. However, depending on the underlying line shapes, data quality from a mathematical point of view changes in importance. For narrow photoemission-lines data quality is of greater importance. That is, deformations of narrow peaks by instrumental factors represent a greater proportion of shape information in data. For broad peaks where signal varies more slowly and instrumental influences on shape is a lower proportion of the final shape, data reproduction by synthetic line shapes is often achieved with greater ease. Hence for broad photoemission lines data quality is of lesser importance.

The pass energy used to acquire spectra must be appropriate for all photoelectron lines measured from a sample and provide a correct quality of data to allow chemical state determination by curve fitting.

Gold 4d photoemission is an example of a broad doublet for which the principal difference between data collected using pass energy 40 and 50 on a Thermo K-Alpha+ (University of Cardiff) is reduced

intensity for PE 40 compared to PE 50. In terms of fitting Au 4d data, an identical peak model yields almost identical results (Figure 108).

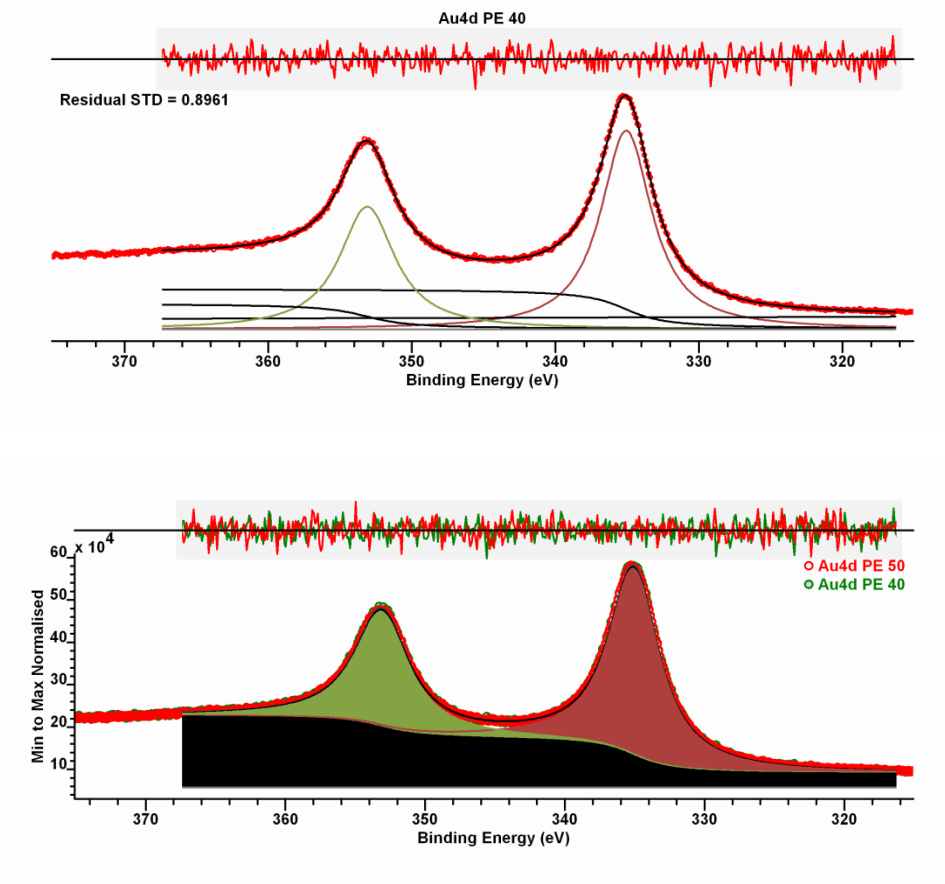

Figure 108. Owing to the width of the underlying line shape for Au 4d spectra, a peak model developed for an Au 4d spectrum measured using pass energy 40 eV can be applied to the equivalent spectrum measured using pass energy 50 eV with similar success to the pass energy 40 eV spectrum.

C 1s Nylon-6

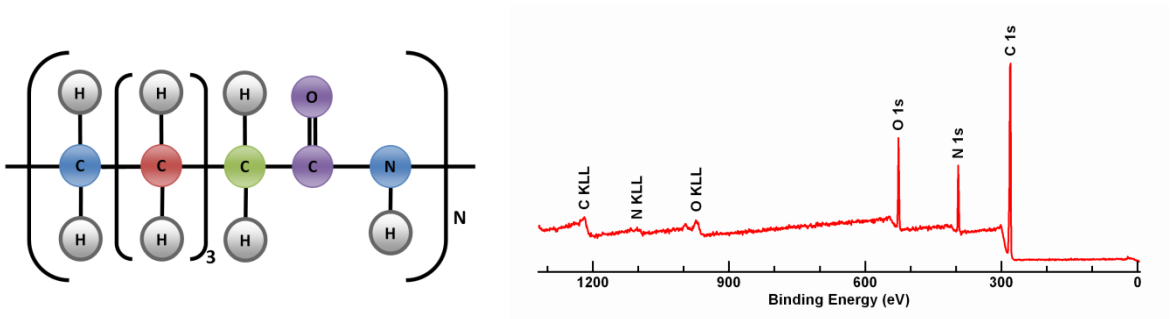

Figure 109. Expected chemistry for Nylon-6 and the result of measuring a survey spectrum from a Nylon-6 sample.

Line shapes are often limited by a photoemission process for electrons rather than instrumental response to photoemission signal. Two C 1s spectra measured from Nylon-6 (Figure 109), fitted using a peak model based on four synthetic components with Voigt line shapes and constrained in component area to follow the expected area ratio for C-$\underline{C}H_2$, O=C-$\underline{C}H_2$ and N-$\underline{C}H_2$, namely, 3:1:1

allows data reproduction consistent with signal-to-noise in both cases (Figure 110). These peak models suggest equivalent FWHM for each C 1s chemically shifted component despite the use of pass energy 40 eV full slot selected area aperture for one spectrum while pass energy 20 110 µm selected area aperture for the other measurement. These two modes on a Kratos Axis Nova yield different peak widths from HOPG for C 1s photoemission. The implication is line widths for C 1s data measured from Nylon-6 are limited by the sample rather than instrumental response.

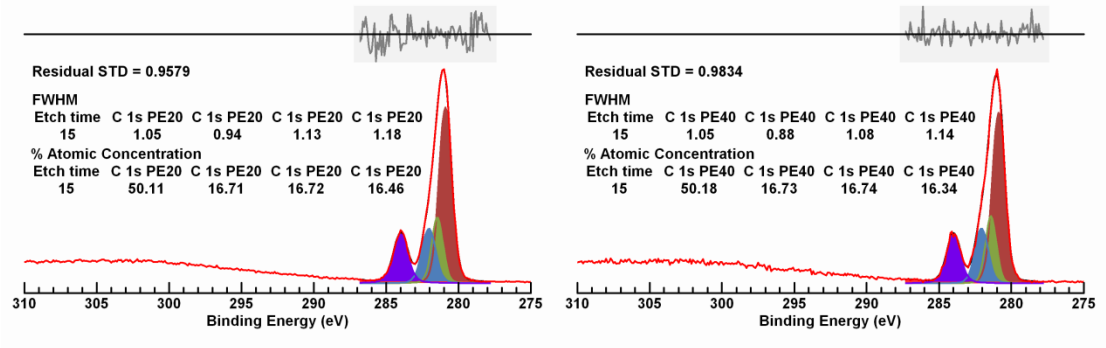

Figure 110. C 1s spectra measured from Nylon-6 using pass energy 20 eV and pass energy 40 eV.

By comparison, graphitic carbon produces C 1s photoelectrons with an inherently narrow asymmetric line shape. Making use of pass energy 5 eV and limiting the effective entrance aperture to the HSA width to about one quarter the width of the standard slot aperture on a Kratos Axis Nova result in a FWHM for C 1s measured from graphite of 0.46 eV (Figure 111). When HOP graphite is measured using two pass energies PE 40 eV and PE 20 eV equivalent to the measurements performed for Nylon-6, the FWHM for C 1s photoemission are 0.75 eV and 0.62 eV, respectively. The limiting factor for C 1s FWHM of Nylon-6 is therefore unlikely to be instrumental in nature. Moreover, if a C 1s component in a peak model fitted to PE 40 eV spectra arrives through optimisation at a FWHM below 0.75, then the component is probably nonphysical in nature.

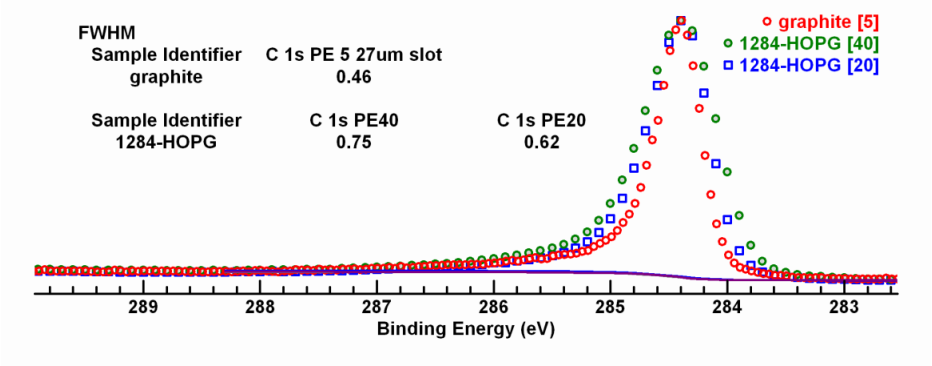

Figure 111. C 1s spectra measured from graphite using pass energy (PE) 5 eV coupled with a narrow aperture that further enhances energy resolution. A comparison to C 1s spectra measured from HOPG using pass energies 20 eV and 40 eV demonstrate a trend of increasing FWHM for C 1s with increasing pass energy. The suggestion is that the underlying line width for C 1s from HOPG is narrower in FWHM than either pass energies 20 eV or 40 eV can achieve.

Molybdenum MoS_2 / MoO_2

Narrow photoemission peaks measured using lower pass energies include instrumental shapes. Low pass energy reduces the influence of the instrument but does not entirely remove deformations due to the measurement process. Making use of low pass energy often requires extended acquisition times and these extended measurements have the potential for introducing deformation due to minor instability within instrumental voltages and/or mechanical components. Modelling shapes in data with synthetic curves with a residual standard deviation expected for pulse counted data tends to be increasingly difficult as acquisition time increases (Figure 112 and Figure 113).

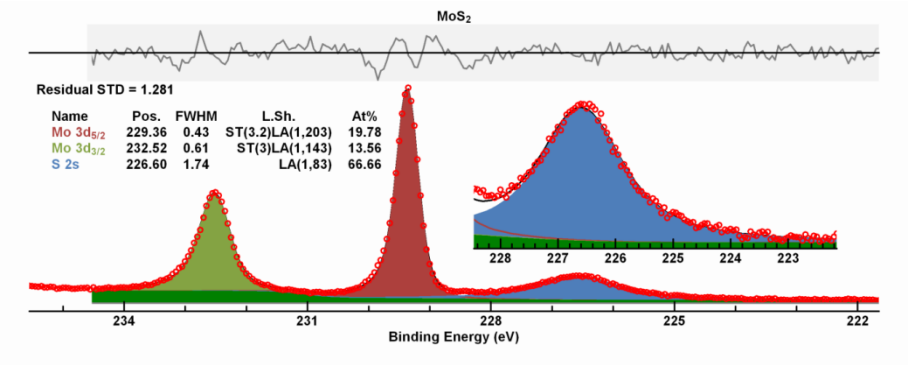

Figure 112. MoS_2 Mo 3d and S 2s photoelectron peak model based on three components. The stoichiometry for MoS_2 is recovered when the peak model is fitted to the spectrum. Note that the residual STD is slightly higher than the expected value of unity, but moreover the residual suggests the Mo 3d model is imperfect for the peak maxima. However, the broader S 2s residual plot is as expected for pulse counted spectra.

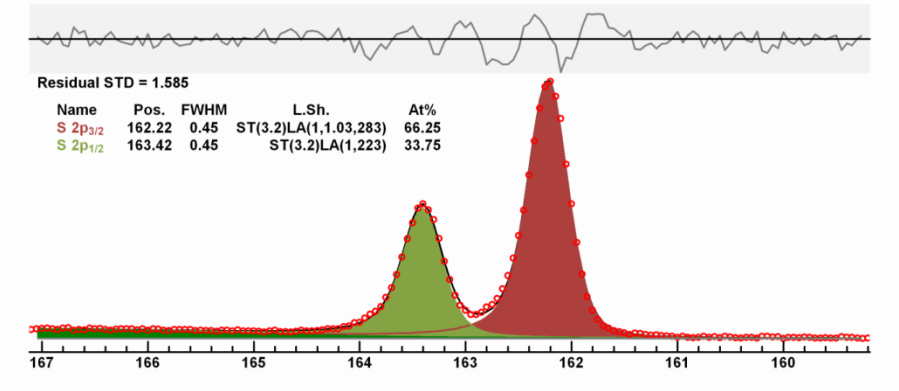

Figure 113. Narrow FWHM for S 2p doublet makes difficult the fitting to data of the peak maxima. This is in contrast to the good fit obtained by the broader S 2s feature in Figure 112.

More complex data envelopes require more components. These additional components introduce flexibility into the peak model which tends to allow good data reproduction, but perhaps without the same physical meaning one might expect based on the figure or merit (Figure 114).

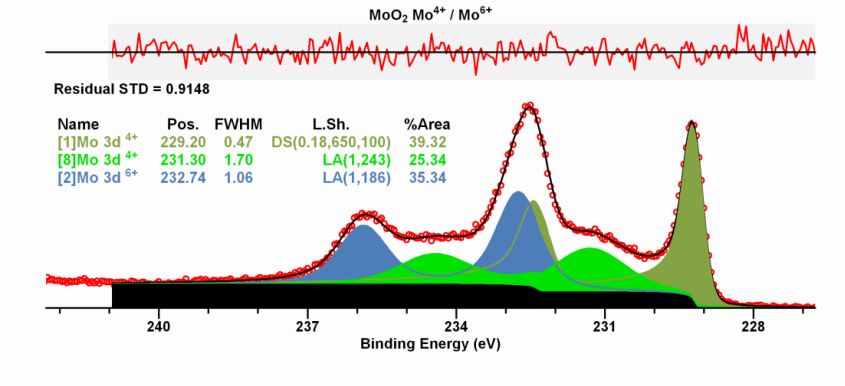

Figure 114. Peak model constructed for molybdenum dioxide, showing evidence of molybdenum trioxide in the sample. The fit to data, in this instance, is close to the expected statistic, however, the residual STD and plot owe much to the use of components representative of background signal. It is also possible that the line shape used to model the asymmetry in the primary Mo^{4+} doublet is sympathetic to these data and therefore permits the fit quality as shown.

Titanium Oxide

Metal oxides with significant band gaps are an example of where a direct calculation of a Shirley background based on data is more difficult to justify than for the metal signal for the same element. Energy loss for photoelectron peaks requires a mechanism for a loss to occur and photoelectron energy loss must be explained in terms of an energy gain by other entities. Bound state electrons in surrounding atoms scattered by photoelectrons are a route by which energy is lost by electrons resulting in background signal with energy close to that of photoemission peaks. For the case of metallic elements energy loss in direct response to photoelectrons from the peak is not limited by a band gap in energy. Hence, modelling such losses by a Shirley background calculated from data can be explained. By contrast, for oxides the same logic would suggest an energy interval close to a photoelectron peak from an oxide should contain little signal due to inelastic scattering. Therefore, modelling background to both metal and oxide by means of a Shirley response to energy loss events needs to be handled differently from a basic Shirley background computed from data.

The problem of fitting photoemission peaks with synthetic components is compounded for heterogeneous materials where energy loss may be caused by a variety of scattering events. For example, the existence of adventitious carbon may alter background shapes and proximity of a response to a photoemission peak. Another example is a film of titanium oxide on titanium metal which alters the response of background intensity as a function of film thickness. The background is important because titanium oxide signal is superimposed on titanium metal energy loss intensity. It is therefore difficult to model backgrounds to such samples by a basic Shirley background, and it is certainly non-trivial to justify, on scientific grounds, the precise form a background should take beneath photoemission from an oxide film on a metal substrate measured following contamination by adventitious materials.

The peak model in Figure 115 makes use of Voigt line shapes for titanium oxide signal, asymmetric line shapes based on the Doniach Sunjic formalism modified by a Shirley response to a DS line shape and background signal modelled using background component curves in the peak model. When fitted to these data, the Shirley-derived components are positioned closer to the Ti photoemission peaks than one might expect. The location with respect to titanium oxide components of these

background components is perhaps a consequence of carbon contamination coupled with these background curves accommodating more subtle structure associated with Ti 2p photoemission often observed in metal oxide multiplet structure.

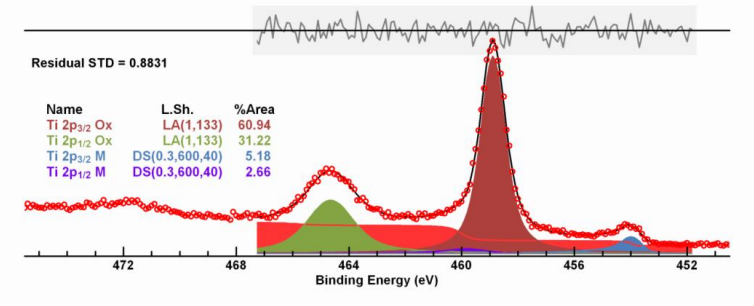

Figure 115. The peak model makes use of Voigt line shapes LA(1,133) for titanium oxide signal, asymmetric line shapes DS(0.3,600,40) based on the Doniach Sunjic formalism modified by a Shirley response to a DS line shape to model the low intensity metallic-like signal, while background signal is modelled using components in the peak model with Shirley characteristics.

A direct comparison of relative intensity for overlayer and substrate materials does not provide useful information about a sample unless the sample is well understood in the first place. Escape depth considerations and location of materials relative to the surface mean that %Area for photoemission reported by a basic quantification by XPS is by no means representative of true sample composition. The following example illustrates these points.

Heterogeneous samples are sometimes an unintended consequence of sample preparation (Figure 116). The following sequence of spectra is measured from a sample prepared with Ti^{4+} oxide on a silicon oxide substrate. However, the titanium layer was compromised in one location on the sample where silicon oxide from the substrate contributed to spectra.

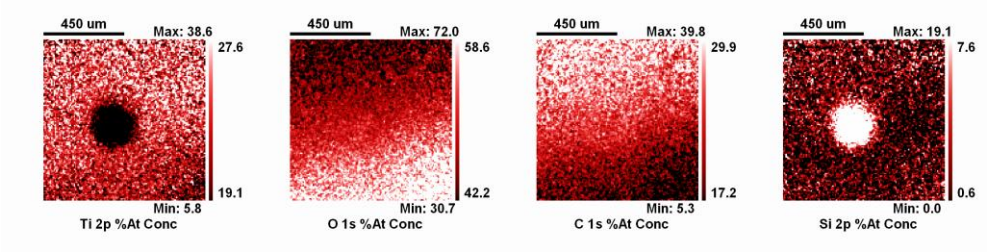

Figure 116. Imaging XPS shows that a sample prepared with the intention of creating a film of titanium on silicon, in reality, included a hole in the titanium that exposed silicon to XPS at the surface.

The spectra presented in Figures 117 to 122 were measured using pass energy 80 in FoV2 making use of a 55 µm selected area aperture on a Kratos Axis Nova. The analysis position and analysis area allow both titanium and silicon signal to be recorded simultaneously. Making use of the 55 µm selected area aperture projects an image of the sample into the entrance aperture to the HSA that is about half the width of the standard full slot (700 x 300 μm^2) used for the more sensitive slot-slot aperture settings for pass energy 80. The benefit of using 55 µm selected area aperture is the analysis area, as implied by the name, is smaller and therefore preserves to a greater extent the

spatial identity for spectra. Further, energy resolution improves and recorded photoemission peak shapes are higher quality compared to the more sensitive mode, as well as potentially improving consistency of charge state for signal measured from an insulating sample requiring charge compensation.

Titanium oxide is of value in a pedagogic sense (regarding aspects of quantification by XPS) because Ti 2p is located in energy close to O 1s and Ti 3p is similarly close to O 2s but at high kinetic energy compared to Ti 2p. It is therefore possible to obtain relative amounts of titanium and oxygen measured using four photoemission lines from the sample. Oxygen signal from oxygen bonded to silicon is shifted to higher binding energy than oxygen bonded to titanium therefore peak models can be constructed for Ti 2p, Ti 3p, O 1s and O 2s that separate Ti oxide from Si oxide.

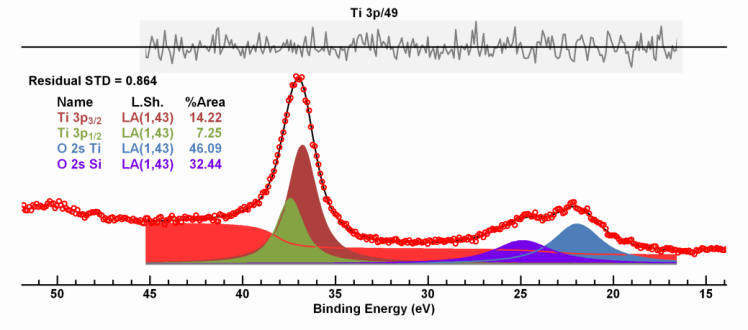

Figure 117. Peak model designed to compute the photoelectron intensity from titanium and oxygen emanating from Ti 3p and O 2s core-level electrons.

The background signal to Ti 3p and O 2s is constructed using components with line shapes formed by application of the Shirley algorithm to specific bell-shaped line shapes representing primary photoemission signal. A Voigt line shape is used to model primary photoemission signal from both Ti 3p and O 2s (Figure 117).

Spectra are also presented corresponding to Si 2p (Figure 118), Si 2s (Figure 119) and C 1s (Figure 120) as a means of demonstrating the validity of a peak model incorporating oxygen signal chemically shifted in binding energy representing Si oxide within the Ti 3p/O2s peak model.

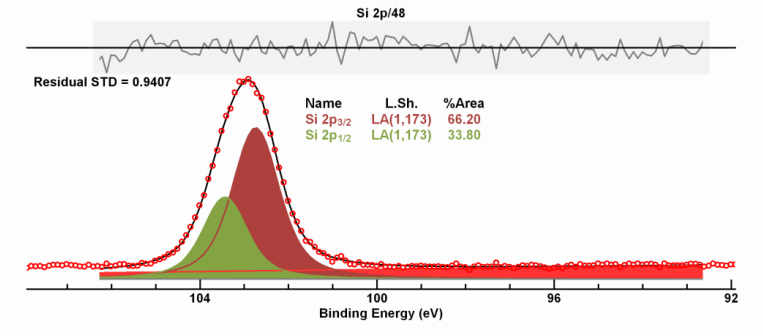

Figure 118. Si 2p spectrum fitted using two component peaks to model the unresolved doublet peaks expected for p-orbitals for silicon. Figure 103 provides an example of a Si 2p spectrum that exhibits elemental signal with strong evidence for the use of two components when modelling Si 2p photoelectrons.

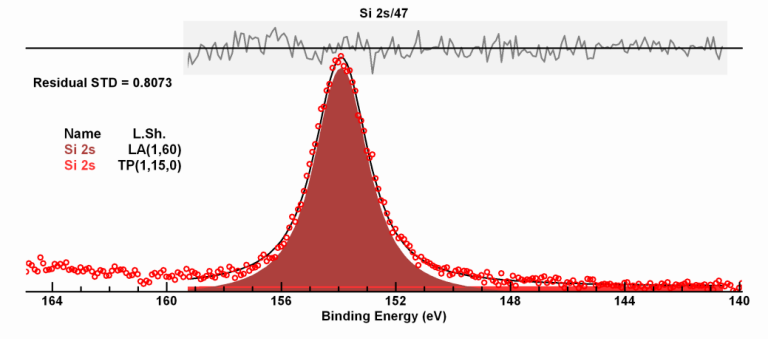

Figure 119. The physics of s-orbital photoionization is in contrast to p-orbital excitation. For the emission of Si 2s electrons, a single component representing photoelectrons is expected. However, to obtain the appropriate peak intensity for Si 2s, the line shape must be strongly Lorentzian.

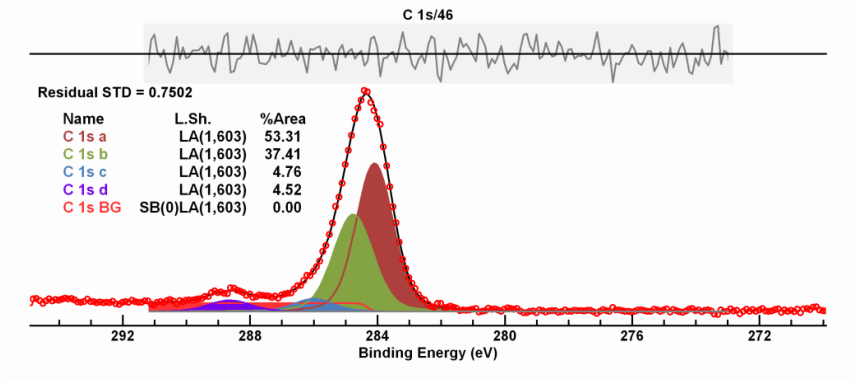

Figure 120. Peak model for C 1s photoelectrons.

A peak model for C 1s (Figure 120) demonstrates that a small amount of carbon bonded to oxygen is present in these samples. In principle O 1s and O 2s should also include synthetic peaks corresponding to C-O and C=O type signal. However, the low intensity of these components and the complexity of the peak models would present a challenge to optimisation in determining the correct energy, FWHM and area, so oxygen bonded to carbon is assumed to be accommodated by shapes in background or imperfections in data reproduction by fitting oxygen in 1s (Figure 121) and 2s (Figure 117) emission with only two component peaks per photoelectron peak.

A comparison of relative intensities for Ti and O measured using Ti 2p /O 1s (Figure 122) and Ti 3p/O 2s (Figure 117) suggests remarkable agreement for the ratio of Ti to O and a remarkable agreement for the ratio of Si oxide to Ti oxide computed from these peak models. The implication from these results is both Ti oxide and Si oxide are bulk materials homogeneous in nature. That is, despite Ti 2p/O 1s and Ti 3p/O 2s corresponding to different ranges of kinetic energy Ti 2p/O 1s quantify similarly to Ti 3p/O 2s, so it is unlikely there is any in-depth structure such as one forming a layer above the other. If this were the case then one might expect significant differences between Ti and Si bonded to O determined from O 1s and O 2s as a result of escape depth differences. Indeed, these circumstantial findings based on peak models are supported by the XPS images measured from the sample, namely, silicon signal is due to a circular hole in the titanium oxide layer (Figure 116).

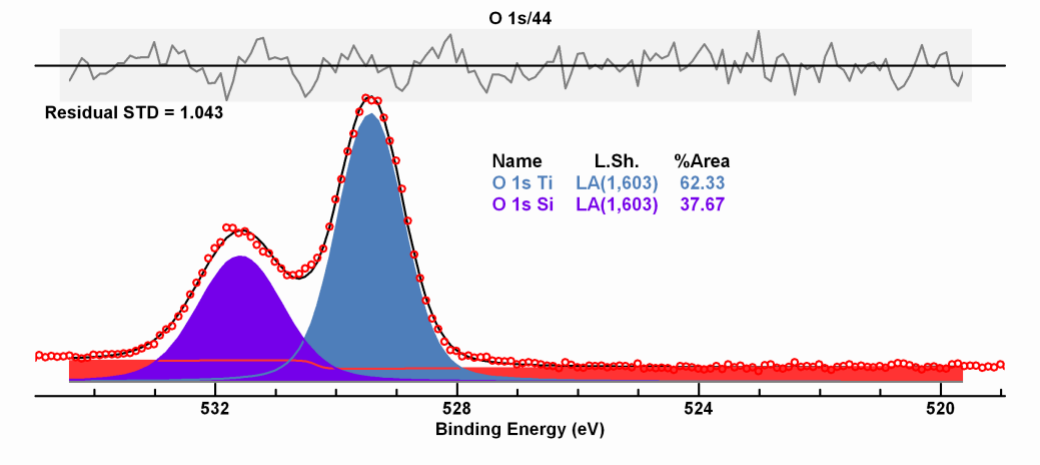

Figure 121. Peak model for O 1s which clearly shows two chemical environments for oxygen. The assignment of the higher binding energy O 1s component to silicon bonded to oxygen is made by an analysis of aTiO_2/SiO_2 multilayer sample, where the coordination of silicon to oxygen and titanium to oxygen clearly shifts O 1s photoelectrons to higher binding energy when bonded to silicon compared to titanium.

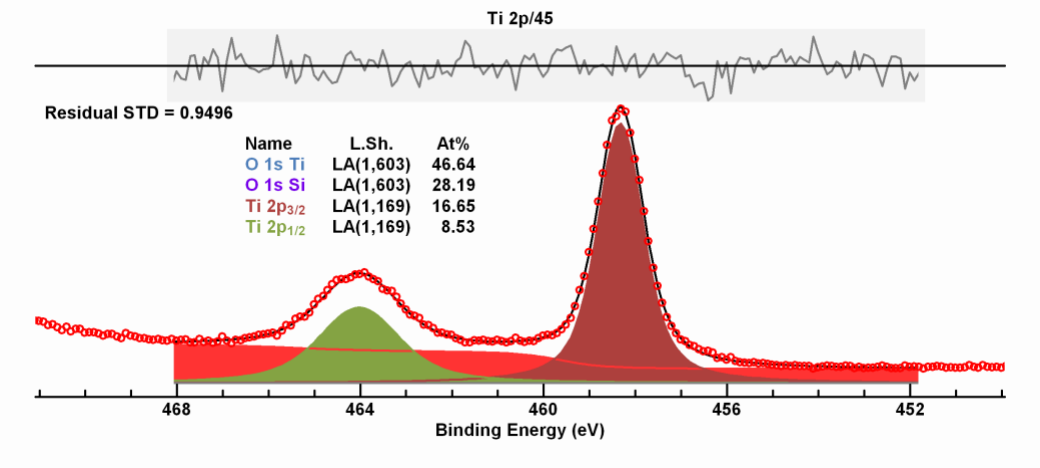

Figure 122. Titanium peak model with two Voigt line shapes used to model photoelectrons split in energy by spin-orbit interactions in the final state ion. The atomic concentration table displayed over the Ti 2p doublet is constructed using the Annotation dialog window using the Quantification property page. The Ti 2p and O 1s spectra are from the same row in the righthand-pane of CasaXPS and both are selected to allow the source for components from O 1s and Ti 2p to be available for constructing the quantification table as seen.

Poly lactic acid

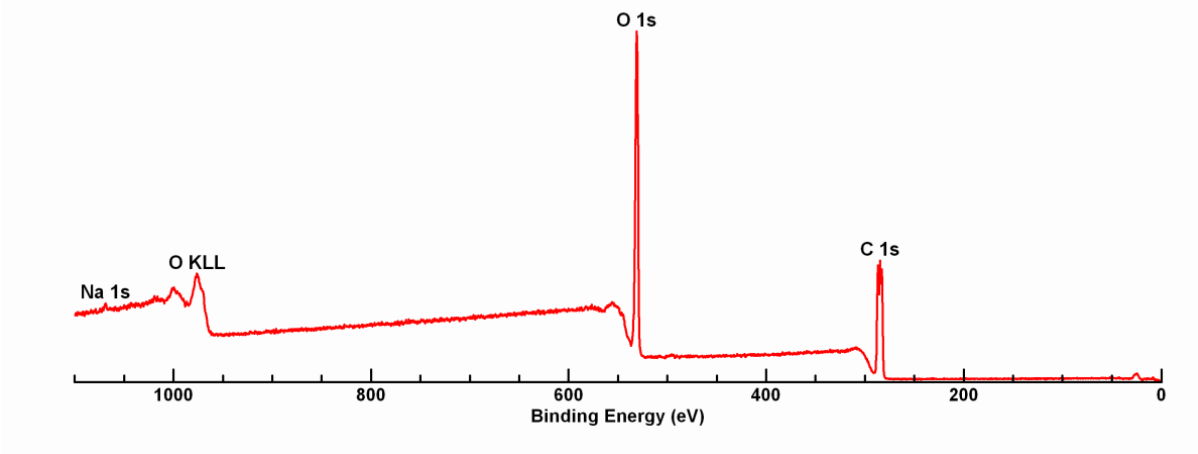

Figure 123. Survey spectrum measured from poly (lactic acid).

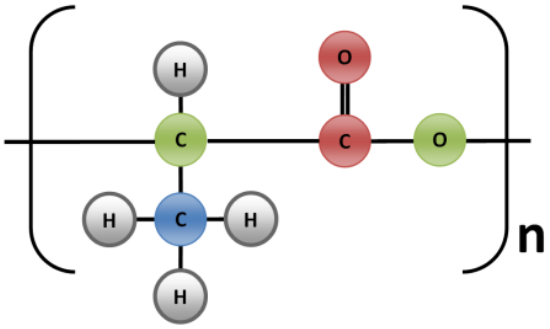

Figure 124. Expected chemistry for poly (lactic acid).

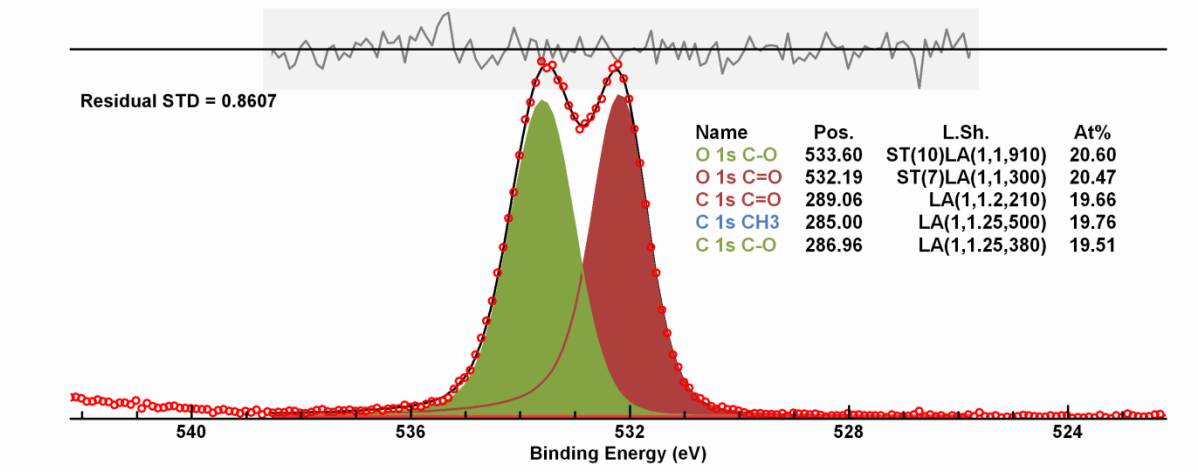

Figure 125. O 1s spectrum measured from poly (lactic acid). The quantification table is constructed using the two components fitted to O 1s data as shown and three components for C 1s fitted to the spectrum in Figure 126.

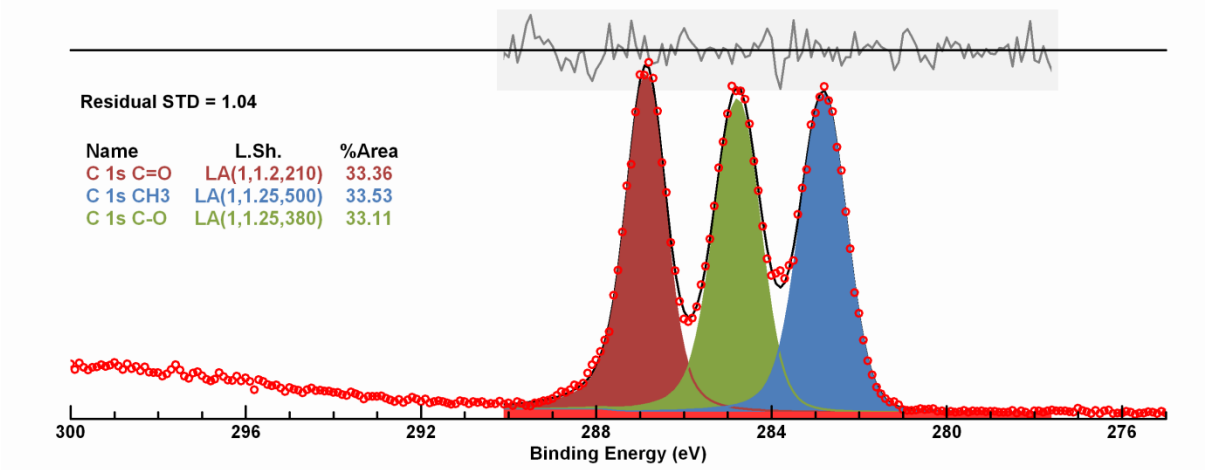

Figure 126. C 1s spectrum measured from poly (lactic acid). The table of components is added to the display of these three chemically shifted C 1s components using the Annotation dialog window and the Components property page.

An important means of supporting a peak model is demonstrating relationships applying not only between relative intensities within a peak model but also correlating with related information from other photoemission processes. The example shown here is poly lactic acid (Figure 123 and Figure 124) analysed using two peak models, one for O 1s (Figure 125) and the other C 1s (Figure 126), and for these data all components combined from both peak models yield consistent relative intensities for the material analysed (Figure 125). While results such as these are highly desirable there are several factors at play that make these results possible.

The first and necessary factor is the sample is homogeneous in area and homogeneous in depth. The importance of this statement is that signal emanating from the sample should be independent of the analysis area on the sample.

It is often assumed that variation in intensity as a function of kinetic energy for photoelectrons can be compensated for by means of a transmission function. However, the fact that a transmission function is required is evidence that electrons are gathered from a sample differently, depending on energy of recorded photoelectrons, and one reason signal intensity changes with energy is the analysis area changes. Another reason is the angular cone of electrons leaving the sample collected by a spectrometer alters, which means at a minimum the surface sensitivity changes with energy for the same reason angle resolved XPS (ARXPS) is possible. A further reason is apertures and iris dimensions that limit electrons accepted by the energy analyser are dependent on lens modes. Essentially, the origin from which photoelectrons leaving the sample arrive at the detectors is not identical for all photoemission peaks. If the sample is not truly homogeneous comparing O 1s intensity to C 1s intensity should be done with care.

Further, for a bulk homogeneous material, the correction to photoelectron intensity due to attenuation as a consequence of inelastic scattering by atoms within the sample is generally understood. Accounting for changes in intensity due to inelastic scattering is performed using an exponential decay model. The purpose of an exponential attenuation model is to correct energy dependence of sampling depth. Any in depth distribution of materials invalidates these escape

depth corrections, once again alters the ratio between peaks with different photoemission energies. If the material is a thin film, less than the sampling depth of XPS, then obtaining the expected relative intensity for photoemission peaks requires knowledge about the film thickness.

Secondly, if the sample is homogeneous then correlating intensities for photoemission with different energy requires an accurate transmission function for each operating mode for an instrument. These data measured from PLA were measured using an instrument for which a true transmission function was available. The procedure to compute the true transmission for the operating conditions used to measure narrow scan spectra for O 1s and C 1s is based on characterising a sensitive mode (pass energy 80) for the instrument. Using the NPL intensity calibration method applied to pass energy 80 spectra is beneficial because numerical fitting of data is best performed for data with good signal to noise. Then computing transmission for less sensitive modes such as pass energy 20, the transmission function is constructed relative to the pass energy 80 NPL transmission function using a simple piece-wise linear approximation included in the acquisition data system.

Thirdly, relative sensitivity factors for photoemission compatible with escape depth and transmission corrections must be available. In this example the RSFs are Scofield cross-sections. These Scofield cross-sections are theoretically determined probabilities for the scattering of a core-level electron by a photon of a given energy. The merit of using theoretical RSFs is the three corrections discussed to this point, namely, escape depth, transmission and RSF are traceable in the sense each factor is separate and the origin of these corrections is clear.

The fourth factor required for the comparison of different photoemission lines is angular distribution correction (ADC). Simply stated, photoemission intensity when measured in different directions varies with respect to angle between the X-ray source and the direction used to sample signal. While ADC is important in general, for the special case of s-orbitals these intensity variations due to sampling direction are the same for all elements.

Other factors including charge compensation and sample roughness can influence a comparison between photoelectron peak intensities. When taken en masse obtaining the type of results displayed here for PLA is somewhat remarkable. Nevertheless, a well characterised instrument combined with traceable quantification corrections is a powerful tool for understanding samples.

The real power is experienced when quantification fails to follow expectation and, by examining the steps leading to quantification results, clues about a sample are formed. Clues gained by quantification may extend beyond analysis of a sample. For example, the following spectrum is measured from a sample rich in sodium which is expected to be homogeneous in nature. The instrument in question is well characterised for the mode used to acquire these data and so the expected ratio for photoemission from Na 1s compared to Na 2s would be 1:1 (Figure 127). The ratio for these photoemission lines as measured is 2:3 (Figure 128). Such a difference might be explained by a significant layer of carbon contamination, but on observing the anomaly in these peak intensities it was possible to identify, in this case, the instrument malfunctioned. Repeating the experiment demonstrated a step-in-signal occurred beneath the S 2s photoemission peak. Confidence in quantification procedures is important beyond attempting to support peak models.

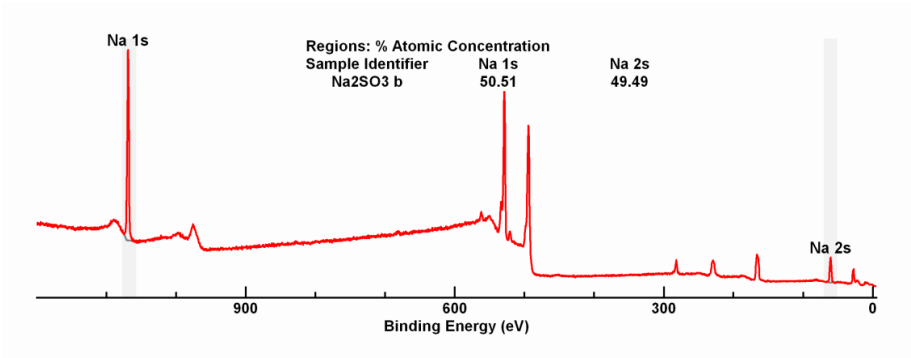

Figure 127. Survey spectrum measured from an instrument operating correctly. The estimate for sodium obtained from either Na 1s or Na 2s photoelectron peaks is entirely consistent.

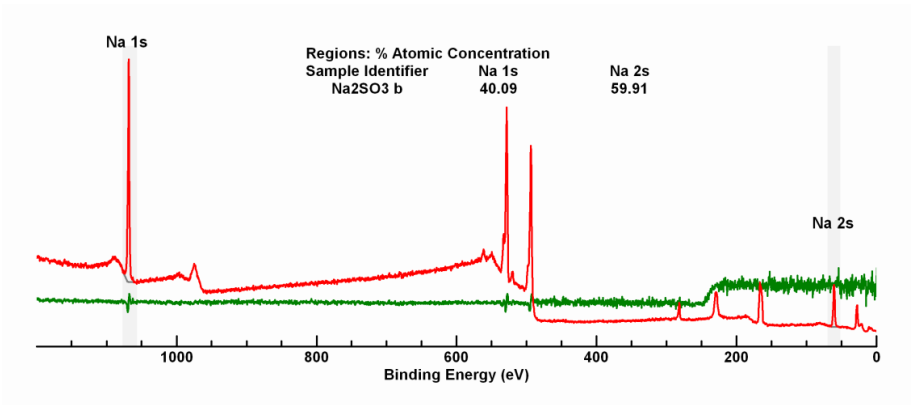

Figure 128. Survey spectrum measured from a malfunctioning instrument. The estimate for sodium obtained from either Na 1s or Na 2s photoelectron peaks is inconsistent. The ratio of the spectrum to the spectrum shown in Figure 127 is plotted in green and shows evidence of instability in the instrument during the measurement of the survey spectrum with poor estimates for the amount of sodium.

Curve Fitting using Edge Measurement Background Types

The complementary error function is obtained by the integral of a Gaussian as follows.

$$erfc(x) = \frac{2}{\sqrt{\pi}} \int_x^{\infty} e^{-y^2}\, dy$$

Estimating an edge position and width is implemented through background types based on the complementary error function. These backgrounds are defined in terms of *erfc* and a constant function. Four parameters a_0, a_1, a_2 and a_3 are used to fit the background functional form to a step in signal. For kinetic energy KE:

Background types Step Up and Edge Up (Figure 129) have the form:

$$Up(KE) = \frac{a_0}{2} erfc\left(\frac{a_1 - KE}{a_2}\right) + a_3$$

Background types Step Down and Edge Down have the form:

$$Down(KE) = \frac{a_0}{2} erfc\left(\frac{KE - a_1}{a_2}\right) + a_3$$

Where a_1 identifies the location of the step and $(2\sqrt{ln2})a_2$ is the full width at half maximum of the Gaussian that when integrated fits to the step in signal. The parameter a_0 scales the step height and the fourth parameter a_3 represents a constant required to account for an offset in signal necessary when fitting these edge measurement background types to data.

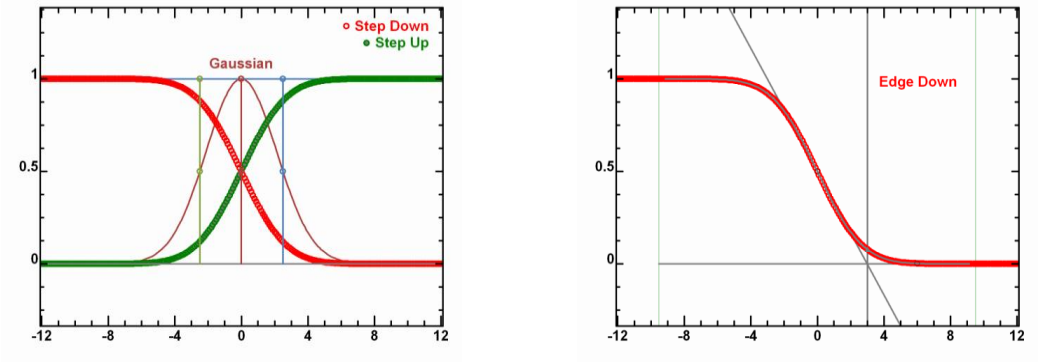

Figure 129. Step Down and Step Up differ from Edge Down and Edge Up only with respect to the definition for the edge position. Step Down and Step Up define the position to be the point of inflection for *erfc*. Edge Down and Edge Up compute the position for an edge by intersecting a line passing through the point of inflection in *erfc* with gradient equal to the gradient of *erfc* at the point of inflection and the line $I = a_3$.

An important use of these background types is to establish a systematic approach to energy calibration for a spectrometer. Aligning measured photoemission peaks based on peak maxima is not always appropriate, particularly for instrument modes designed for sensitivity rather than quality of line shapes. A step when measured with high pass energy is less prone to extreme deformations associated with narrow photoemission peaks such as Ad $3d_{5/2}$. These erfc based backgrounds have the added advantage that the width of the edge is more representative of instrumental resolution than Ag 3d as life-time broadening of photoemission peaks is inherently wider than the physical processes involved in thermal broadening of Fermi edge signal at room temperature (Figure 130).

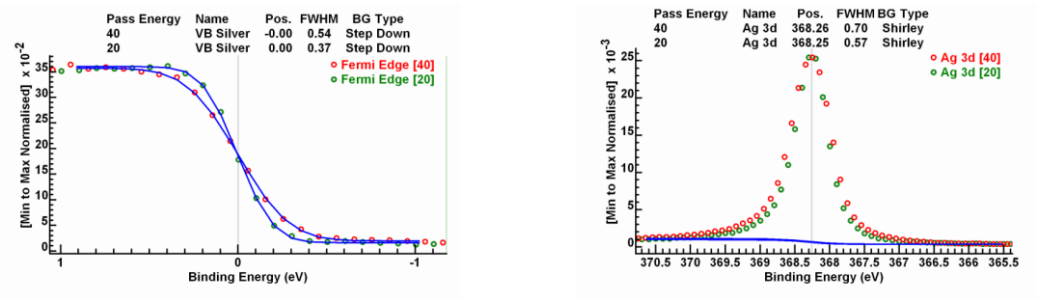

Figure 130. Comparison between characterising the energy resolution of an instrument using Step Down background types fitted to the Fermi edge of silver and estimating the FWHM for the corresponding Ag $3d_{5/2}$ photoelectron peak.

One might question why there should be a constant offset required to obtain a fit to Fermi edge measured by XPS. The explanation for dual anode X-ray sources is these X-ray sources induce X-rays with energies greater than the resonant X-ray energy for Kα emission. These X-rays with greater energy than Kα X-rays create photoemission electrons with energy greater than the Fermi edge due to Kα emission only. Therefore, inelastic scattered background is possible with signal above the Fermi edge assigned to Kα emission. When monochromatic X-rays are used the existence of a background is less obvious, but some inelastic scattered electrons are also possible due to the same properties of the quartz crystal diffraction and the Bragg angle law used by monochromatic X-ray guns that allow the use of anode materials such as aluminium, silver and chromium. X-rays with energy in multiples of 1486.6 eV are diffracted by the quartz crystal similarly and while resonant X-ray lines from Al, Ag and Cr anode materials satisfy the Bragg law, non-resonant X-ray signal from Al anodes will also arrive at the sample with relatively low intensity, nevertheless inelastic scattered background signal above the Fermi edge is also possible for, so called, monochromatic Al X-ray guns.

Peaks in Spectra that are neither Photoelectron or Auger in Origin

The example of a peak model in Figure 131 illustrates how spectra measured assuming the X-ray source delivers a narrow width in photon energy, if false can result in confusing peaks in spectra. While the data in Figure 131 are contrived to illustrate this point, so called, cross-talk between different anode materials in an X-ray gun may manifest as unexpected peaks in spectra. The spectrum in Figure 131 should be compared to the spectrum in Figure 132. Both spectra are measured from an aluminium metal foil, but the Auger lines indicated in Figure 131 are not possible when the X-rays are generated purely from a monochromatic X-ray gun using an aluminium anode only. Figure 133 is a spectrum made possible by X-rays with energies corresponding to Cr K_β, which is evidence that Al 1s photoelectrons are generated by a monochromatic X-ray gun using a chromium anode. The Auger lines in Figure 131 are only possible if Al 1s core-level holes are created.

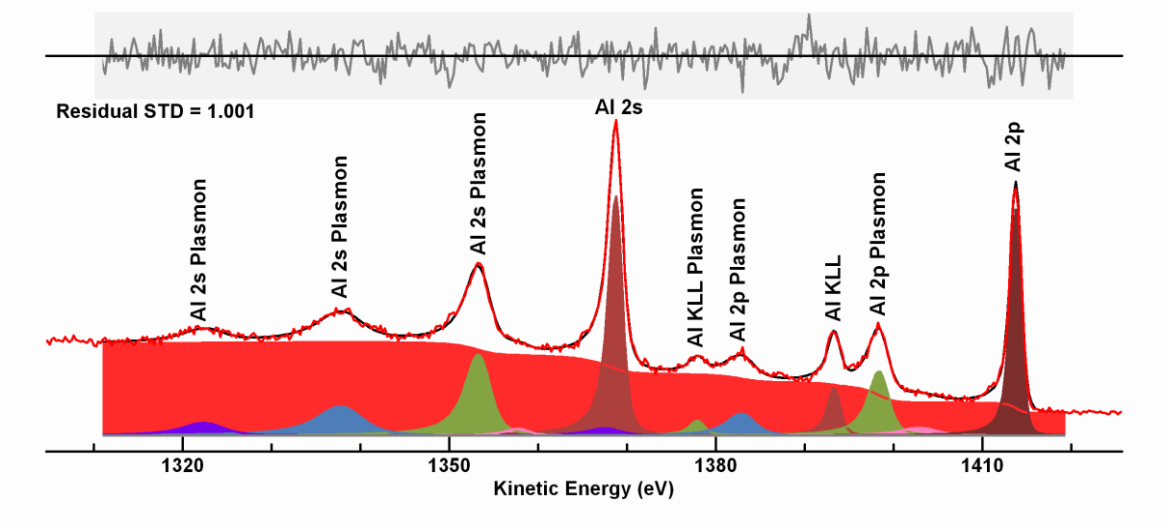

Figure 131. Aluminium metal sample measured using Scienta ECSA300 Daresbury Laboratory by Graham Beamson. Photoemission generated by the X-ray gun monochromator allows both Al K_α (1486.6 eV) and Cr K_β (5946 eV $\approx 4 \times 1486.6$) X-rays to reach the sample simultaneously thus creating both Al 2p photoemission due to Al Kα and Al KLL Auger emission due to Cr K_β. Al Kα X-rays alone are not capable of creating K shell holes in aluminium metal required to induce Al KLL Auger emission.

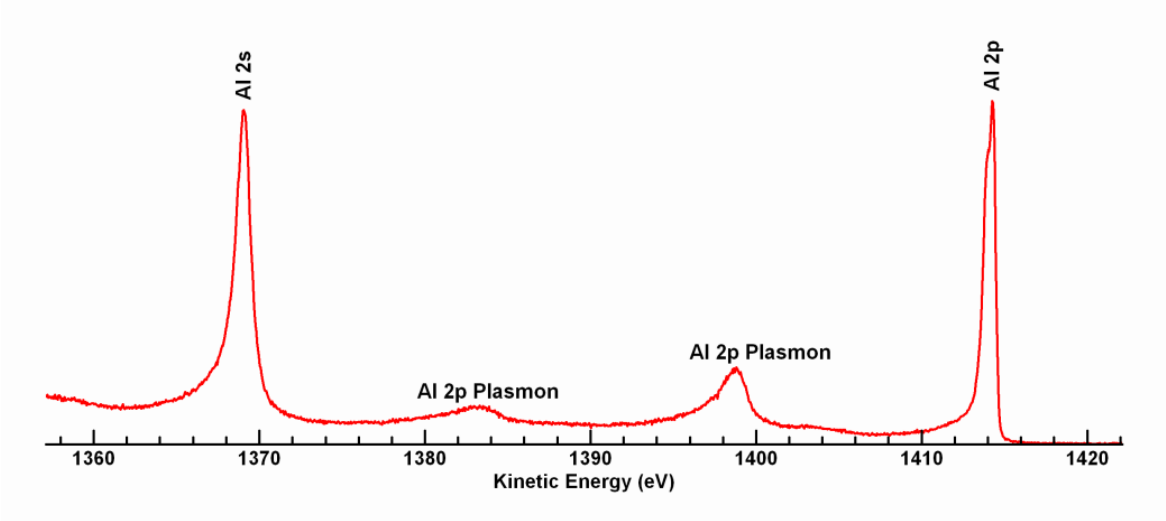

Figure 132. Aluminium metal measured using monochromatic Al K_α (1486.6 eV) X-rays only.

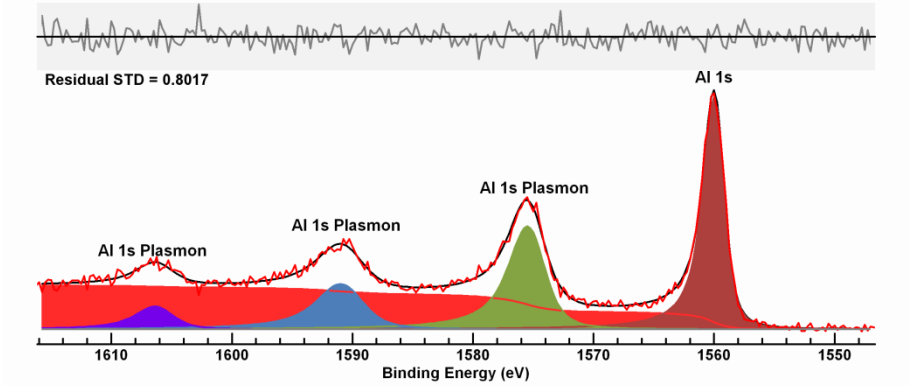

Figure 133. Aluminium metal Al 1s photoemission due to Cr K_β (5946 eV) monochromatic X-rays. The existence of Al 1s photoemission is evidence Cr K_β X-rays create holes in the K shell necessary for Al KLL Auger emission from aluminium. Note that the binding energy for Al 1s is greater than the energy of photons emitted due to Al K_α (1486.6 eV) X-rays and explains the absence of detectable Al KLL Auger signal in spectra acquired using Al anode monochromatic X-ray guns.

Curve Fitting and the Informed Sample Model Approach to Chemical State Analysis

Whenever data are available from samples related to one another the possibility exists to manipulate these original spectra to obtain spectral forms not necessarily available in the original data set but which can be interpreted as chemical state in origin. If it is possible to construct spectral forms that are capable of reproducing measured spectra, in the sense that simply scaling and summing these derived spectra result in adequate approximation to experimental data, then intensity can be measured for different chemical states by the means of integration regions.

Experimental design is central to such a methodology. That is, spectra rich in chemical state information of good quality underpin the informed sample model approach. Good signal-to-noise is important for the success of this method since derived spectral forms are created by creating lists of difference spectra. Subtraction of spectra tends to amplify noise just as summing spectra tends to suppress noise, hence good quality spectra with good signal to low noise is advantageous.

Also involved in these types of analyses are numerical techniques for calculating spectral envelopes that fit experimental data in the same sense as traditional nonlinear least squares curve fitting

allows sets of synthetic components to fit experimental data. These numerical techniques are now illustrated in terms of spectral forms computed from data collected from PVEE films on PS substrate.

Linear Least Squares for Spectra

XPS creates spectra by allocating intensity to different data bins. While these data are typically plotted as a continuous curve where these intensities are visualised as changes in a functional form due to changes in energy, these data are in fact a histogram representing discrete energy bins used to record signal sequentially at specific energies over a given time interval. Data considered as a histogram are open to interpretation as vectors in a vector space with dimension at most equal to the number of data-bins and, on the basis of such an interpretation it is possible to apply techniques from linear algebra to obtain fits to experimental data in terms of spectra of known origin.

If it is assumed spectra of known origin are available and that these spectra are capable of reproducing spectra of interest, then the fitting procedure can be derived by adopting a least squares criterion as the measure of goodness of fit.

A least squares criterion is defined for spectra constructed from histograms with n data bins $\boldsymbol{d} = \{d_1, d_2, d_3, \dots, d_n\}$ as follows.

Given a set of linearly independent vectors in an n dimensional vector space $\{\boldsymbol{v_1}, \quad \boldsymbol{v_2}, \quad \boldsymbol{v_3}, \dots, \boldsymbol{v_m}\}$, a vector $\boldsymbol{y} = \{y_1, y_2, y_3, \dots, y_n\}$ can be defined by

$$\boldsymbol{y} = c_1\boldsymbol{v}_1 + c_2\boldsymbol{v_2} + c_3\boldsymbol{v_3} + \cdots + c_m\boldsymbol{v_m} \quad \dots \quad (1)$$

where $c_1, c_2, c_3, \dots, c_m$ are constant values. The vector $\boldsymbol{y}$ is an approximation to $\boldsymbol{d}$. Each $\boldsymbol{v_j}$ is a spectral form representative of chemical state.

The figure of merit used to select a set of constants $c_1, c_2, c_3, \dots, c_m$that fit $\boldsymbol{y}$ to $\boldsymbol{d}$ is

$$L(c_1, c_2, c_3, \dots, c_m) = \sum_{i=1}^{n} (y_i - d_i)^2 \quad \dots \quad (2)$$

The condition for minimising the function $L(c_1, c_2, c_3, \dots, c_m)$ is

$$\frac{\partial L}{\partial c_j} = 0 \; for \; all \; j = 1,2,3, \dots, m$$

If a matrix $\boldsymbol{A}$ is defined in terms of the vectors $\boldsymbol{v_j}$

$$\boldsymbol{A} = [\boldsymbol{v_1}, \boldsymbol{v_2}, \boldsymbol{v_3}, \dots, \boldsymbol{v_m}]$$

Then the set of simultaneous equations resulting from minimising Equation (2) written in matrix notation becomes

$$\boldsymbol{A}^T\boldsymbol{A}\boldsymbol{c} = \boldsymbol{A}^T\boldsymbol{d} \quad \cdots \quad (3)$$

where $\boldsymbol{c} = \{c_1, c_2, c_3, \dots, c_m\}$. A least squares problem has a theoretical solution, provided the inverse matrix $(\boldsymbol{A}^T\boldsymbol{A})^{-1}$ exists, in the form

$$\boldsymbol{c} = (\boldsymbol{A}^T\boldsymbol{A})^{-1}\boldsymbol{A}^T\boldsymbol{d} \quad \dots \quad (4)$$

$\boldsymbol{A^T A}$ is a real symmetric matrix and therefore singular valued decomposition provides a least squares solution even when $\boldsymbol{A^T A}$ is singular, hence an approximation $\boldsymbol{y}$ to $\boldsymbol{d}$ can always be obtained. However, not all solutions $\boldsymbol{y}$ are feasible solutions for spectra and therefore constraints forcing solutions with positive area must be introduced rather than simply a direct solution of Equation (4).

The problem when attempting a linear least squares (LLS) solution is to identify a set of physically meaningful vectors for use in Equation (1) leading to a solution via Equation (4) that yields a residual standard deviation consistent with the expected noise in the data. The term consistent needs explaining in the context of fitting spectra by spectral forms. For pulse counted data, the residual standard deviation should be close to unity. However, spectral forms computed from data may fit spectra within a data set with precision unexpectedly good for pulse counted data. If so, this is a mathematical artefact and does not imply a superior result nor is this a problem. On the otherhand, failure to obtain the expected residual standard deviation in the opposite sense, that is, a magnitude significantly greater than unity should be considered a problem.

Least Squares Analysis of PVEE Film on PS

Designing LLS solutions require all spectra (analysed data and spectral components) used in the analysis to be energy calibrated and all have the same number of data bins. These operations involve appropriately distributing intensities into data bins to permit the use of a common energy interval and energy increment between data bins for all spectra. Appropriate adjustments to measured spectra are critical to the success of fitting data with spectral shapes by means of LLS.

The alternative to LLS is to make use of spectral components within a peak model designed for non-linear optimisation approach to fitting of data by peak shaped curves. Non-linear optimisation will compute offsets in energy required to obtain the best fit of components to data. Such an approach is possible, but shifting component positions automatically as part of optimisation may fit data well but may also result in less well-defined relative intensities for chemical state. Adopting the LLS approach forces greater care in aligning spectra. Misalignment of energy in spectra (Figure 134) yield poor fits for LLS which point to short comings in data that non-linear optimisation might incorrectly accommodate.

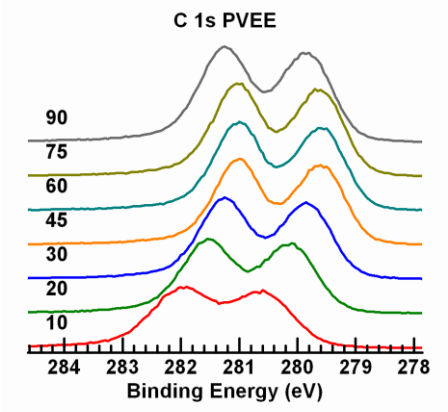

Figure 134. C 1s spectra measured from a bulk PVEE standard acquired at different take-off angles.

For the analysis of PVEE films on PS the question of component spectral forms ought to be simple to answer. In principle, the problem should be as simple as measuring spectra shapes from bulk

homogeneous PVEE and PS. However, this is not always so straight forward. Charge compensation is required for these polymer samples which necessitates energy calibration. Peak shapes for these standard spectra must match the shapes formed by measuring spectra from the PVEE film on PS so experimental conditions must be identical for all measurements. This point is emphasized by observing changes to peak shapes from PVEE induced by tilting the sample through a range of take-off angles between 10° and 90° (Figure 134). Each take-off angle changes the experimental conditions and these differences are sufficient to alter measured data envelopes for PVEE, most obviously seen in the depth of the valley between peaks deriving from CH and CO within C 1s data and shifts in energy due to varying charge compensation between measurements at different angles.

An alternative to using spectra from standard materials in the LLS decomposition is to compute spectral shapes from data measured from samples for which the analysis is required. A motivation for such an approach is samples may not be exactly the sum of their parts. There is the possibility, when forming a film of PVEE on PS, changes to the chemistry occurs at the interface between these two polymers. A further advantage of using sample data rather than standard spectra is the charge compensation state for these samples can be gauged by O 1s signal which is present for all samples due to the PVEE film. Aligning O 1s peaks in energy should in theory also align C 1s signal in terms of energy. However, should charge compensation be imperfect and consequentially a sample potential evolves slowly with time, then aligning O 1s may result in a misalignment for C 1s intensity. The analysis that follows makes use of the O 1s spectra from PVEE to corroborate the results for charge correction based on C 1s analysis using synthetic components. Alignment for C 1s spectra measured from PVEE films on PS is performed here using the CO peak from PVEE to create a systematic adjustment to the energy scale (Figure 135).

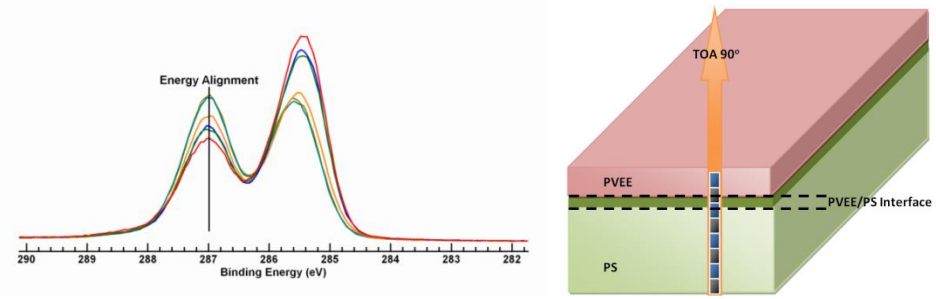

Figure 135. Charge corrected C 1s spectra where calibration of energy aligns CO peak from PVEE.

Once energy alignment is achieved the next step requires the re-binning of intensities which is necessary because each spectrum must be formed from the same number of data bins and following energy calibration the meaning for each data bin within calibrated spectra changes. Re-binning intensities recovers the ability to treat spectra as vectors from the same vector subspace.

Computing spectral forms from PVEE films on PS data is simplified by the fact that two samples appear to be sufficiently thick films of PVEE that identical ratios for C 1s to O 1s are obtained for data acquired at normal TOA and 10° TOA. By this observation the use of spectra from one of these samples is justified as representative of bulk PVEE data. The problem reduces to computing a spectral form characteristic of the material below PVEE. Difference spectra between the spectra with greatest PS proportion and the sample representative of bulk PVEE are formed. The spectral forms created by these difference spectra approach the expected PS spectrum but do not permit a full

reproduction of PS C 1s data. It is not possible to fully remove CO type intensities without deforming the spectral shapes for both C 1s and O 1s (Figure 136). For this reason, there is the suspicion that at the interface between PVEE and PS a hybrid form of material is created.

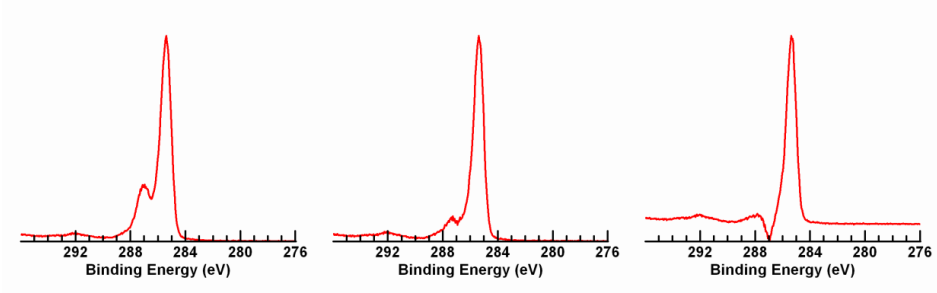

Figure 136. Spectral form calculated from the difference between a spectrum representative of bulk PVEE and a sample where a thin film of PVEE on PS allows PS type signal to be recorded. The spectrum representative of the substrate still includes the characteristic of CO type bonds.

The computed spectral shape for the substrate is further analysed by introducing the spectrum for pure PS and performing a further difference analysis with the view of removing pure PS from the substrate spectral form.

These steps lead to three spectral forms that can be used in LLS calculations applied to each spectrum measured from PVEE films on PS with different preparations for the PVEE film for each sample (Figure 137).

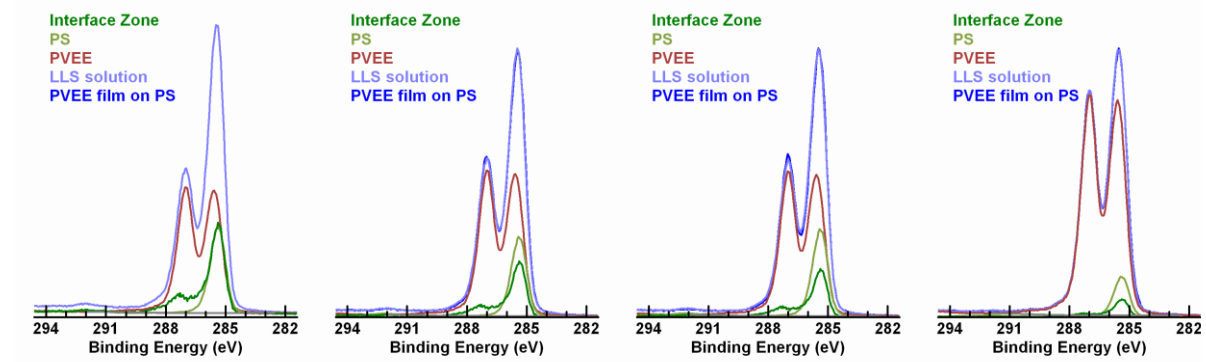

Figure 137. Linear least squares decomposition of spectra measured from PVEE films on PS. Spectral forms used in the LLS calculation are spectra computed from PVEE films on PS, a spectrum representative of bulk PVEE and a standard PS spectrum. All data are measured using 90° take-off angle.

An analysis of these samples in terms of film thickness via the Hill equation indicate two of these samples have similar thickness of PVEE film, namely approximately 5.65 nm in depth. However, the analysis into three spectral forms shows these two samples may contain a difference in the interfacial zone. Indeed, all four spectra exhibit different relationships between the proposed interfacial zone chemistry and PS.

The results from the analysis of these PVEE films on PS demonstrate that spectra can be decomposed in to shapes characteristic of chemistry associated with a sample. Such an approach is

even more appropriate for materials with spectra formed from complex multiplet structures such as iron or chromium oxides as these tend to have spectra without a clear relationship between bell shaped curves and chemical state. While LLS provides the means of fitting data and measuring amount of substance, understanding gained regarding the samples and spectra is a significant benefit of such an analysis. The merit of these steps applied to an investigation is far greater than the ability to measure the relative proportions of PVEE and PS from overlayer and substrate. The act of creating difference spectra and observing how choices made during the analysis alter outcomes should be viewed as food for scientific thought.